# Cerium Oxide Nanoparticles Act As A Unique Catalyst And Scavenge Nitric Oxide And Peroxynitrite And Decrease Rns In Vitro And In Vivo

2012

Janet Dowding
*University of Central Florida*

Find similar works at: https://stars.library.ucf.edu/etd

University of Central Florida Libraries http://library.ucf.edu

Part of the Molecular Biology Commons

University of Central Florida

STARS
Showcase of Text, Archives, Research & Scholarship

CeO$_2$ NPS ACT AS A UNIQUE CATALYST AND SCAVENGE ·NO AND ONOO$^-$ AND DECREASE RNS *IN VITRO* AND *IN VIVO*

by

JANET MARIE DOWDING
B.S. Northern Illinois University, 1982
M.S. Illinois State University, 1990
M.S. University of Central Florida, 2010

A dissertation submitted in partial fulfillment of the requirements
for the degree of Doctor of Philosophy
in the Burnett School of Biomedical Sciences
in the College of Medicine
at the University of Central Florida
Orlando, Florida

Fall Term
2012

Major Professor: William T. Self

# ABSTRACT

Cerium oxide nanoparticles ($CeO_2$ NPs)(nanoceria) have been shown to possess a substantial oxygen storage capacity via the interchangeable surface reduction and oxidation of cerium atoms, cycling between the $Ce^{4+}$ and $Ce^{3+}$ redox states. Reduction of $Ce^{4+}$ to $Ce^{3+}$ causes oxygen vacancies or defects on the surface of the crystalline lattice structure of the particles, generating a cage for redox reactions to occur. The study of the chemical and biological properties of $CeO_2$ NPs has expanded recently, and the methods used to synthesize these materials are also quite diverse. This has led to a plethora of studies describing various preparations of $CeO_2$ NPs for potential use in both industry and for biomedical research. Our own work has centered on studies that measure the ability of water-based $CeO_2$ NPs materials to reduce reactive oxygen and nitrogen species in biological systems, and correlating changes in surface chemistry and charge to the catalytic nature of the particles. The application in experimental and biomedical research of $CeO_2$ NPs began with the discovery that water-based cerium oxide nanoparticles could act as superoxide dismutase mimetics followed by their ability to reduce hydrogen dioxide similar to catalase. While their ROS scavenging ability was well established, their ability to interact with specific RNS species, specifically nitric oxide ($\cdot$NO) or peroxynitrite ($ONOO^-$) was not known. The studies described in this dissertation focus on the study of RNS and cerium oxide nanoparticles.

Our *in vitro* work revealed that $CeO_2$ NPs that have higher levels of reduced cerium sites (3+) at the surface (which are effective SOD mimetics) are also capable of accelerating the

decay of peroxynitrite *in vitro*. In contrast, CeO$_2$ NPs that have fewer reduced cerium sites at the particle surface (which also exhibit better catalase mimetic activity) have ·NO scavenging capabilities as well as some reactivity with peroxynitrite. Our studies and many others have shown cerium oxide nanoparticles can reduce ROS and RNS in cell culture or animal models. The accumulation of ROS and RNS is a common feature of many diseases including Alzheimer's disease (AD). Testing our CeO$_2$ NPS in cortical neurons, we used addition of Aβ peptide as an AD model system. CeO$_2$ NPs delayed Aβ-induced mitochondrial fragmentation and neuronal cell death. When mitochondrial ROS levels are increased, mitochondrial fission is activated by DRP1 S616 phosphorylation. Specifically, our studies showed the reduction of phosphorylated DRP1 S616 in the presence of CeO$_2$ NPs. Results from our studies have begun to unravel the molecule mechanism behind the catalytic nature of how CeO$_2$ NPs reduce ROS/RNS in biological systems and represents an important step forward to test the potential neuroprotective effects of CeO$_2$ NPs in model systems of AD.

A plethora of studies describing various preparations of CeO$_2$ NPs for potential use in both industry and for biomedical research have been described in the past five years. It has become apparent that the outcomes of CeO$_2$ NPs exposure can vary as much as the synthesis methods and cell types tested. In an effort to understand the disparity in reports describing the toxicity or protective effects of exposure to CeO$_2$ NPs, we compared CeO$_2$ NPs synthesized by three different methods; H$_2$O$_2$ (CNP1), NH$_4$OH (CNP2) or hexamethylenetetramine (HMT-CNP1). Exposure to HMT-CNP1 led to reduced metabolic activity (MTT) at a 10-fold lower concentration than CNP1 or CNP2 and surprisingly, exposure to HMT-CNP1 led to substantial

decreases in the ATP levels. Mechanistic studies revealed that HMT-CNP1 and CNP2 exhibited robust ATPase (phosphatase) activity, whereas CNP1 lacked ATPase activity. HMT-CNP1 were taken up into HUVECs far more efficiently than the other preparations of $CeO_2$ NPs. Taken together, these results suggest the combination of increased uptake and ATPase activity of HMT-CNP1 may underlie the mechanism of the toxicity of this preparation of $CeO_2$ NPs, and may suggest ATPase activity should be considered when synthesizing $CeO_2$ NPs for use in biomedical applications.

Overall the studies have uncovered two new catalytic activities for water-based $CeO_2$ NPs (·NO scavenging and accelerated decay of peroxynitrite), demonstrated their ability to reduce RNS in an AD cell culture model as well as identifying a catalytic activity (phosphatase) that may underlie the observed toxicity of $CeO_2$ NPs reported in other studies.

I dedicate this dissertation first, to my beloved husband, Fred. Fred 'you are the wind beneath my wings' and I couldn't have chosen a more wonderful man to spend my life with. Thank you for believing in me and helping me achieve this goal of mine.

I also dedicate my PhD journey to all the women throughout my life, especially Janka, Brittany, Kishka, Makenzie, Emma, Jillian, Lois, Bunny, Barbara and my mom. You all have touched me, helped me, inspired me to become a better woman in countless ways and this dedication is to remind YOU to NEVER give up on your dreams and aspirations. Please live passionately and believe in yourself!

# ACKNOWLEDGMENTS

My completion of this work is a compilation of the many amazing people I have met throughout my life. First and foremost I thank my incredible mentor, Dr. William Self, for his encouragement and inspiration. The time spent in his lab has been some of the happiest and challenging in my life. I feel very fortunate to have been able to complete this chapter of my life under his guidance.

I thank my graduate committee members Dr. Sudipta Seal, Dr. Ella Bossy-Wetzel, Dr. Swadeshmukul Santra, and Dr. Anthony Zervos for their advice, suggestions and encouragement. I thank all my UCF friends, classmates, and lab members both past and present especially Self lab members, Milan and Sanjay, and Seal lab members, Soumen, Amit and Ajay.

When did my PhD journey begin? I cannot not pinpoint the start but I need to acknowledge my colleagues and friends in the Ridgway lab at the University of Colorado, Health Science Center: Thank you Chip, Bill, David, Bryan, Virginia, Suzie, Nicole, Alex, Rhonda and especially Whitney. The time I spent working, growing and laughing with you in Colorado were joyful.

# TABLE OF CONTENTS

# LIST OF FIGURES

# LIST OF TABLES

# LIST OF ABBREVIATIONS

| | |
|---|---|
| Aβ | Amyloid beta |
| AD | Alzheimer's disease |
| APF | 3'-($p$-aminophenyl) fluorescein |
| ATP | Adenosine triphosphate |
| $CeO_2$ | Cerium oxide |
| CNP1 | Cerium nanoparticle 1, water-based high $Ce^{3+}/Ce^{4+}$ ratio |
| CNP2 | Cerium nanoparticle 2, water-based low $Ce^{3+}/Ce^{4+}$ ratio |
| DEA/NO | Diethylamine NONOate diethylammonium salt |
| DEPMPO | 5-(Diethoxyphosphoryl)-5-methyl-1-pyrroline-N-oxide |
| DPR1 | Dynamin-related protein 1 |
| DTPA | Diethylenetriaminepentaacetic acid |
| Hb | Hemoglobin |
| HMT | Hexamethylenetetramine |
| HMT-CNP | Hexamethylenetetramine-cerium nanoparticles |
| $H_2O_2$ | Hydrogen peroxide |
| ICP-MS | Inductively coupled plasma mass spectroscopy |
| MESG | 2-Amino-6-mercapto-7-methylpurine riboside |
| MTT | Thiazoyl blue tetrazolium bromide |
| NAC | $N$-Acetyl-$L$-cysteine |

| | |
|---|---|
| NMDA | *N*-Methyl *D*-aspartate |
| ·NO | Nitric oxide |
| NOS | Nitric oxide synthase |
| NPs | Nanoparticles |
| 3-NP | 3-Nitropropionic acid |
| ONOO⁻ | Peroxynitrite |
| ROS | Reactive oxygen species |
| RNS | Reactive nitrogen species |
| SNAP | S-Nitroso-*N*-acetylpenicillamine |
| SNOC | *S*-Nitrosocysteine |
| SOD | Superoxide dismutase |
| TEM | Transmission electron microscopy |
| ZP | Zeta potential |

# CHAPTER 1: INTRODUCTION

## Aging

Progressive accumulation of damaged molecules or tissues are associated with aging and are believed to be responsible for the ever-increasing susceptibility to disease and death (1). In 1956, Harman proposed the 'free radical theory of aging' (2) which implicated increasing levels of oxidatively damaged biomolecules is due to the formation of reactive oxygen species. These reactive species including free radicals (*i.e.* superoxide, hydroxyl, carbonate) lead to deleterious side effects on most cell constituents (2). Reactive oxygen species (ROS) and reactive nitrogen species (RNS) are reactive molecules that can damage all types of biomolecules, including DNA, proteins, and lipids with the formation of toxic and mutagenic products. ROS/RNS can originate from exogenous sources such as ultraviolet light (UV), ionizing radiation, and other environmental stress or they can be generated intracellularly as a consequence of normal metabolism (3). Aerobic organisms possess antioxidant enzymes (*i.e.* superoxide dismutase, catalase, peroxiredoxins), antioxidants (*i.e.* glutathione, uric acid) and mis-folded protein degradation defense systems that deal with ROS produced as a consequence of aerobic respiration and oxidation of biomolecules (4). Macrophages of the immune system can create ROS by deliberately producing superoxide to rid itself of foreign material such as bacteria and viruses (5). Mammalian cells and tissues can tolerate certain levels of these species, but excessive levels of ROS leads to damage to cells and tissues (6). Life expectancy has also been shown to decline with an increase in the generation of ROS in many species (7). In addition to the normal levels of oxidative stress formed during regular metabolism,

neurodegenerative disease models have suggested that cells may also be subjected to damage by RNS resulting from elevated levels of nitric oxide (·NO) and its reactive intermediate compounds, including peroxynitrite ($ONOO^-$) (8). The pathogenesis of diseases including many degenerative diseases involve the generation of ROS and RNS associated with mitochondrial dysfunction (9). Exposure to pesticides, toxins and other exogenous factors as well as endogenous factors may trigger the over-production of ROS and RNS (10). For organisms to withstand this imbalance and prevent or diminish ROS and RNS induced damage, it is important to evaluate new modes of therapy and treatment.

<u>Antioxidants</u>

Decreasing the levels of ROS and RNS is the role many antioxidant molecules play. Cellular protective effects of antioxidants have been extensively studied and have demonstrated their ability to directly scavenge ROS/RNS or their precursor molecules by attenuating the catalysis of ROS/RNS generation in most instances using metal dependent coenzymes (11). Effectively managing diseases is the foremost goal in medical research today and many studies have used therapeutic antioxidants in their research which did not have satisfactory pharmacological outcomes. In recent human studies, several antioxidants including β-carotene, vitamins C and E, NAC (12), coenzyme $Q_{10}$ (13) and tetra-hydrocurcumin have been shown to provide protective effects in cellular and animal models of AD (14). However, their efficacy in human trials provided at best only modest changes in disease progression (12, 15, 16). Among the problems are their poor stability and repetitive dosing, underscoring the need for alternative strategies.

Treatment efficacy of diseases that respond to antioxidants should be improved by using catalytic antioxidants, which would then decrease the need for repetitive dosing. This would allow the breakdown of toxic molecules without the catalytic antioxidants themselves becoming inactivated (11). It has become apparent that identifying compounds for treating the excessive formation of ROS and RNS in diseases without interfering with normal metabolism or resulting in additional adverse effects is an important standard (17).

Nitric Oxide

The role of ROS and its effect on aging has received considerable attention since Dr. Harman first proposed the 'free radical theory of aging.' More recently, the role of RNS have been shown to have a direct role in cell signaling, vasodilatation and the immune response (18). Nitrosative stress, defined by the excessive production of reactive nitrogen species, causes damage to macromolecules and can lead to degenerative diseases, contribute to metabolic diseases and if in great excess can lead to cell death through a variety of molecular mechanisms. The role that RNS play in many age related diseases is now just being appreciated.

Nitric oxide has many physiological functions (neurotransmitter, blood vessel dilation) but also ·NO can convert into a highly reactive and toxic molecule, peroxynitrite, that readily reacts with proteins, DNA, and lipids to alter their function (19). Nitric oxide reacts with various molecules *in vitro* and *in vivo* and the products of these reactions can damage the cell through a variety of mechanisms. One mechanism, S-nitrosylation is a post-translational, redox-related modification of cysteine thiols by nitric oxide (20). Additionally, tyrosine residues can be modified to generate 3-nitrotyrosine, and subsequently this modified amino acid is used as a

3

biomarker of nitric oxide -related oxidants (21). Accumulating evidence suggests that the specific proteins are regulated through S-nitrosylation and tyrosine nitration, and these sites play key roles in human health and disease. S-nitrosylation is a reversible reaction, often tied to regulation of enzyme activity (22-24) whereas and 3-nitro tyrosine is a stable covalent adduct (25). Nitric oxide, if present in excess of antioxidant defense systems, can trigger nitrosative damage to macromolecules through its reactive intermediates, which in turn may contribute to degenerative diseases due to various reasons including the structural alteration of proteins, inhibition of enzymatic activity, and interferences of the regulatory function (18).


Peroxynitrite


A primary reaction in the production of RNS is the diffusion limited reaction of $\cdot$NO and superoxide radical ($O_2^-\cdot$) to form $ONOO^-$ (26). $ONOO^-$ is a powerful oxidant and has been shown to react with all classes of biomolecules including thiols (27), lipids (28), carbohydrates (29) and DNA (30). The oxidative chemistry of peroxynitrite in biological systems depends upon the availability of targets (31), but the primary deleterious effect of $ONOO^-$ is the inactivation of enzymes (32). Modification of amino acid residues on the active site of key proteins may result in detrimental change in function of the proteins. Tyrosine nitration of proteins has become an important marker for inflammation and for nitrosative stress and has been detected in a number of diseases and pathological conditions (33). Likewise, disproportionate amounts of nitric oxide can compete with oxygen causing the interruption of electrons from the respiratory chain which results in increased formation of $O_2^{\bullet-}$ (33) and thus increased peroxynitrite leading to the post-translational modification of proteins. Tyrosine nitration occurs with the

4

incorporation of a nitro group (-NO$_2$) at position 3 of the aromatic ring of tyrosine and  the majority of nitration  is due to the simultaneous availability of a tyrosyl radical (Tyr·) and nitrogen dioxide  radical (·NO$_2$) (34). Addition of a -NO$_2$ group to tyrosine can alter protein function by various modes including lowering the pK$_a$ of its phenolic –OH.  This bulky substituent which if placed on a relevant tyrosine, can alter protein function and conformation, impose steric restrictions, and also inhibit tyrosine phosphorylation. (35).

Several specific proteins and systems have been shown to be modified by ONOO$^-$ . Peroxynitrite has been shown to cause tyrosine nitration of complex I of the respiratory chain thus effecting mitochondrial injury (36). Increased levels of nitrated proteins have been reported in AD brains as well as cerebrospinal fluid in patients with AD (37). Several proteins present in AD have been shown to be nitrated by peroxynitrite (33). Peroxisome proliferator-activated receptor gamma (PPARγ) expression protects neurons from A*β*- mediated toxicity (38) however its nitration prevents its translocation to the nucleus, thereby preventing mitochondrial biogenesis (39). Protection against peroxynitrite damage *in vivo* is provided by several antioxidants (40) as well as eliminated by many of the anti-oxidant enzymes, peroxiredoxins (41).  The rate of reduction of peroxynitrite by ascorbate (42), glutathione (43) , and uric acid (44) is too slow during the course of disease or increased nitrative stress to prevent damage (45).  Effective antioxidants that can selectively quench ROS/RNS species such as peroxynitrite or superoxide and provide lasting effects are needed. Finding a specific ONOO$^-$ scavenger is of considerable importance.

## Manganese (Mn) Porphryins

Aerobic organisms evolved antioxidant defense systems that deal with ROS produced as a consequence of aerobic respiration (4). Superoxide dismutase (SOD) developed as a defense mechanism against oxidative stress to more rapidly convert $O_2^{\cdot-}$ to $H_2O_2$ (46), even though the spontaneous reaction with protons is nearly as effective as the enzyme catalyzed reaction. $H_2O_2$ is then acted upon by catalase, glutathione peroxidase and/or peroxiredoxins to maintain a healthy level of peroxide in cells and tissues. These endogenous enzymes work in concert to limit ROS, and their synthesis and expression is generally tissue and cell type specific. SOD belongs to a diverse group of enzymes that have metal ions which are usually coordinated by nitrogen, oxygen or sulfur centers, to assist in the process of electron transfers (47) called metalloenzymes. Since its discovery many chemists and biochemists have developed synthetically produced metal based small molecule catalysts to try and mimic the active site of SOD. These so called SOD mimics have been shown to increase the lifespan of nematodes (48) and a number of studies have shown their ability to scavenge $O_2^{\cdot-}$ and/or $H_2O_2$ utilizing various metalloprophyrin motifs (49-51).

## Cerium Oxide Nanoparticles

The use of $CeO_2$ nanoparticles (NP) for potential therapy in cancer, age-related and neurodegenerative diseases represents a novel strategy for a unique technology. Cerium is a rare-earth element belonging to the lanthanide series. In bulk, $CeO_2$ is in the 4+ oxidation state. Cerium is distinctive in that in its oxide nanoparticle form, the cerium atom can exist in either

3+ (fully reduced) or 4+ (fully oxidized) and may interchange between the two states (52). Babu *et al* (53) have synthesized $CeO_2$ NPs that vary in the amount of 3+ and 4+. The oxidation state can be represented by $CeO_{2-x}$. Cerium oxide also contains oxygen vacancies or "defects" in the lattice structure caused by loss of oxygen and/or its electrons (54). $CeO_2$ NPs have similar chemical and physical properties to bulk cerium but due to the increased surface area to volume ratio, along with oxygen vacancies, $CeO_2$ NPs have the potential as a unique catalyst (55) and can act as a free radical scavenger or antioxidant. The valence and defect structure of cerium oxide is therefore dynamic and may change spontaneously or in response to physical or biological parameters (56). Preliminary biocompatibility testing has shown no toxicity or other adverse reactions to $CeO_2$ NPs in the eyes of rats (57). Further work from this group demonstrated $CeO_2$ NPs additionally extend photoreceptor cell lifespan in tubby mice by modulation of apoptosis/survival signaling pathways by slowing the progression of retinal degeneration. The protective effect by $CeO_2$ NPs was demonstrated by decreasing ROS, down-regulating apoptosis signaling pathways and upregulating the expression of neuroprotection-associated genes resulting in slowing of photoreceptor degeneration (58). Treatment with $CeO_2$ NPs reduced total nitrated proteins in transgenic MCP-1 mice using $CeO_2$ NPs in the $Ce^{4+}$ state (59). Continuing work from this lab indicate that $CeO_2$ NPs can inhibit the ROS induced by cigarette smoke extract in cardiomyocytes (60). Interestingly, the $CeO_2$ NPs used in this second study contained an increased concentration of $Ce^{3+}$ on their surface. Elevated ROS from chronic cigarette exposure can result in cardiomyopathy and may also activate nuclear factor-kB (NF-kB), a redox-sensitive transcription factor. $CeO_2$ NPs were able to inhibit this activation. The reactivity of the cerium atoms at the surface of $CeO_2$ NPs is critical to their catalytic properties

and reactivity is reflected in their $Ce^{3+}/Ce^{4+}$ ratio. These studies approach the on-going issue of what happens to the oxidation state of the $CeO_2$ NPs once they are inside cells or animals and suggests that $CeO_2$ NPs may indeed act as regenerating catalytic antioxidants. Exploring the surface properties and catalytic abilities of $CeO_2$ NPs to scavenge free radicals *in vitro* and *in vivo* will aid in the search for future effective therapies for management of diseases where radicals have been proposed to play a role.

Numerous synthetic catalytic scavengers of ROS and RNS have been made and tested in various model systems. Copious metalloporphyrins have been synthesized to have high reactivity with $O_2^{\cdot-}$, $H_2O_2$, $\cdot NO$ and $ONOO^-$ (8, 50, 61, 62). Most studies affirm metalloprophyrins are useful tools for researching and understanding the roles that ROS and RNS may play in diseases, however, their potential toxicity due to metals has often come into question for their use humans. The health effects of $CeO_2$ NPs are not as yet well understood and there are reports which claim that $CeO_2$ NPs are both protective and toxic (63-66). In considering $CeO_2$ NPs as potential therapeutic agents it is important to pay attention to their synthesis method, concentration, and surface chemistry. The preparation/synthesis methods of $CeO_2$ NPs result in particles with a wide variety of surface functionalities and modifications, and these properties will dictate whether a nanoparticle will be protective or deleterious. There are well established synthesis methods in which $CeO_2$ NPs are consistently shown to exhibit SOD mimetic activity (55, 56) , catalase mimetic activity (67) or NO scavenging abilities (68) whereas other synthesis methods result in $CeO_2$ NPs without comparable antioxidant properties (66). Thus these factors as well as concentrations used and cell type studied might account for the seemingly conflicting reports.

## Alzheimer's Disease

Alzheimer's Disease (AD) is among the most common neurodegenerative disorders. AD is a progressive and irreversible disorder of the central nervous system that confers an enormous economic as well as emotional burden on patients, caregivers and society (69). Reactive oxygen species (ROS) and RNS are formed during normal metabolism but an imbalance may result from the increase production of free radicals or from the failure of antioxidants and antioxidant enzymes to adequately scavenge the damaging molecules. This imbalance has been documented to be involved in AD (70).

The mechanism of how $ONOO^-$ promotes neurotoxic effects is still being elucidated but mitochondrial injury seems to be a primary cause (71, 72) due to $ONOO^-$ ability to oxidize or nitrate all biomolecules. Strong evidence suggests that mitochondrial dysfunction is an early event in AD (73). Among the reported changes are altered morphology and ultrastructure of mitochondria, inhibition of respiration and ATP production, and increased ROS production (74). However, what causes the failure in mitochondrial function is unclear.

Widespread $ONOO^-$ mediated damage is seen in brain tissue from AD in the form of increase protein nitration in neurons (75). This increase in nitration, the result of increased nitrosative stress, has been attributed to the aggregation of the Aβ peptide into amyloid plaques, one of the defining morphological features of AD (76). The molecular basis of this increase of Aβ-induced RNS has been shown to be an impaired synaptic transmission, specifically the modulating of NMDA-type glutamate receptors (77). In addition, AD pathology is

also characterized by self-assembly of the tau protein into neurofibrillary tangle (NFT). Tyrosine

nitration of the tau proteins has been demonstrated in many studies (78, 79) further implicating

ONOO$^-$ in AD.

# CHAPTER 2: CERIUM OXIDE NANOPARTICLES Ce$^{3+}$ RATIO DETERMINES REACTIVITY TOWARDS NITRIC OXIDE RADICAL (·NO) AND PEROXYNITRITE (ONOO$^{-}$)

## Introduction

The study of the chemical and biological properties of CeO$_2$ NPs has expanded recently. However, most of the focus has been on the ability of these materials to reduce reactive oxygen (ROS). CeO$_2$ NPs have been shown to protect several cell types and animal models against ROS mediated diseases (80) with little study of their effect on specific reactive nitrogen species (RNS). In these studies, we have obtained evidence that cerium oxide nanoparticles (CeO$_2$ NPs) are able to interact with two very important nitrogen species, nitric oxide radical (·NO) and peroxynitrite (ONOO$^{-}$). For the scavenging of ·NO, this activity is present in CeO$_2$ NPs with a lower level of cerium in the 3+ state (CeO$_2$ NPs with low 3+/4+ ratio (CNP2) and therefore a reduced number of oxygen vacancies), in contrast to the superoxide scavenging properties which are correlated with an increased level of cerium in the 3+ state (CeO$_2$ NPs with high 3+/4+ ratio (CNP1) and therefore an increased number of oxygen vacancies). In the case of peroxynitrite, CNP1 and CNP2 share the catalytic ability of reducing the effect of peroxynitrite, though to different degrees.

## Materials and Methods

*Nanoparticle Synthesis and Characterization*

The cerium oxide nanoparticles were synthesized by wet chemical process as previously described (81). Chemicals for $CeO_2$ nanoparticle synthesis, Ce $(NO_3)_3$, $H_2O_2$, were obtained from Sigma-Aldrich (St. Louis, MO). In brief, to prepare CNP1 with a high ratio of $Ce^{3}+/Ce^{4+}$, Ce $(NO_3)_3 \cdot 6H_2O$ (5 mM) was dissolved in $dH_2O$ and the nitrate precursor was stirred for 15 min then $H_2O_2$ (2% v/v) was rapidly added while stirring at 300 rpm. The solution was continuously stirred for 1 h to obtain a stable dispersion of cerium oxide nanoparticles. Samples were stored at room temperature. All preparations were sonicated to ensure single nanoparticles (Branson, Danbury, CT) for 45-60 min prior use. CNP2 was synthesized using ammonium hydroxide $NH_4OH$ precipitation method. Briefly, cerium nitrate hexahydrate was dissolved in deionized sterile water and stoichiometric amount of $NH_4OH$ was added and stirred for 4 h at room temperature. Cerium oxide nanoparticles were separated by centrifugation at 8000 g for 10 min. $SiO_2$ nanoparticles were purchased from Corpuscular Inc. (Cold Spring, NY). The surface chemistry of the cerium oxide nanoparticles was studied using a Physical Electronics (5400 PHI ESCA) spectrometer with a monochromatic Al Kα X-ray source operated at 300 W and base pressure of $1 \times 10^{-9}$ Torr. The binding energy of the Au (4f7/2) at 84.0±0.1 eV was used to calibrate the binding energy scale of the spectrometer.

*Assay for Nitric Oxide*

A ferrous hemoglobin assay was adapted from Murphy & Noack (82) in which ferrous hemoglobin (Hb) (Sigma-Aldrich) and ·NO react to form oxidized ferric hemoglobin. S-nitroso-*N*-acetylpenicillamine (SNAP) (Molecular Probes), was used to generate ·NO. Briefly, 200 µM of SNAP was added to 25 mg/mL ferrous Hb in the presence or absence of nanoparticles or the spin-trap DEPMPO (Enzo Life Sciences) in 100 mM phosphate buffer (pH 7.0). The oxidation of Hb was monitored using a Hewlett-Packard 8453 diode array spectrophotometer. We followed changes to spectra at wavelengths of 411 nm (isosbestic point) and 421 nm. The change in absorbance per unit time was measured for 10 min at 30 s intervals. The concentration of ·NO reacting with Hb was obtained by the difference in absorbance between 401-421 nm using an extinction coefficient of 77 mM$^{-1}$cm$^{-1}$ (82).

*Surface Chemistry Alteration by Phosphate Ions*

Phosphate buffer was prepared by dissolving monosodium phosphate (13.8 g/L) and its conjugate base, disodium phosphate (14.1 g/L), in 1 L of water to give a 0.1 M solution, and the pH was adjusted by titration with 1 M HCl to reach a pH value of 7.4. Water dispersed $CeO_2$ NPs with higher levels of oxygen vacancies at their surface (200 µM) were suspended in equimolar phosphate buffer (pH 7.4) for 24 h at room temperature. The UV-visible spectra were recorded to determine surface chemistry of cerium using a UV-viable Hewlett-Packard 8453 diode array spectrophotometer in a 1.0 cm path length quartz cuvette.

*·NO Detection Using Copper-fluorescein Method*

To measure ·NO by an alternate method we followed ·NO levels using a copper-fluorescein (Cu-FL) probe as previously described (83). In these experiments, 100 µM of the ·NO generator, diethylamine NONOate diethylammonium salt (DEA/NO) (Sigma) was added to CuFL probe (1 µM) (Strum Chemicals, Newburyport, MA). Fluorescence was followed at an emission wavelength of 530 nm using an excitation wavelength of 503 nm in 50 mM sodium phosphate buffer, pH 7.0, containing 20 µM DPTA using a Varian Cary Eclipse fluorescence spectrophotometer (Palo Alto, CA) for 20 min at room temperature. Assays were carried out in the presence or absence of $CeO_2$ NP, $SiO_2$ NPs or glutathione (Fisher Scientific, Pittsburg, PA).

*Zeta Potential (ZP) and Particle Size Measurement*

Water dispersed $CeO_2$ NPs with different 3+/4+ ratios were suspended in buffers according to the various conditions used in these studies and ZP and particle size measured. For surface chemistry alteration experiments, NPs were incubated for 24 h followed by ZP and particle size measurements using Zeta sizer (Nano-ZS) from Malvern Instruments.

*Peroxynitrite Decay Using Spectroscopy*

Peroxynitrite (20 µM) was added under stirring into a 1 ml quartz cuvette with a 1 cm path length. Each sample was analyzed for a total of 600 seconds with a cycle time of 0.5 seconds at a wavelength of 302 nm in 100 mM sodium or potassium phosphate buffers, pH 8.0, and 100 µM diethylenetriaminepentaacetic acid (DPTA) to minimize any potential interference by adventitious metal ions using a Hewlett-Packard diode array UV-visible 8453

spectrophotometer. Absorbance was normalized by subtracting the final absorbance from initial absorbance and dividing by the amplitude.

*Peroxynitrite Decay Using APF* in *vitro*

To measure the effects of nanoceria (100 µM), Glutathione (0.5 mM) or uric acid (1 mM) on the decay of peroxynitrite (20 µM), APF (10 µM) fluorescence was measured at excitation/emission wavelengths of 490 nm/515 nm in 0.1 mM sodium phosphate buffer, pH 7.4, containing 100 µM DPTA using a Varian Cary Eclipse fluorescence spectrophotometer (Palo Alto, CA). We followed fluorescence for 1 min at room temperature using a quartz fluorometer cell (Starna Cells, Inc. Atascadero, CA). Peroxynitrite was added last due to the short-half of peroxynitrite at pH 7.4. End-point assays fluorescence was read after 10 min incubation using same buffer conditions as kinetic studies. As stock solutions of ONOO$^-$ contain 0.3 M NaOH, control incubations were performed with equivalent amounts of NaOH.

*Dot Blot Assay*

500 ng BSA treated with 10 µM peroxynitrite (ONOO$^-$)(Cayman Chemicals)   in the absence and presence of 500 nM  NPs, 100 µM NPs or 1 mM GSH @ RT for 20 min . Nitrocellulose (Hybond ECL, GE Healthcare) was equilibrated using  1X TBS and placed in Hydri-Dot manifold (BRL). Reactions were pipetted in to the membrane and allowed to incubate for 20 min. After 3 washes, membrane was blocked in 5% milk, 1X TBS+0.1% Tween. Blot was probed with antibody specific for 3-nitro-tyrosine modification (Sigma #N0409) followed by

HRP-conjugated secondary (ECL). For detection, West Dura substrate (Thermo Scientific) was used as per protocol.

## Results

Reactive oxygen species (ROS) and reactive nitrogen species (RNS) are normal byproducts of oxidative metabolism in mammals. If unchecked, they can cause damage to proteins, DNA, and lipids contributing to diseases ranging from atherosclerosis and aging to neurodegenerative disorders such as Parkinson's and Alzheimer's disease. Nitric oxide radical ($\cdot$NO) is a gaseous free radical which exhibits multifaceted biological effects, both beneficial and damaging. Nitric oxide functions as an important messenger molecule, as an essential neurotransmitter, (84) and regulator of cardiovascular physiology (85). $\cdot$NO is not particularly toxic *in vivo*, however, recent evidence indicates the cytotoxicity attributed to $\cdot$NO is due to formation of the potent oxidant peroxynitrite ($ONOO^-$), formed by the diffusion limited interaction of superoxide ($O_2\cdot^-$) with $\cdot$NO (86). While neither $\cdot$NO nor $O_2\cdot^-$ are strong oxidants, $ONOO^-$ is highly reactive and can oxidize DNA, proteins and lipids(34).

Cerium oxide ($CeO_2$) is a rare earth metal oxide catalyst known for its ability to remove carbon monoxide (CO), hydrocarbons and nitric oxide species ($NO_x$) from exhaust gas (87) and is widely used as a catalyst in industrial applications because of its potent redox-active properties(88). The adsorption and reaction of $\cdot$NO on $CeO_2$ has been shown to be influenced by the valence state of the surface cerium (89). and bulk $CeO_2$ has been shown to adsorb $\cdot$NO only on reduced or partially reduced sites (90). Weakly absorbed $\cdot$NO on pure $CeO_2$ at room temperature has been reported (91) as well as evidence for the transfer of the unpaired

16

electron from ·NO to Ce in the 4+ state (92). These catalytic studies have been performed in the absence of water and under non-biological conditions. Whether $CeO_2$ NPs react with ·NO under physiologically relevant conditions has yet to be determined. Other redox active catalysts, especially manganese porphyrins, have been shown to interact with ·NO (8). In this first study we determined the reactivity of $CeO_2$ NPs with ·NO under biologically relevant conditions.

To study $CeO_2$ NPs ability to react with ·NO, water-based $CeO_2$ NPs with different 3+/4+ ratios were synthesized and characterized. High resolution transmission electron microscopy (HR-TEM) as well UV-visible spectroscopy confirmed that the CNP1 and CNP2 used in ·NO studies were indicative of HR-TEM images and absorbance's of $CeO_2$ NPs as previously reported (68). The ratios of $Ce^{3+}/Ce^{4+}$ were determined by XPS and sizes ranged 3-8 nm (determined by TEM) for CNP1 and CNP2 (68).

*CNP2 Scavenge ·NO*

The reaction between ·NO and the oxygenated, ferrous form of Hb can be used as a sensitive means to measure dissolved ·NO. We used S-nitroso-*N*-acetylpenicillamine (SNAP) to generate ·NO and we followed the conversion of the ferrous form of Hb to the ferric form of Hb by ·NO (82). Addition of CNP1 with high 3+/4+ ratio (75% 3+) had no effect on ·NO's ability to oxidize Hb suggesting no interaction with these NPs (Figure 1A). However, the addition of CNP2 with low 3+/4+ ratio (20% 3+) inhibited the ability of ·NO to oxidize Hb in a dose dependent manner (Figure 1B). This pattern was similar to that observed with the known ·NO scavenger DEPMPO (Figure 1C). This result suggests that CNP2 prevent ·NO from oxidizing Hb.

17

To elucidate the scavenging efficiency of CeO$_2$ NPs, we additionally determined the amount of

dissolved ·NO in the presence and absence of CeO$_2$ NPs or DEPMPO translating the data

obtained from Hb assay experiments. The concentration of ·NO was obtained by difference in

absorbance 401-421 nm using an extinction coefficient of 77 mM$^{-1}$cm$^{-1}$ (82)(Figure 2A-C). We

observed concentration-dependent decreases in ·NO in the presence of varying levels of

Ce$^{3+}$/Ce$^{4+}$ ratio and were able to calculate the rates of radical formation in the presence or

absence of the catalyst (Table 1).


*Scavenging of ·NO by CNP2 Confirmed Using Alternate Detection Method*

In order to corroborate the data obtained from the Hb assay, we used an alternate

detection method to determine CeO$_2$ NPs ability to react with ·NO. A derivatized copper-

fluorescein conjugate (Cu-FL) has been shown to be a specific detector of ·NO production (93)

though not as sensitive as Hb assay. We followed fluorescence emission at 530 nm upon

addition of 100 µM of the NONOate DEA/NO, another ·NO donor, in the presence and absence

of CeO$_2$ NPs. The addition of CNP1 had no effect on the ability of dissolved ·NO to oxidize the

Cu-FL probe (Figure 3A). When CNP2 were included, we observed that the NPs prevented the

oxidation of the Cu-FL probe and the fluorescent signal was decreased in a dose dependent

manner (Figure 3B). This reduction in fluorescent signal by CNP2 is similar in efficacy as

glutathione, a known ·NO scavenger (Figure 3C). By contrast, silicon oxide (SiO$_2$) control NPs of

similar size, were unable to prevent the ·NO-mediated Cu-FL oxidation (Figure 3D) suggesting

that the changes in dissolved ·NO are specific to CNP2. Collectively, these data elucidate a

previously unidentified catalytic property for CeO$_2$.

*CNP1 Can Convert to ·NO Scavenging Catalyst Upon Incubation with Phosphate.*

Recently, we have shown that incubation of $CeO_2$ NPs with phosphate ions can interconvert these particles between the two catalyst (SOD or catalase mimetic) states (94). To determine whether this property also applies to ·NO scavenging, we incubated CNP1 with phosphate and followed the presence of cerium atoms in the 3+ state (Figure 4). The absorbance peak between 230-260 nm (consistent with $CeO_2$ NPs with higher levels of oxygen vacancies) disappears after addition of phosphate (Figure 4A) as previously described (94). After this conversion, $CeO_2$ NPs are now able to effectively scavenge ·NO (Figures 4B & C) indicating this surface chemistry 'switch' also correlates with ·NO scavenging.

Discussion

In summary, this study establishes the ·NO scavenging capability of CNP2 - $CeO_2$ NPs with low 3+/4+ ratio. ·NO can be both electrophilic or nucleophilic in nature (95). The nature of this heterogeneous catalysis is not yet fully understood. Yet one could envision a mechanism by which $CeO_2$ NPs scavenge ·NO through formation of an electropositive nitrosyl ligand due to internal electron transfer from ·NO to a $Ce^{4+}$ site:

$$Ce^{4+} + ·NO \rightarrow [Ce^{4+} - NO \leftrightarrow Ce^{3+} - NO^+] \tag{1}$$

This mechanism has been found in various synthetic ferric porphyrin species (96) and manganese complexes (97). *In vivo* ·NO reacts with $O_2^{·-}$ to form $ONOO^-$, a potent oxidant that can lead to 3-nitrotyrosine (3-NT) modification of tyrosine residues in proteins(34). 3-NT is frequently used as a biomarker for nitrosative stress. Recently, a reduction in 3-nitrotyrosine

levels in a neural brain slice model was observed after treatment with $CeO_2$ NPs(98) and in a cardiovascular disease model(99). It is likely that the observed scavenging of $\cdot NO$ in this study contributed to the protective effects seen in these studies. $CeO_2$ NPs surface chemistry is just now starting to be described and understood in respect to their ability to ameliorate cellular damage caused by both oxidative (superoxide, hydrogen peroxide) and nitrosative ($\cdot NO$ and thus $ONOO^-$) stress.  For $CeO_2$ NPs to become a viable therapeutic, their material properties must be optimized and thoroughly understood.

Cerium Oxide Nanoparticles and Their Reactivity with $ONOO^-$

Peroxynitrite is formed from the reaction of nitric oxide radical ($\cdot NO$) with superoxide ($O_2^{\bullet -}$). The biochemistry of $ONOO^-$ is vastly complicated due to the multiple reactions possible in the presence and absence of $CO_2$, $H^+$ and metals during its decomposition (34, 100). Determining $CeO_2$ NP ability to scavenge $ONOO^-$ *in vitro* is imperative to begin to understanding it's biological capabilities. We have begun to discern the reactivity of CNP1 and CNP2 with peroxynitrite using three different assays.

Dependent on their 3+ or 4+ oxidation states, nanoceria exhibit either SOD or catalase activity (55, 56, 67). Recent reports suggested that nanoceria are able to reduce nitrosative stress in various cell types (98, 99, 101). However, the underlying mechanism of their nitrosative stress reducing activity remains unknown. Given their redox cycling properties, it is conceivable that nanoceria might scavenge peroxynitrite. To test this idea we employed a cell-free system *in vitro*. Physical and chemical analysis of the nanoceria preparations used were

confirmed and the CNP1 3+ oxidation state, CNP2 4+ oxidation state as well as fluorite structure

and cerium spectrum  were previously reported (CD&D under review,(67)).

*CNP1 Accelerates Decay of Peroxynitrite in a Cell-free System in vitro*

Peroxynitrite exhibits a strong absorbance at 302 nm, hence its rapid decay can be

measured within seconds using spectroscopy (102) Exploiting these properties, we observed

that nanoceria dramatically accelerated the normal decay rate of peroxynitrite and with similar

efficacy as uric acid or glutathione, two well established  peroxynitrite scavengers (Figure 5A)

(103). By contrast, silicon oxide ($SiO_2$) nanoparticles of similar size had no effect on the half-life

of peroxynitrite.. A second addition of  peroxynitrite after complete decay resulted in renewed

nanoceria-mediated peroxynitrite decomposition (data not shown), indicating that nanoceria is

acting as a catalyst in the reaction with peroxynitrite.

*Accelerated Decay of ONOO⁻ by CNP1 Confirmed Using APF Dye*

To confirm the novel peroxynitrite-lowering properties of CNP1, we followed the

oxidation of 3'-(*p*-aminophenyl) fluorescein (APF) by fluorescence spectrometry *in vitro* (Figure

5B). APF has no fluorescence at baseline, but when oxidized by peroxynitrite it exhibits

fluorescence (104). Using this probe, we observed that CNP1 prevented the oxidation of APF *in*

*vitro*, similar to glutathione and uric acid (Figure 1B) (105). Again, silicon oxide nanoparticles

were unable to prevent the peroxynitrite-mediated APF oxidation.  Collectively, these data

illustrate a previously unknown catalytic property of $CeO_2$ NPs, namely their ability to reduce

peroxynitrite *in vitro*.

*3-Nitrotyrosine Protein Modification Diminished in the Presence of CNP1 or CNP2*

3-Nitrotyrosine (3-NT), a specific marker of protein nitration by ONOO⁻, is an established

marker for RNS damage  (106). CeO$_2$ NPs can be synthesized with high or low ratios of

Ce$^{3+}$/Ce$^{4+}$. Reduction of Ce$^{4+}$ to Ce$^{3+}$ causes oxygen vacancies or defects on the surface of the

lattice structure, hence provides a platform for redox cycles to occur. Though the nanoparticles

have measurable starting ratios, it is conceivable that due to redox interactions, the ratios

would change *in vivo*. To compare how CNP1 and CNP2 may act in the presence of cellular

components, we tested whether CNP1 and CNP2 would be able to reduce peroxynitrite-

induced protein tyrosine nitration using bovine serum albumin (BSA) as an in vitro model. When

BSA was pre-incubated with CNP1 or CNP2 alongside peroxynitrite, they prevented the 3-NT

modification by peroxynitrite in a dose dependent manner (Figures 6A and B).  These findings

suggest that CNP1 and CNP2 are accelerating the decay of peroxynitrite in a manner that can

prevent the modification of tyrosine residues.


<u>Discussion – Accelerated Decay of Peroxynitrite</u>

Using cell-free assays we provide evidence for the ability of CeO$_2$ NPs to accelerate the

decay of peroxynitrite. The changes observed in the presence of cerium oxide nanoparticles

represents compelling yet preliminary evidence that these nanomaterials readily react with

peroxynitrite, or one or more of its breakdown products.  The mechanism by which these

materials can alter the catalytic decomposition of peroxynitrite has yet to be elucidated. Others

have shown that thiols, metals and carbon dioxide are the most likely targets of peroxynitrite *in*

*vivo* (34). Assuming cerium oxide reacts directly with peroxynitrite (and not decay products such as carbonate radical), a putative scheme of one electron oxidation and reduction reactions is shown that could explain the acceleration of peroxynitrite decay (Equation 2).

$$O2^{\cdot-} + {}^{\cdot}NO \leftrightarrow ONOO^- + H^+ \rightarrow [{}^{\cdot}OH + {}^{\cdot}NO_2]\ ^{(34)} \quad\quad (2)$$

$$Ce^{3+} + {}^{\cdot}NO_2 \rightarrow Ce^{4+} + NO_2^- \quad\quad (3)$$

$$Ce^{3+} + {}^{\cdot}OH \rightarrow Ce^{4+} + OH^- \quad\quad (4)$$

$$Ce^{3+} + O2^{\cdot-} \rightarrow Ce^{4+} + O_2^{2-} \qu\quad (5)$$

$$2Ce^{4+} + O_2^{2-} \rightarrow O_2 + 2Ce^{3+} \quad\quad (6)$$
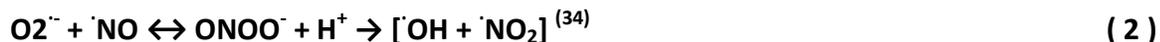
The proton-dependent decay of peroxynitrite results in production of nitrogen dioxide (Equation 3) radical and hydroxyl radical (Equation 4). Each of these potent radicals, which are one-electron oxidants, could react with cerium oxide nanoparticles at the particle surface (in an oxygen vacancy) to oxidize $Ce^{3+}$ to $Ce^{4+}$ (Equations 5 and 6) with the concomitant release of hydroxyl ion or nitrite. In our UV-visible measurements an absorption peak near that of nitrite (229 nm) was observed that paralleled the decrease in peroxynitrite levels (data not shown). Superoxide, derived from the back reaction of peroxynitrite to nitric oxide and superoxide could also serve as an oxidant with the products reducing cerium in the oxygen vacancy both *in vitro* and *in vivo*, especially given the location of the particles in the vicinity of the mitochondria. Although quite speculative, this putative pathway is a starting point for studies to determine the intermediates and rate constants for the reaction of cerium oxide nanoparticles with peroxynitrite and/or its decay products.
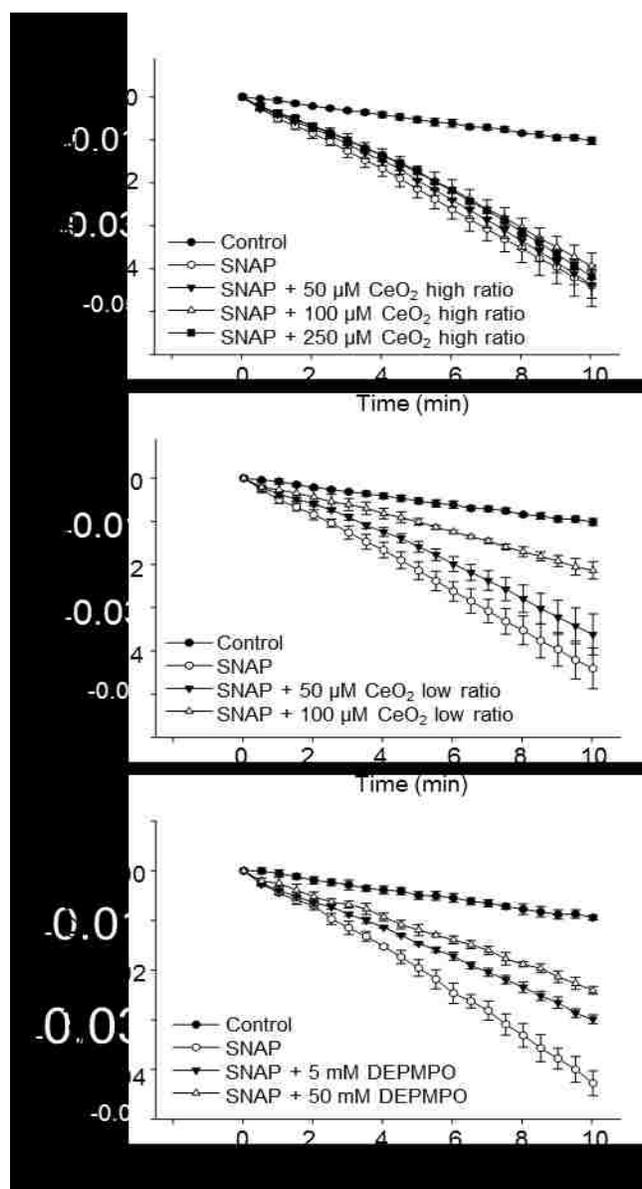
**Figure 1: CNP2 - CeO$_2$ NPs with low 3+/4+ ratio scavenge ·NO.**

Represented in all graphs: closed circles = 25 mg/mL Hb alone; open circles = 25 mg/mL Hb + 200 µM SNAP. A) CNP1- CeO$_2$ NPs with high 3+/4+ ratio. B) CNP2- CeO$_2$ NPs with low 3+/4+ ratio. C) DEPMPO addition. CeO$_2$ NPs or DEPMPO were added at the concentrations indicated. Graph is representative of 3 or more experiments.
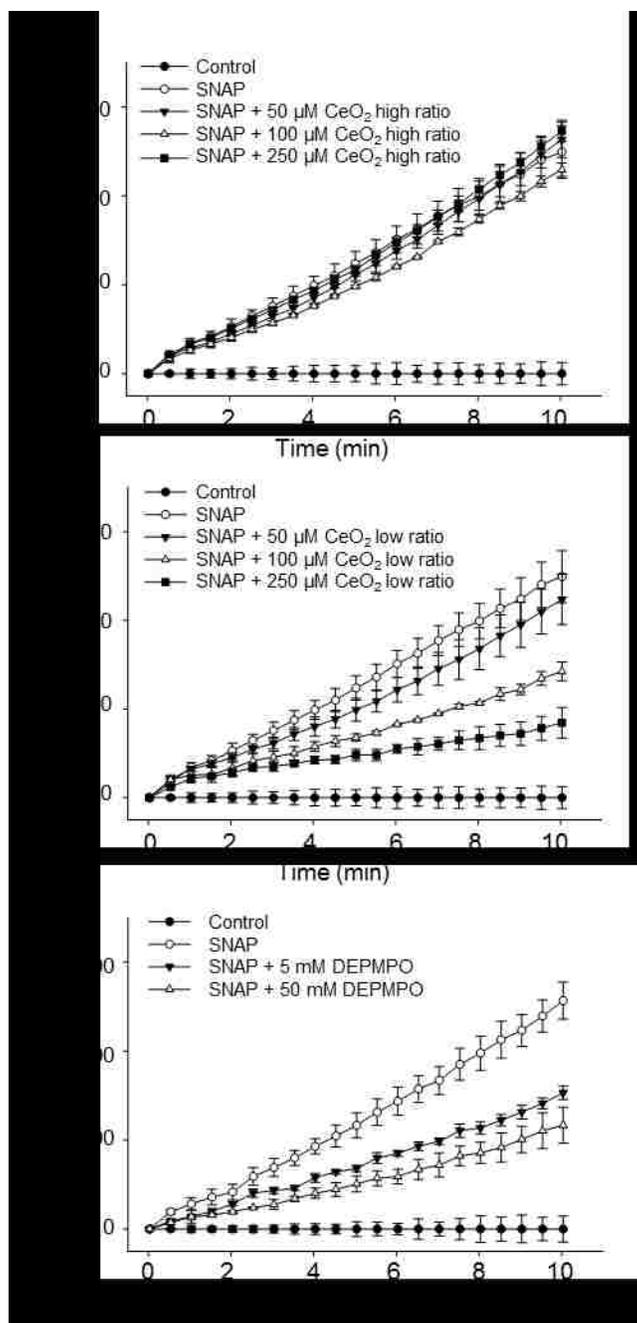
**Figure 2: Effective scavenging of ·NO by CeO$_2$ NPs lacking surface oxygen vacancies.**

The concentration of ·NO in the presence or absence of CeO$_2$ NPs was quantified using the extinction coefficient for reaction with ferrous Hb (82). Data are derived from experimental data shown in Figure1. Represented in all graphs: closed circles = 25 mg/mL Hb alone; open circles = 25 mg/mL Hb + 200 µM SNAP. A) CNP1- CeO$_2$ NPs with higher levels of oxygen vacancies at their surface. B) CNP2- CeO$_2$ NPs with reduced levels of oxygen vacancies. C) DEPMPO addition. CeO$_2$ NPs or DEPMPO were added at the concentrations indicated. Graph is representative of 3 or more experiments.

**Table 1: Changes in ·NO levels in the presence of CeO$_2$ nanoparticles**

| Reaction conditions | NP conc. (µM) | NO production rate[a] (pmol min$^{-1}$ +/- SD |
|---|---|---|
| SNAP (200 µM) control | 0 | 51.6 ± 4.4 |
| SNAP + CNP2 | 50 | 42.1 ± 5.7 |
| | 100 | 25.8 ± 2.9 |
| | 250 | 14.3 ± 3.3 |
| SNAP + CNP1 | 250 | 52.5 ± 2.9 |
| SNAP + CNP1 + PO$_4$ | 200 | 39.7 ± 5.9 |

[a]Rates are pmol min$^{-1}$ and were calculated by determining the rate of change in absorbance per unit time, based on the molar extinction coefficient of conversion of HbO$_2$ to metHb in the presence of ·NO (401 nm-421 nm) ($\Delta\epsilon$ = 77 mM$^{-1}$cm$^{-1}$). SD = standard deviation
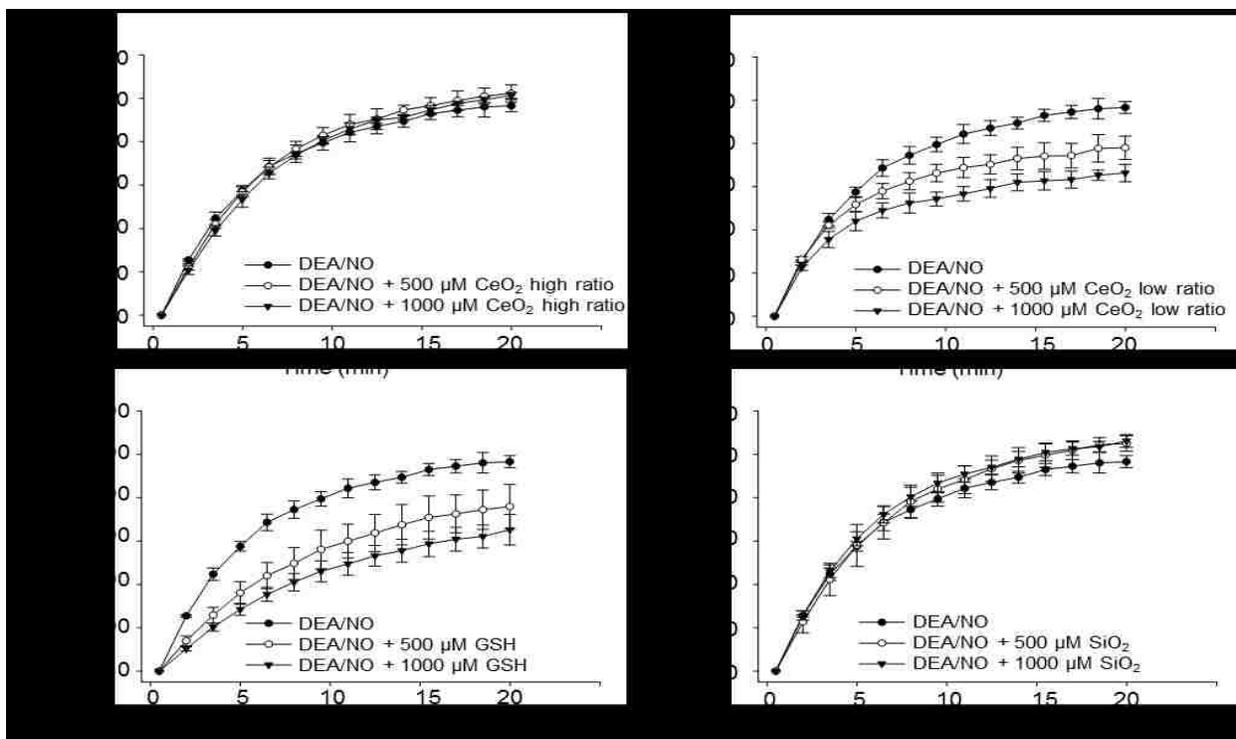
**Figure 3: Scavenging of ·NO by CeO$_2$ NPs confirmed using alternate detection method.**

Fluorescence emission was monitored at 530 nm upon excitation at 503 nm. Represented in all graphs; closed circles = 100 μM DEA/NO. A) CNP1 - CeO$_2$ NPs with high 3+/4+ ratio. B) CNP2 - CeO$_2$ NPs with low 3+/4+ ratio. C) GSH addition. D) SiO$_2$ NPs addition. CeO$_2$ NPs, GSH or SiO$_2$ NPs were added at concentrations indicated. Graph is representative of 3 or more experiments.
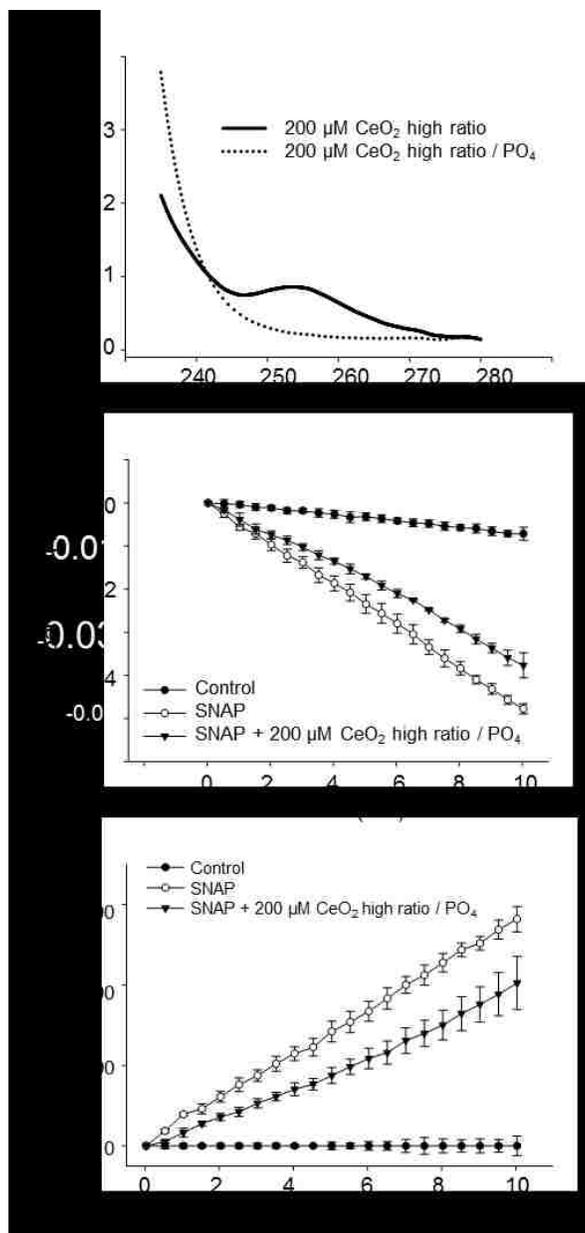
**Figure 4: CNP1 - CeO₂ NPs with high level of surface oxygen vacancies can convert to ·NO scavenging catalyst upon incubation with phosphate.**

A) CNP1 were incubated in 200 μM sodium phosphate buffer at RT for 24h. Solid line represents CNP1 - CeO₂ NPs with higher levels of oxygen vacancies at their surface and dotted line represents sample incubated in phosphate. B) ·NO scavenging by CeO₂ NPs after incubation in phosphate. C) Effective scavenging of ·NO by CNP1 after incubation in phosphate. Closed circles = 25 mg/mL Hb alone; open circles = 25 mg/mL Hb + 200 μM SNAP; closed triangles = 25 mg/mL Hb + 200 μM SNAP + 200 μM CNP1 - CeO₂ high Ce³⁺/PO₄. Graph is representative of 3 or more experiments.

28
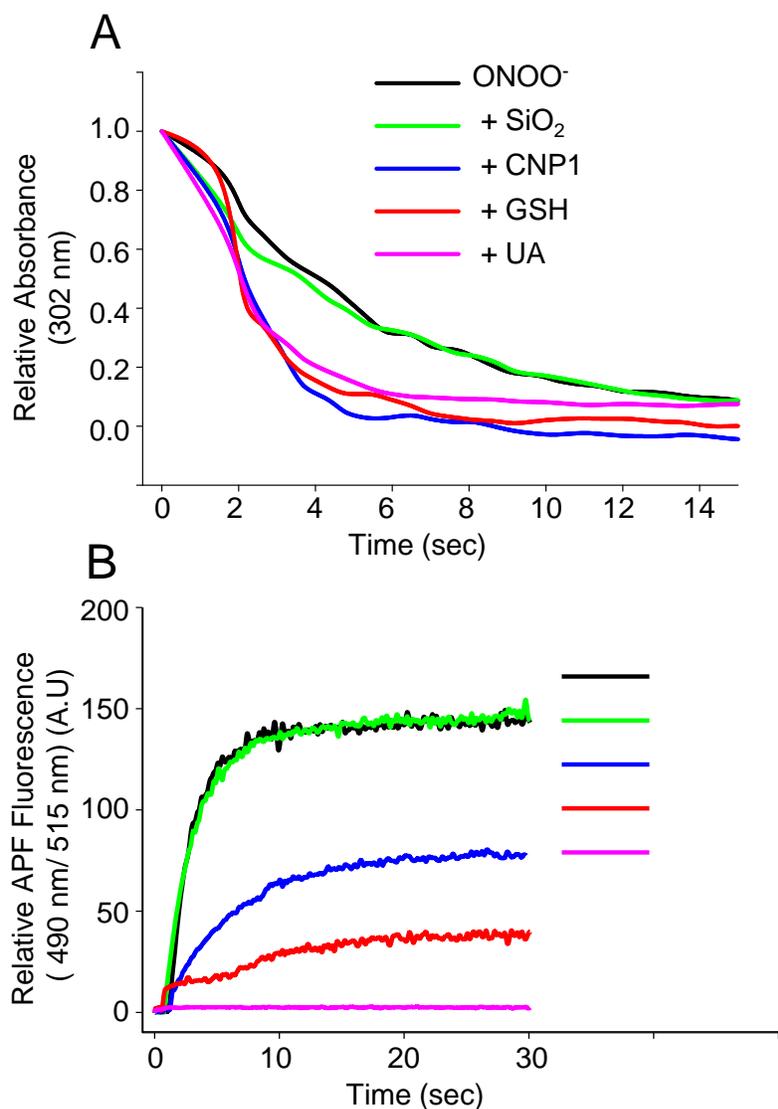
**Figure 5: CNP1 scavenge peroxynitrite *in vitro*.**

(A) Relative absorbance of peroxynitrite (25 µM) at 320 nm over time (seconds) either in the absence or presence of CeO$_2$ nanoparticles (100 µM), SiO$_2$ nanoparticles (100 µM), uric acid (UA) (1mM), or glutathione (GSH) (0.5 mM) using spectrometry. (B) Relative APF (10 µM) fluorescence at 490 nm excitation and 515 nm emission wavelength of either peroxynitrite (20 µm) alone, or in combination with CeO$_2$ nanoparticles (100 µM), SiO$_2$ nanoparticles (100 µM), uric acid (1mM), or glutathione (0.5 mM) measured over a time period of 14 seconds. Data are representative of three or more experiments.
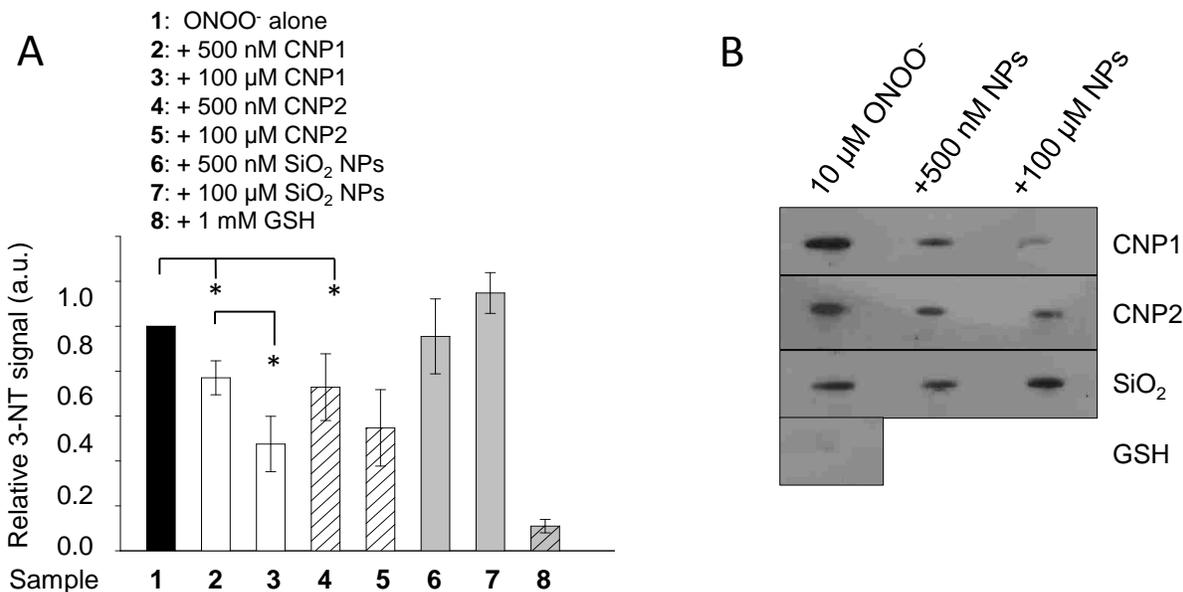
**Figure 6: 3-nitrotyrosine protein modification diminished by CeO$_2$ NPs.**

A) Graphical representation of BSA western blots protected from nitration with dose dependent addition of CeO$_2$ NPs. B) Representative blots. All lanes contain 500 ng BSA treated with 10 µM peroxynitrite (ONOO$^-$) in the absence and presence of 500 nM NPs, 100 µM NPs or 1 mM GSH. Blots were probed with anti-3-nitrotyrosine antibody. Individual experiments were normalized to their individual BSA/ONOO$^-$ treated lane. Data are representative of three or more independent experiments. $p \leq 0.001$. Statistics: Student's $t$ test.

# CHAPTER 3: CERIUM OXIDE NANOPARTICLES DELAY Aβ-INDUCED MITOCHONDRIAL FRAGMENTATION AND NEURONAL CELL DEATH

## Introduction

Nitric oxide ($\cdot$NO) is an important neurotransmitter and neuromodulator normally required for learning and memory (84, 107). $\cdot$NO is generated by nitric oxide synthases (NOSs), a group of enzymes that produce $\cdot$NO from L-arginine in mammals. In addition to its role in normal physiology, $\cdot$NO is implicated in pathophysiology. When overproduced, $\cdot$NO combines with superoxide anions ($O_2^{\cdot-}$), byproducts of oxidative phosphorylation in mitochondria, to form peroxynitrite anions ($ONOO^-$) which are highly reactive as well as neurotoxic and can oxidize DNA, proteins, lipids. The accumulation of reactive oxygen species (ROS) and nitrogen species (RNS), also known as oxidative or nitrosative stress respectively, is a common feature of many diseases including Alzheimer's disease (AD) (84, 107). Excessive nitrosative stress in the nervous system can originate from glial cell activation and release of inflammatory cytokines. Alternatively, nitrosative stress can be caused by excessive accumulation of excitatory amino acids such as glutamate and $N$-methyl-D-aspartate (NMDA), which results in overstimulation of synaptic NMDA-type glutamate receptors, increased cytoplasmic $Ca^{2+}$, neuronal NOS activation, and subsequent overproduction of $\cdot$NO/$ONOO^-$.

Excessive nitrosative stress causes neuronal damage and cell death by impinging on several cellular pathways. RNS can react with the cysteine or tyrosine residues of protein targets, altering their structure and/or function (84, 107). These protein modifications of S-nitrosylation or nitration play a role in protein aggregation, a central hallmark of

neurodegenerative disorders. In AD nitrosative stress contributes to insoluble protein deposits of A$\beta$ and phosphorylated tau protein (84). Furthermore, nitrosative stress can activate signaling pathways and kinases, including Jun amino terminal kinase (JNK) and p38 mitogen-activated protein kinase (MAPK) (108-110). Moreover, nitrosative stress can induce mitochondrial fragmentation, resulting in mitochondrial dysfunction (111).

Mitochondria are a source of free radicals. Disrupted energy metabolism from A$\beta$ resulting in inhibition of mitochondrial oxidative phosphorylation and respiration is implicated in AD. Normally an accumulation of ROS such as superoxide and $H_2O_2$ are neutralized by the enzymes superoxide dismutase 1 and 2 (SOD1, SOD2) and catalase. Peroxynitrite can inhibit complex I and IV of the mitochondrial respiratory chain, culminating in bioenergetic failure and a vicious cycle of ROS production (112, 113). When ROS detoxifying mechanisms fail or become overwhelmed, the event causes irreversible damage to biomolecules and can result in functional decline, characteristic of aging and age-related disorders (114).

Neurons depend on mitochondrial energy production to fuel processes including synaptic transmission, ion pump and channel activity, and axonal and dendritic transport (111). Strong evidence suggests that mitochondrial dysfunction is an early event in AD (73). Among the reported changes are altered morphology and ultrastructure of mitochondria, inhibition of respiration and ATP production, and increased ROS production (74). However, what causes the failure in mitochondrial function is unclear. We recently postulated that the defects in mitochondrial function are caused by an imbalance in mitochondrial fission and fusion (71, 84, 107, 111). Notably, peroxynitrite, generated by exogenous ·NO donors or neurotoxic insults like

NMDA or A$\beta$ induces mitochondrial fragmentation caused by activation of fission and/or inhibition of counterbalancing fusion (71, 75).

To maintain their energy producing function, mitochondria must frequently divide and fuse. Evidence suggests that an imbalance in mitochondrial division and fusion plays a causal role in AD (115). Mitochondrial division and fusion is regulated by large GTPases of the dynamin family. Dynamin-related protein 1 (DRP1) is required for mitochondrial division. Inhibition of mitochondrial division by expression of the GTPase defective DRP1[K38A] mutant provides protection against excessive ·NO, NMDA, or A$\beta$ (71). The exact mechanism that accounts for the ·NO-induced mitochondrial fragmentation remains unclear. A recent report suggested that S-nitrosylation of DRP1 at cysteine 644 increases DRP1 activity and is the cause for the peroxynitrite-induced mitochondrial fragmentation in AD (107, 116). However, the work remains controversial, suggesting alternative pathways might be implicated (107, 117). Nitrosative stress causes rapid DRP1 Serine 616 (S616) phosphorylation, which promotes its translocation to mitochondria and organelle division (117, 118). In mitotic cells DRP1 S616 phosphorylation is mediated by Cdk1/cyclinB1 and synchronizes mitochondrial division with cell division (119, 120). Interestingly, p-DRP1 S616 levels are markedly increased in brains of individuals with AD, suggesting that this event might contribute to the change in mitochondrial morphology and energy metabolism in AD (117, 119). The kinase responsible for DRP1 S616 hyperphosphorylation in AD is unknown, but Cdk5/p25 is a potential candidate kinase mediating this process (75, 121). Notably, aberrant Cdk5/p25 signaling causes tau hyperphosphorylation in postmitotic neurons and is implicated in A$\beta$-mediated neurodegeneration (119, 122-124).

While it is clear that nitrosative stress is at the heart of AD and other common age-related disorders, effective antioxidants that can selectively quench ROS/RNS species such as superoxide, $H_2O_2$, ·NO and/or peroxynitrite and provide lasting effects are missing. Cerium (Ce) is a rare earth element and its oxide nanoparticle form uniquely exists in both 3+ and 4+ oxidation states. Reduction of $Ce^{4+}$ to $Ce^{3+}$ causes oxygen vacancies or defects on the surface of the crystalline lattice structure of the particles, generating a cage for redox reactions to occur (125). Accordingly, nanoceria mimic the catalytic activities of the antioxidant enzymes SOD (55, 126) and catalase (67) as well as scavenge dissolved ·NO (127). The specificity of the catalytic activities depends upon the ratio of $Ce^{3+}/Ce^{4+}$ (94, 127). Given these unique antioxidant properties, we hypothesized that nanoceria, specifically CNP1 with increased ratio of Ce3+/Ce4+, detoxify ROS/RNS and protect against A$\beta$-induced DRP1 S616 hyperphosphorylation, mitochondrial fragmentation and neuronal cell death.

## Materials and Methods

### *Reagents*

EBSS (Earle's Balanced Salt Solution), Hanks buffer, Glutamax, B-27® supplement, LipoFectamine2000®, and penicillin-streptomycin were purchased from Invitrogen (Carlsbad, CA). Neurobasal medium and Dulbecco's Modified Eagle's Medium (DMEM) were purchased from Hyclone (Logan, UT). Poly-L-lysine, Hepes, glutamine, formaldehyde, *N*-acetyl-*L*-cysteine (NAC), anti-3-nitrotyrosine, *N*-methyl-D-aspartate (NMDA), Ponceau S reagent, Durcupan ACM, 3-nitropropionic acid (3-NP), Aβ peptides and chemicals for cerium oxide nanoparticle synthesis

were obtained from Sigma-Aldrich (St. Louis, MO). Hoechst 33342, pluronic acid, 3'-(*p*-aminophenyl) fluorescein (APF) (for cell culture) were purchased from Molecular Probes (Eugene, OR). PVDF membrane was purchased from Bio-Rad Laboratories (Hercules, CA). The DsRed2-Mito vector was obtained from Clontech (Mountain View, CA). Vector Shield was purchased from Vector Laboratories, Inc., (Burlingame, CA). T-Per protein extraction reagent was purchased from Pierce Biotechnology, Inc., (Rockford, IL). Peroxynitrite and 2-[6-(4-aminophenoxy)-3-oxo-3H-xanthen-9-yl]-benzoic acid (APF) (for *in vitro* experiments) were purchased from Cayman Chemicals (Ann Arbor, MI). All reagents for transmission electron microscopy (TEM) were purchased from Ted Pella (Redding, CA). $SiO_2$ nanoparticles were purchased from Corpuscular Inc. (Cold Spring, NY). In addition the following antibodies were used: monoclonal mouse-anti-DRP1 antibodies (clone 8/DLP1, BD Bioscience), rabbit polyclonal anti-p-DRP1 S616 antibodies (Cell Signaling), rabbit polyclonal 3-nitrotyrosine (Sigma), rabbit β-actin antibody (Cell Signaling); sheep-anti-mouse IgG-HRP (GE Healthcare), donkey-anti-rabbit IgG-HRP (GE Healthcare), goat-anti-mouse AlexaFlour488 (Invitrogen), goat-anti-rabbit AlexaFluor594 (Invitrogen).

*Primary Cortical Neurons*

Pure cortical neurons were isolated from Sprague-Dawley rat embryos (E18) as previously described (71, 128).

*Mitochondrial Fragmentation and Neuronal Cell Death*

Neurons were grown on poly-Lysine coated glass cover slips as described before and transfected with DsRed2-Mito after 5 days *in vitro* (DIV) using Lipofectamine2000®. 3-NP was prepared as previously described (128). The Aβ peptides were preaggregated as described before (71). Cell death was induced with 3-NP (10 mM, 8 h), glutamate (150 μM, 6 h), NMDA (150 μM, 12 h) Aβ (10 μM, 6 h) at 11–14 DIV or with SNOC (100 μM, 3 h) at 8 DIV. After various time periods neurons were fixed using 3.7% formaldehyde and 5% sucrose in PBS for 20 min at 37$^{º}$C. Nuclei were labeled with Hoechst 33342 (1 μg/ml). Quantification of mitochondrial fragmentation and neuronal cell death was performed as described (129). Fluorescence microscopy and image acquisition of mitochondrial morphology was performed as previously described (130).

*Western Blotting*

To detect protein nitration, neurons were lysed using T-Per extraction reagent (Pierce) supplemented with Complete Protease Inhibitor Cocktail (Roche Applied Science, US). Protein concentrations were determined using the Bradford assay (Pierce Biotechnology, Inc., Rockford, IL). Proteins were separated by 4-20% SDS-PAGE gradient gels (Invitrogen) and transferred to PVDF membranes (0.2 μm, Bio-Rad).  Nonspecific protein binding was blocked by incubating the membranes with TBS (50 mM Tris-Cl, pH 8.0, 150 mM NaCl), 0.02% Tween20, and 5% nonfat milk for 3 hours at room temperature. The membranes were then probed with primary rabbit polyclonal antibodies for 3-nitrotyrosine (Sigma) (1:500) overnight at 4°C. After four washes (5 min) of TBS (0.02% Tween20), membranes were incubated for two hours at room temperature

with anti-rabbit horseradish peroxidase-conjugated secondary antibodies (GE Healthcare) (1: 15,000) in blocking solution. After four washes (5 min) of TBS (0.02% Tween20), immunocomplexes were detected using the Super-Signal West-Dura chemiluminescence substrates (Pierce, Thermo Scientific, Rockford, IL). Restore Western Blot Stripping Buffer (Thermo-Scientific) was used to strip blots. Membranes were successively probed with anti-β-actin antibody (Cell Signaling, 1:1000).  To measure the levels of p-DRP1 S616, neurons were lysed in buffer containing 50 mM Tris-Cl, pH 7.0, 150 mM NaCl, 1 mM MgCl$_2$, 1 mM NaF, 1 mM NaVO$_4$, 1 % NP40, 10 % glycerol and complete Protease Inhibitor Cocktail Tablets (Roche Applied Science, US). Membranes were blocked with 5 % nonfat milk in TBS (pH 8.0) with 0.05% Tween20 for 3 h at room temperature (RT) and were incubated with primary rabbit polyclonal antibodies for p-DRP1 S616 (Cell Signaling) (1:1000) overnight at 4°C. The membranes were then washed four times (5 min) with TBS (0.05% Tween) and incubated for 2h at room temperature with anti-rabbit horseradish peroxidase-conjugated secondary antibodies (GE Healthcare)(1:15,000) in blocking solution. After 4 washes (5 min) of TBS (0.05% Tween), immunocomplexes were then detected using the Super-Signal West-Dura or Femto chemiluminescent substrates (Pierce, Thermoscientific, Rockfod, IL). For reprobing the membranes were stripped with Restore Western Blot Stripping Buffer (Thermo-Scientific) according to the manufacturer and incubated with mouse monoclonal antibodies for DRP1 (BD Biosciences, clone 8/DLP1) (1:1000) antibody or with polyclonal rabbit antibodies for β-actin (Cell Signaling) (1:1000).

*Immunocytochemistry for 3-nitrotyrosine*

For immunocytochemistry, neurons were grown on poly-Lysine coated glass coverslips as previously described (71) and fixed with 4% formaldehyde (Ted Pella, Inc.) in PBS for 10 minutes at room temperature. Fixed neurons were then permeabilized with 0.1 % Triton X-100 in PBS for 5 minutes. Unspecific binding was blocked with 3% BSA, 3% FBS in PBS for one hour at room temperature. Fixed neurons were then probed with antibodies for 3-NT (1:500, Sigma) and an antibody specific for MAP 2 protein (1:200, Invitrogen) (RT, 2h), a neuronal marker followed by conjugated fluorescent secondary antibodies AlexaFluor594 or AlexaFluor488 (respectively) at dilutions of 1:500 (RT, 2h). Chromatin was stained by incubating fixed samples with Hoechst 33342 (1 µg/ml) in PBS at RT for 5 min. To visualize 3-NT using AlexaFluor594, the excitation filter was S555/28× (Chroma) and the emission filter was S617/73m (Chroma), to visualize neurons using AlexaFluor488, the excitation filter was S490/20× and the emission filter was S528/38m (Chroma) and to visualize Hoechst 33342 the excitation filter was S403/12× and emission filter S475/50m. Immuno-staining conditions for 3-NT were first optimized along with a blocking control, using 10 mM nitro-tyrosine, to confirm specificity of 3-NT signal. Fluorescence microscopy was performed as previously described (112). Quantification of fluorescence from 3-NT was as follows. Exposure time, brightness and contrast of randomly selected cortical neurons were held constant for all images within same experiment. Using MetaMorph 7.5, a region of interest was selected around each neuron using the MAP 2 label as a guide. This region was transferred to the 3-NT image channel. The fluorescence intensity for each neuron was measured using Show Region Statistics function. Area and intensity/fluorescence data was logged for each neuron. Twenty five to fifty neurons from each

treatment were evaluated for a total of over 100 neurons per experiment. Three areas were selected randomly within each image and the average of their fluorescence intensity was considered as background. The background was subtracted within each image. 3-nitrotyrosine immuno-fluorescence quantification is expressed as fluorescence per $\mu m^2$.

*APF Live Cell Imaging*

Neurons were cultured on poly-Lysine coated MatTek dishes. To visualize peroxynitrite in neurons, cell permeable APF (2.4 µM) (Molecular Probe) was loaded in Neurobasal medium (phenol red free) containing 0.2 % pluronic acid, 1.8 mM $CaCl_2$, 0.8 mM $MgCl_2$, Hoechst 33342 (1 µg/ml) for 30 minutes at 37°C in a humidified 5% $CO_2$. Dye was then removed and replaced with conditioned phenol red-free Neurobasal medium. The APF fluorescent signals were measured in response to SNOC (100 µM) at two hours. Z-stacks were acquired keeping the exposure time, brightness and contrast constant using excitation S490/20× and emission S528/38m filters (Chroma). Using MetaMorph 7.5 software (Molecular Devices), equal backgrounds were subtracted from each z-stack image (as determined from each experiments control images) then z-stack series were summed. Cell soma and processes were selected, as previously described, using region of interest drawn around cell. This region was transferred to the APF image channel. The fluorescence intensity for each neuron was measured using Show Region Statistics function. Intensity/fluorescence data was logged for each neuron and data exported to Excel for further analysis.

*Nanoceria Preparation*

Nanoceria were synthesized by a wet chemical process as previously described (81). In brief, to prepare nanoceria with a high ratio of $Ce^{3}+/Ce^{4+}$, $Ce\,(NO_3)_3 \cdot 6H_2O$ (5 mM) was dissolved in $dH_2O$ and the nitrate precursor was stirred for 15 min then $H_2O_2$ (2% v/v) was rapidly added while stirring at 300 rpm. The solution was continuously stirred for 1 h to obtain a stable dispersion of cerium oxide nanoparticles. Samples were stored at room temperature. All preparations were sonicated to ensure single nanoparticles (Branson, Danbury, CT) for 45-60 min prior use. For cell experiments, nanoceria were diluted in sterile water.

*Transmission Electron Microscopy (TEM)*

Neurons were cultured on poly-Lysine coated 35 mm MatTek glass bottom dishes and fixed with 2 % paraformaldehyde, 0.15 M sodium cacodylate, pH 7.4, 2.5 % glutaraldehyde for five minutes at room temperature and followed by an additional 30 minutes on ice. The fixed cells were then washed three times with ice-cold 0.15 M sodium cacodylate and 3 μM calcium chloride for three minutes on ice and followed by postfixation in 1 % osmium tetroxide, 0.8 % potassium ferrocyanide, 3 μM calcium chloride in 0.15 M sodium cacodylate for 60 minutes on ice. After washing cells three times with ice-cold $ddH_2O$ for three minutes each, the cultures were stained in 2 % uranyl acetate for 30 minutes on ice. Samples were dehydrated with ice-cold 20, 50, 70, 90 % ethanol and then with 100 % ethanol at room temperature. The samples were first infiltrated in 50 % ethanol/50 % Durcupan ACM (Fluka/Sigma) for 1 hour at room temperature and under agitation, followed by three changes of 100 % Durcupan for three hours. The resin was polymerized at 80 $^{\circ}$C for three to four days under vacuum. Sectioning was

40

performed using AO/Reichert Ultramicrotome. Ultrathin (80 nm) sections were post-stained

with uranyl acetate (five minutes) and lead salts (two minutes) prior to imaging using a JEOL

1200FX transmission EM operated at 80 kV. A subset of sections was imaged without poststain.

Negatives were shot at a magnification of 20,000. The negatives were digitized at 1800 dpi

using a Nikon CoolScan system, giving an image size of 4033 × 6010 pixels and a pixel resolution

of 0.71 nm.

The nanoparticle morphology was characterized using high-resolution transmission

electron microscopy (HRTEM). The nanoceria preparation was deposited on the carbon-coated

copper grid (SPI supplies) for HRTEM analysis. The TEM grid was dipped into the nanoceria

preparation by the dip coating technique.  HRTEM micrographs were obtained using FEI Tecnai

F30 operated at 300 keV.

*Statistics*

Results were collected from at least three or more independent experiments and are

expressed as mean ± standard deviation (s.d.). Statistical analysis of two populations was

compared using two-tailed non-paired Student's *t* test.

Results

*Nanoceria Accumulate at Mitochondria in Neurons*

First, we determined the properties of our CNP1 preparation to confirm their $Ce^{3+}$

oxidation state, fluorite structure and cerium spectrum (CD&D under review). To assure sterile

conditions during growth of cortical neuronal cultures, CNP1 were filtered prior to use. To assure that CNP1 would not be prevented from going through 2 μm filter, possibly due to electrostatic attractions, the UV-visible spectrum before and after filtering were analyzed (Figure 7) and were determined to be identical. Previous reports suggest that CNP1 are readily internalized by cells, owing to their small size of ~ 5 nm (98, 131). We first checked for CNP1 (100 nM) uptake in our cultured cortical neurons using inductively coupled plasma mass spectroscopy (ICP-MS) over a time-course of twenty four hours (Figure 8). Cerium was easily detected in neurons after 1 h and reached steady state concentrations after 2 h.

CNP1 are internalized by cells owing to their small size (98, 131). However, their subcellular localization in neurons remains unclear. Therefore, we tracked the presence of CNP1 in primary rat cortical neurons using transmission electron microscopy (TEM). While untreated neurons exhibited no detectable signal (Figure 9A), we obtained clear evidence of electron dense particles in neurons cultured with CNP1 for three, twelve or twenty four hours. Specifically, CNP1 were present at two primary locations: the mitochondrial outer membrane and inner leaflet of the plasma membrane (Figure 9B,C). To verify that the electron dense granules indeed reflected CNP1, we repeated the EM preparation using samples void of post-staining. Using this modification we still detected electron dense particles, suggesting that they are not an artifact and indeed represent the nanoparticles (Figure 9D). The size of our CNP1 particles were ~ 3 to 8 nm (Figure 9E), in agreement with previous reports (101). However, the electron dense particles within neurons were larger, measuring 20.6 nm (± 2.9 nm s.d.). This increased size is expected since oxide nanoparticles rapidly agglomerate in cells, owing to their surface interactions with biological material. Further quantification of the association of CNP1

particles with mitochondria (Figure 9F) or the plasma membrane (Figure 9G) confirmed that

their location aligns with sites of increased ROS/RNS production in neurons. Analyses of the

nuclei from non-post-stained images revealed very few CNP1 (data not shown). In summary,

the data suggests that CNP1 become internalized by neurons and accumulate at the

mitochondrial outer membrane and inner leaflet of the plasma membrane.


*CNP1 Protect Against Nitrosative Stress*

Next, we tested whether CNP1 would lower nitrosative stress in neurons exposed to the

·NO donor *S*-nitrosocysteine (SNOC). The levels of nitrosative stress were measured by live cell

labeling with the RNS/ROS-sensitive fluorescent probe 3'-(*p*-aminophenyl) fluorescein (APF).

Fluorescence microscopy indicated that neurons exposed to either aged SNOC, - which released

all ·NO owing to its poor stability-, or CNP1 alone displayed low baseline APF fluorescence

(Figure 10A(a) and 10A(b)). By contrast, neurons exposed to fresh SNOC showed a clear

increase in fluorescence, reflecting APF oxidation (Figure 10A(c)). Importantly, neurons

pretreatment with CNP1 for 3 hours abolished the SNOC-induced increase in APF fluorescence,

suggesting that CNP1 were able to neutralize ROS/RNS in neurons (Figure 10A(c) and 10A(d)).

Notably, the APF fluorescent signal in SNOC-exposed neurons revealed a mottled cytoplasmic

pattern (Figure 10A(c)). It is possible the APF marks mitochondria, exhibiting increased

RNS/ROS levels. Further quantitative analyses confirmed a significant decrease of APF oxidation

in SNOC plus CNP1 treated neurons compared to SNOC alone treated neurons (Figure 10B).

Finally, CNP1 significantly protected neurons from SNOC-induced cell death (Figure 10C).

*CNP1 Reduce Peroxynitrite-induced Protein Tyrosine Nitration*

The modification of tyrosine residues can elicit changes in protein structure and function. Protein tyrosine nitration is a frequently used diagnostic marker for nitrosative stress and neurodegeneration (132). We tested whether CNP1 would reduce the burden of SNOC-induced protein tyrosine nitration using immunocytochemistry of fixed neuronal cultures and pan antibodies for 3-nitrotyrosine. Using fluorescence microscopy we observed that control neurons, - treated with either aged SNOC or CNP1 alone-, exhibited low background 3-nitrotyrosine immunofluorescence (Figure 11A(a) and 11A(b)). By contrast, SNOC-exposed neurons showed a robust increase in fluorescence, reflecting increased protein tyrosine nitration (Figure 11A(c)). Remarkably, CNP1 prevented SNOC-induced tyrosine nitration, evidenced by the reduced fluorescent intensity (Figure 11A(d)).  Quantitative analyses confirmed a significant reduction in the relative 3-nitrotyrosine signal in neurons that were pretreated with CNP1 (Figure 11B). Finally, we analyzed the relative 3-nitrotyrosine immunoreactivity of neuronal cell lysates with western blotting. Again, CNP1 reduced the SNOC-induced total protein tyrosine nitration, confirming our *in situ* data using intact neurons (Figure 11C). These findings suggest that CNP1 might be a useful tool to attenuate the harmful effects of protein nitration.

*CNP1 Protect Against Aβ induced Mitochondrial Fragmentation*

Nitrosative stress plays an important role in A$\beta$-mediated neurotoxicity (74, 84). A$\beta$ or nitrosative stress evoke persistent mitochondrial fragmentation, an event that causes bioenergetic failure, impaired $Ca^{2+}$ homeostasis, synaptic injury, axonal transport defects, and

neuronal cell death (71, 133).  To test whether CNP1 would prevent the A$\beta$-induced

mitochondrial fragmentation, we visualized the mitochondrial morphology by fluorescence

microscopy in neurons expressing DsRed2-Mito, a red fluorescent protein targeted to the

mitochondrial matrix. Control neurons, - either left untreated or treated with CNP1 alone (3 h

pretreatment)-, demonstrated an elongated mitochondrial morphology, typical of healthy

neurons (Figure 12A(a) and 12A(b)). By contrast, oligomeric A$\beta$ 25-35 peptide, but not the

reverse A$\beta$ 35-25 control peptide (Figure 12A(g)), induced dramatic mitochondrial

fragmentation evidenced by the appearance of mitochondria with mostly round morphology

(Figure 12A(c)). Remarkably, CNP1 prevented the A$\beta$ 25-35-induced mitochondrial

fragmentation, similar to *N*-acetyl-*L*-cysteine (NAC), a known ·NO/ONOO⁻ neutralizing

antioxidant supplement (Figure 12A(d) and 12A(f)). Further quantitative analysis demonstrated

that CNP1 significantly reduced the A$\beta$-induced mitochondrial fragmentation in neurons (Figure

12B). These results suggest that CNP1 not only accumulate at mitochondria, but can also

preserve their morphology and function in response to neurotoxic insults such as A$\beta$.


*CNP1 Reduce DRP1 Phosphorylation at S616*

There is increasing evidence that mitochondrial fragmentation, owing to excessive

DRP1-dependent  mitochondrial fission, plays a central role in many neurodegenerative

disorders including AD (73, 111, 118, 134). Cdk1/cyclinB1-mediated phosphorylation of DRP1 at

S616 causes its recruitment from the cytoplasm to mitochondria to initiate organelle division in

mitotic cells (119). However, all Cdk's are inactivated in postmitotic neurons with the exception

of Cdk5. Over-activation of NMDA receptors by A$\beta$  triggers excessive nitrosative stress and

cytoplasmic Ca$^{2+}$ levels. (121) possibly leading to increased ·NO production. SNOC triggers DRP1

S616 phosphorylation and mitochondrial fragmentation (71, 117). Notably, p-DRP1 S616 is

increased in AD patient brains (117, 121, 135). Because CNP1 prevented A$\beta$-induced

mitochondrial fragmentation (Figure 12), we questioned whether they might inhibit DRP1 S616

phosphorylation, providing an explanation for the preservation of mitochondrial morphology by

CNP1. Neurons treated with either aged SNOC or CNP1 alone exhibited only low baseline DRP1

S616 phosphorylation (Figure 13A). By contrast, neurons treated with fresh SNOC exhibited

high p-DRP1 S616 levels (Figure 13A). Remarkably, CNP1 significantly reduced the SNOC-

induced increase in DRP1 S616 phosphorylation (Figure 13A). Similarly, CNP1 or NAC abolished

the A$\beta$ 25-35-induced DRP1 S616 phosphorylation (Figure 13B). These results suggest that CNP1

reduce nitrosative stress or A$\beta$-induced mitochondrial fragmentation perhaps by preventing

DRP1 S616 hyperphosphorylation.


*CNP1 Protect Against A$\beta$ -induced Neuronal Cell Death*

Cell death by A$\beta$ or NMDA occurs, at least in part, through endogenous RNS/ROS (71).

Neuronal death by the complex II inhibitor 3-nitropropionic acid (3-NP) triggers secondary

excitotoxicity and RNS/ROS (128). A$\beta$ 25-35, but not the reverse peptide, elicited neuronal cell

death, which was reduced in the presence of either CNP1 or NAC (Figure 14A). Similarly,

neuronal cell death by excess NMDA or glutamate was reduced by CNP1 (Figure 14B and 14C).

Finally, similar neuroprotective effects were observed against respiratory complex II inhibition

by 3-NP (Figure 14D). Thus, CNP1 provide neuroprotection against a variety of insults that

generate endogenous ROS/RNS.

Nitrosative stress and mitochondrial dysfunction are early features of AD, therefore targeting these events might offer therapeutic benefits. Several antioxidants including β-carotene, vitamins C and E, NAC (12), coenzyme $Q_{10}$ (13) and tetra-hydrocurcumin provided protective effects in cellular and animal models of AD (14). However, their efficacy in human trials provided at best only modest effects (12, 15, 16). Among the problems are their poor stability and repetitive dosing, underscoring the need for alternative strategies.

To overcome this problem we integrated nanotechnology with neuroscience. Here, we tested the effects of CNP1, which are inorganic auto-catalysts with antioxidant properties. Thus, a single dose might suffice, unlike conventional antioxidants. Mitochondrial dynamics are sensitive to many stimuli including ROS/RNS (111). Mitochondrial fission is activated by DRP1 when mitochondrial ROS levels are increased (136). We provide evidence that CNP1 are able to reduce ROS/RNS, which in turn lowers DRP1 S616 hyperphosphorylation, mitochondrial fragmentation and neuronal cell death by A$\beta$, NMDA receptor overactivation, and mitochondrial respiratory chain inhibitors.

There are reports which claim that CNP1 are toxic (66). In considering CNP1 as potential therapeutic agents it is important to pay attention to their synthesis method, concentration, and surface chemistry. The preparation of water-based CNP1 in our study has been shown to exhibit SOD mimetic activity (55, 126) whereas other synthesis methods result in CNP1 without comparable antioxidant properties (66). Thus these factors might account for the seemingly conflicting reports. Mild nitrosative/oxidative stress provides cell protective effects and plays an important physiological role. A concern would be that antioxidants might eradicate the

cytoprotective effects of mild stress. Our data shows that CNP1 are not toxic to neurons, suggesting that they do not lower physiological levels of nitrosative/oxidative stress.

We reduced *in situ* ROS/RNS as visualized by decreasing APF oxidation (Figure 10) as well as 3-nitrotyrosine nitration in SNOC stressed neurons (Figure 11A,C) and protection from cell death by A$\beta$ 25-35 exposure (Figure 13A) using CNP1. Increased levels of nitrated proteins have been reported in AD brains as well as cerebrospinal fluid in patients with AD (37). Numerous proteins in AD have been shown nitrated by peroxynitrite (33). Peroxisome proliferator-activated receptor gamma (PPARγ) expression protects neurons from A$\beta$- mediated toxicity (38) however its nitration prevents its translocation to the nucleus, thereby preventing mitochondrial biogenesis (39). A disrupted energy metabolism and ROS/RNS redox balance can activate redox-sensitive transcription factors including activator protein-1 (AP-1). Increased iNOS expression by AP-1 is implicated in AD (137).

Nitrosative stress can activate kinases (109, 110). Specifically peroxynitrite can activate p38 MAP kinase and Cdk5 (108). Neurotoxic signals including A$\beta$ and excess glutamate or NMDA causes an impaired $Ca^{2+}$ homeostasis, which can activate downstream mediators including NOS and calpain (128). ROS/RNS can directly activate Cdk5. Aberrant Cdk5 activation in neurodegeneration can occur by two mechanisms. First, nitrosative stress can directly activate Cdk5 by increasing its phosphorylation. Second, $Ca^{2+}$-dependent calpain cleavage of the Cdk5 activator p35 to p25 increases its stability. Consequently, Cdk5/p25 is constitutively activated. (111, 115, 123, 138). The blockage of mitochondrial fragmentation by CNP1 in response to A$\beta$ was associated with a reduction in DRP1 S616 hyperphosphorylation (Figure 13B). Although it is unlikely that nitrosative stress mediates mitochondrial fragmentation and

neuronal cell death only by phosphorylating a single protein target, such as DRP1, our data describes one possible mode of action how CNP1 may specifically attenuate the downstream effects of RNS/ROS.

Most therapeutic treatments of AD have targeted reducing or clearance of A$\beta$ with disappointing results however, therapeutic strategies aimed at reducing mitochondrial damage, especially through mitochondrial antioxidants (13) show promise. Considering CNP1's proximity to mitochondria (Figure 1F) they may be uniquely situated to protect neurons in AD from nitrosative stress and mitochondrial dysfunction by lowering DRP1 S616 phosphorylation and thereby maintaining bioenergetic function and neuronal viability.

CeO$_2$ NPs have been shown to decrease RNS/ROS-induced damage by many stress stimuli and in several cellular and animal models (101). No toxicity or adverse effects to CeO$_2$ NPs in the eyes of rats was found, where it prevents vision loss due to increased ROS from excess light exposure (139). CeO$_2$ NPs also mitigate ischemic brain injury where CeO$_2$ NPs markedly decreased the levels of 3-nitrotyrosine (3-NT) (98) In addition, CeO$_2$ NPs accumulated on mitochondria, consistent with our results (Figure 9F). The small size of CNP1 allowed passage into our neurons (Figure 9B), but delivery routes into all cell types and tissues must still be tested. These are not trivial issues, yet considering our results that CNP1 protected cortical neurons from multiple nitrosative-associated stressors, they represent a potential exciting alternative strategy compared to traditional antioxidants. Our study represents an important step forward to test the potential neuroprotective effects of CeO$_2$ NPs in *in vivo* animal models of AD.
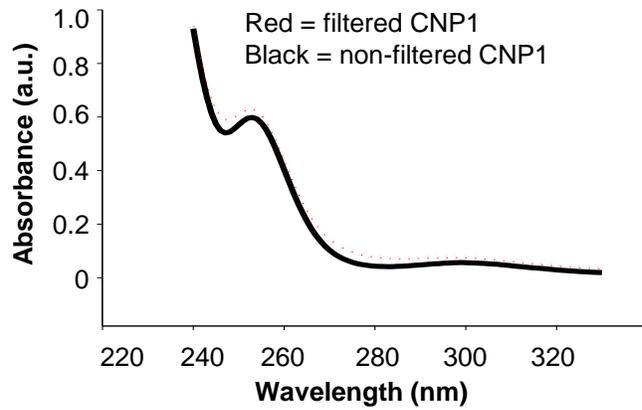
**Figure 7: UV-visible spectroscopy analysis of sterile filtered CNP1 used in tissue culture experiments confirming 3+ oxidation state of CNP1**

Absorbance between 230-260 nm is indicative of Ce $3^{+}$ oxidation state.
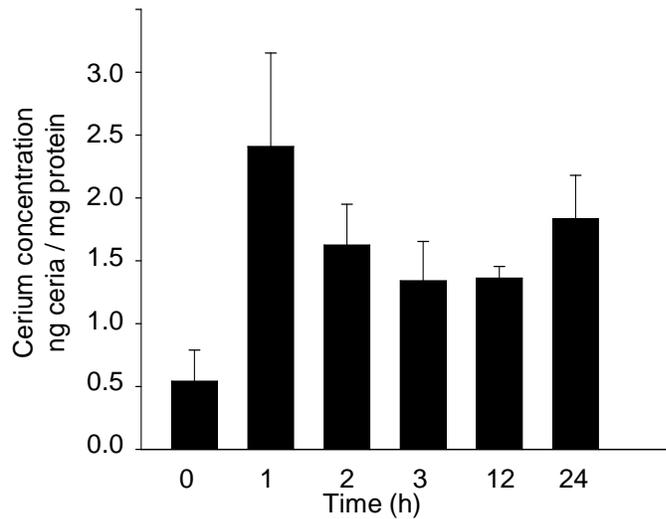


**Figure 8: Time-course uptake of CNP1 measured by ICP-MS.**

Cortical neurons were incubated with 100 nM CNP1 for times indicated and the concentration of cerium inside neurons were measured by ICP-MS.
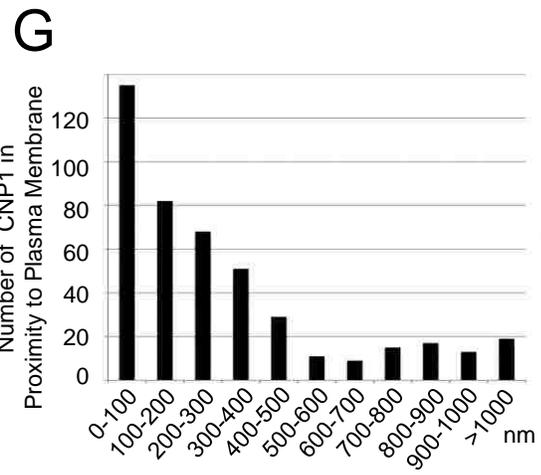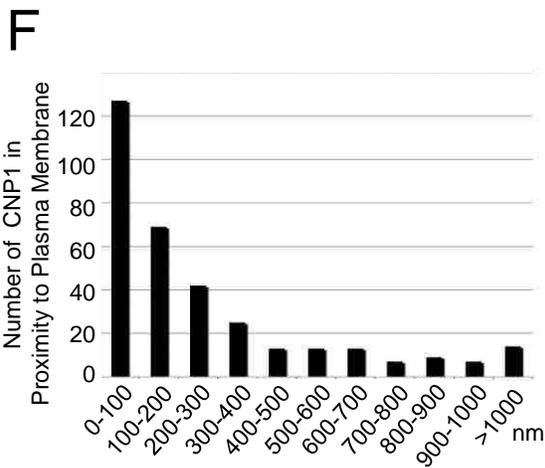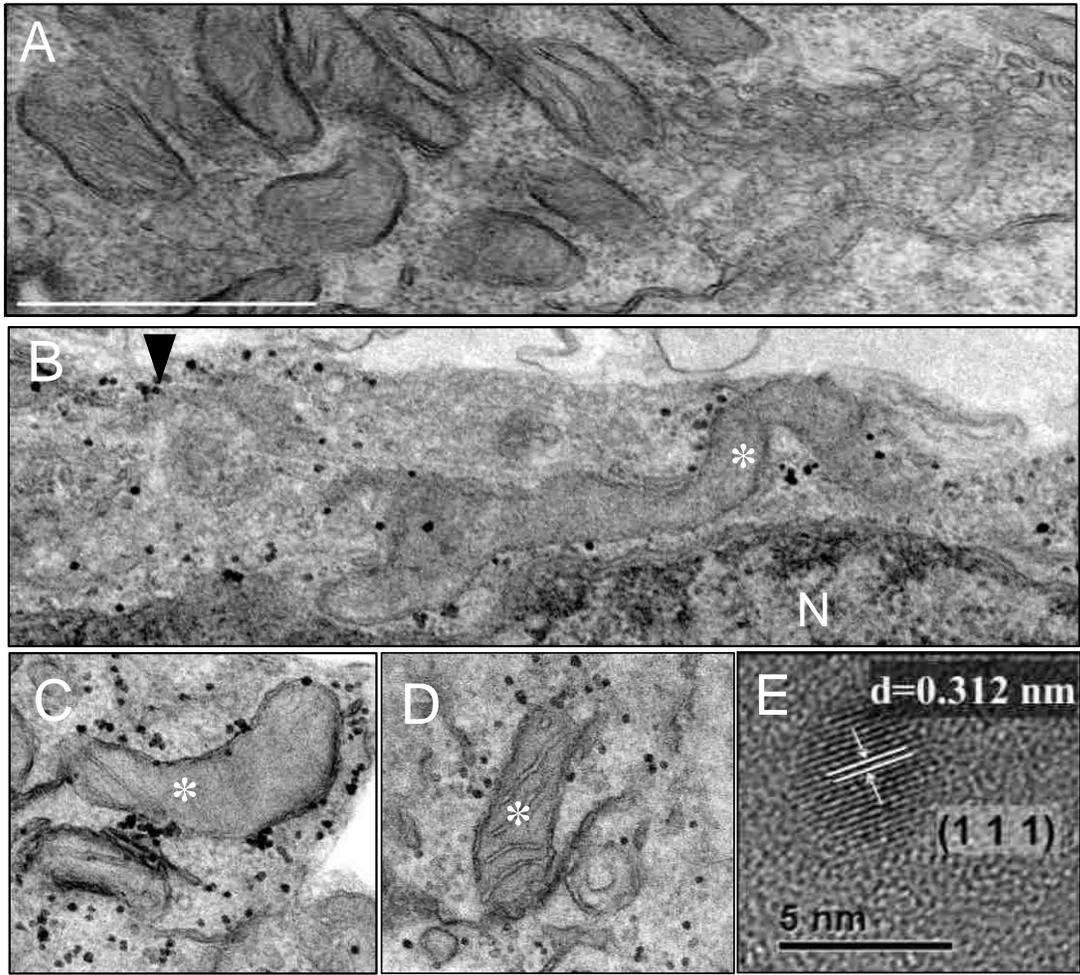
**Figure 9: CNP1 accumulate at the mitochondrial outer mitochondria and the inner leaflet of the plasma membrane in cultured cortical neurons.**

(A) Electron microscopy of an untreated control neuron. Scale bar, 1µm.  (B) Electron microscopy of a neuron treated with $CeO_2$ nanoparticles (100 nM) for 3 hours. Round electron dense particles, indicative of CNP1 particles, concentrate around mitochondria (∗) and the plasma membrane (black arrowhead), but not along the nucleus (N). (C) Electron microscopy of a neuron treated with $CeO_2$ nanoparticles (100 nM) for 12 hours. Mitochondrion (∗) showing clusters of CNP1 particles accumulating at the mitochondrial outer membrane. (D) Electron microscopy of a neuron treated with $CeO_2$ nanoparticles (100 nM) for 3 hours for which the poststaining step was omitted. The mitochondrion is depicted by the (∗) symbol. (E) High resolution transmission electron microscopy of a CNP1 particle. Parallel lines indicate the inter-planar spacing of the atomic arrangement "d" showing the ceria lattice distance of 0.312 nm (as measured by the diffraction pattern, (Supplemental Figure 1C) and a Miller index of (111). Scale bar, 5 nm. (F) Bar graph of number of CNP1 particles in proximity to the mitochondrial outer membrane (G) or the inner leaflet of the plasma membrane. The closest distance between a CNP1 particle and a mitochondrion or the plasma membrane was measured with ImageJ and then binned in 100 nm increments.
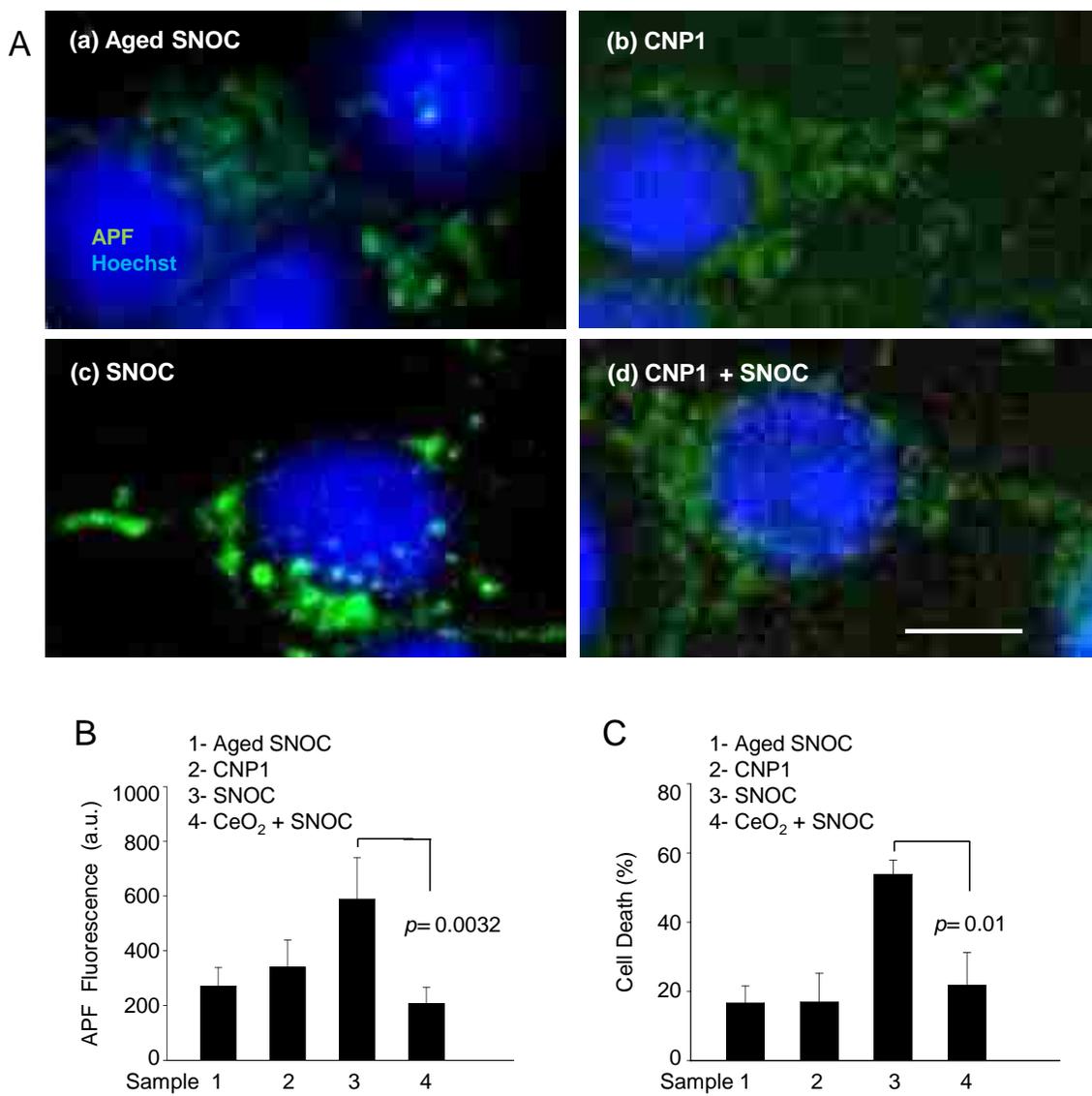
**Figure 10: CNP1 scavenge reactive nitrogen species and rescue cortical neurons from SNOC-induced cell death.**

(A) Fluorescence images of APF (green) and Hoechst 33342 (blue) double staining of neurons treated with (a) aged SNOC (100 µM), (b) CNP1 (100 nM), (c) fresh SNOC (100 µM), or both (d) CNP1 (100 nM) and SNOC (100 µM) for two hours. Scale bar, 10 µm. (B) APF fluorescence of neurons treated with aged SNOC, CNP1, fresh SNOC, or CNP1 and SNOC at two hours. (C) Cell death of neurons at three hours treated with aged SNOC, CNP1, or fresh SNOC alone or in combination of CNP1 plus fresh SNOC. Data represent means ± standard deviation (s.d.). Results are representative of three or more independent experiments. Statistics: Student's *t* test.
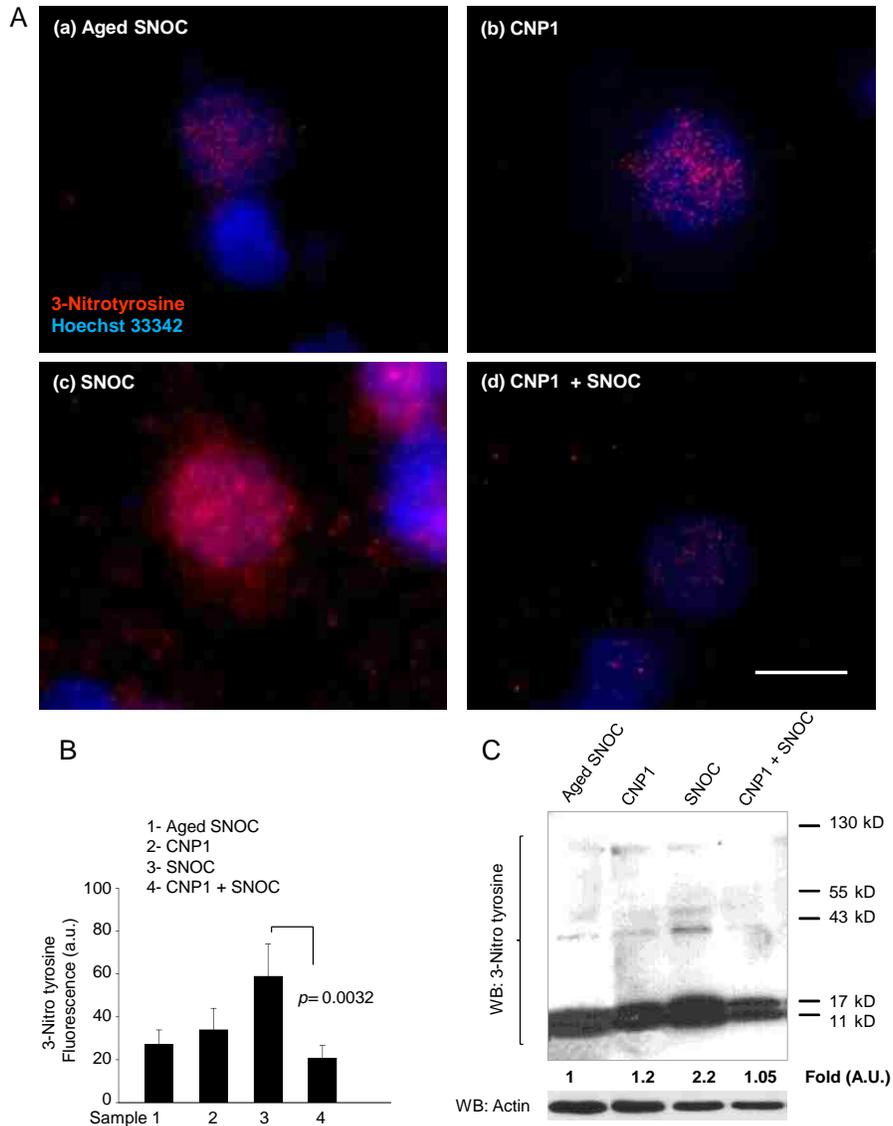
**Figure 11: CNP1 reduce protein tyrosine nitration in SNOC exposed cortical neurons.**

(A) Fluorescence micrographs of 3-nitrotyrosine (red) immunostaining and Hoechst 33342 (blue) staining of neurons treated with (a) aged SNOC (100 µM), (b) CNP1 (100 nM) (3 h pretreatment), (c) fresh SNOC (100 µM) alone, or (d) in combination with CNP1 and SNOC for three hours. Scale bar, 10 µm. (B) 3-Nitrotyrosine fluorescence of neurons treated with aged SNOC, CNP1, fresh SNOC, or CNP1 and SNOC for three hours. Data are means ± s.d. (C) Western blot of 3-nitrotyrosine protein modification in neurons treated with aged SNOC, CNP1, fresh SNOC, or CNP1 and SNOC for three hours. Fold densitometries represent the relative ratios of 3-nitrotyrosine in whole neuronal lysates normalized to control lysates. Data are representative of three or more independent experiments. Statistics: Student's $t$ test.

A

(a) **Untreated**  (b) **CNP1**

(c) **Aβ 25-35**  (d) **CNP1 + Aβ 25-35**

(e) **NAC**  (f) **NAC + Aβ 25-35**
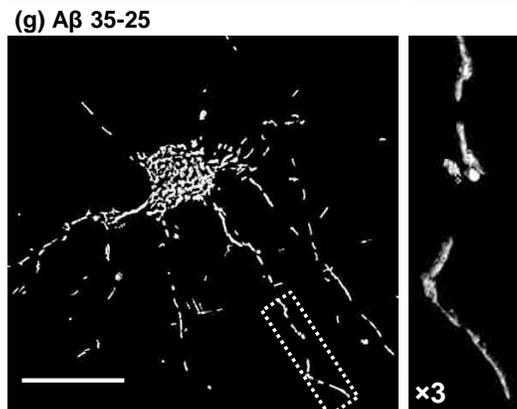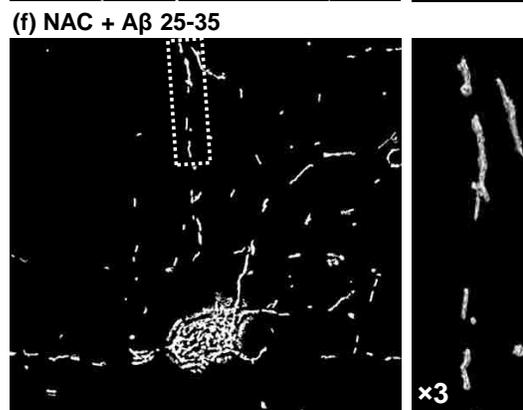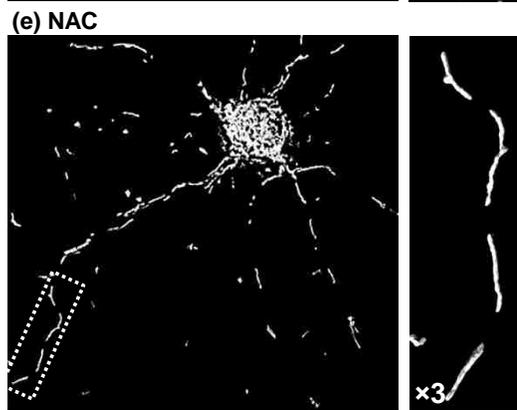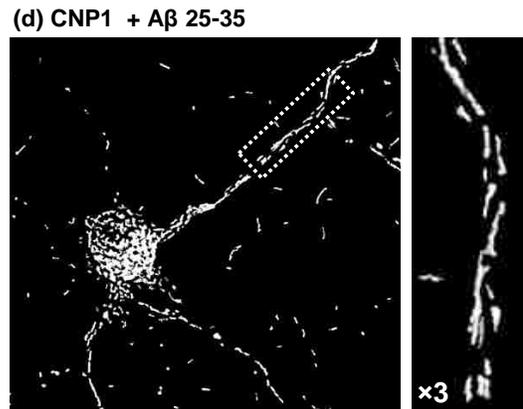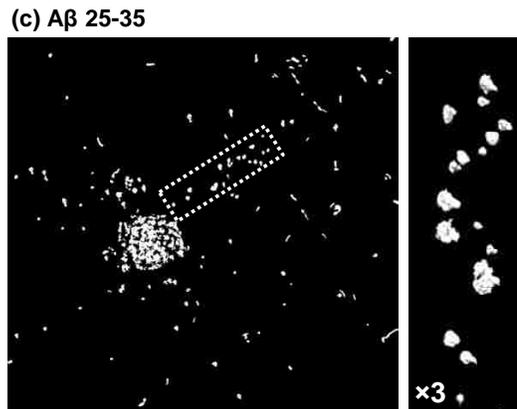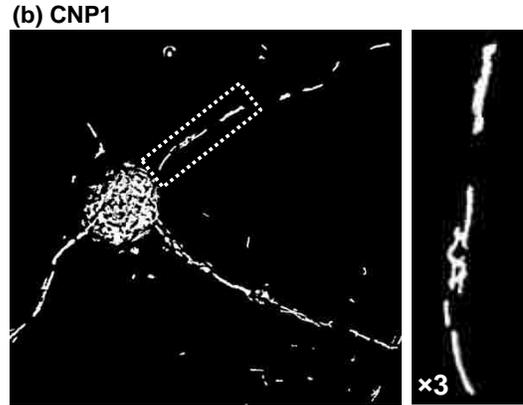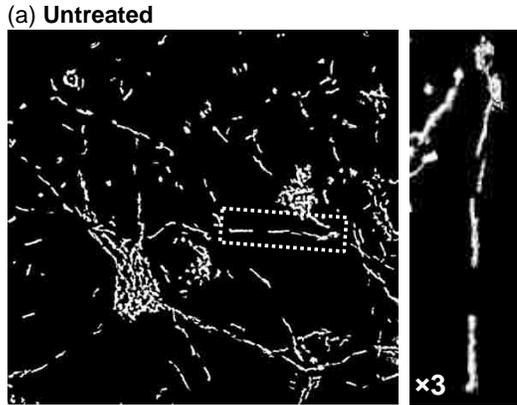
(g) **Aβ 35-25**



B

1- Untreated  5- NAC
2- CNP1  6- NAC + Aβ 25-35
3- Aβ 25-35  7- Aβ 35-25
4- CNP1 + Aβ 25-35

p=0.001  p=0.005

Frag. Mitochondria (% Neurons)

Sample  1  2  3  4  5  6  7
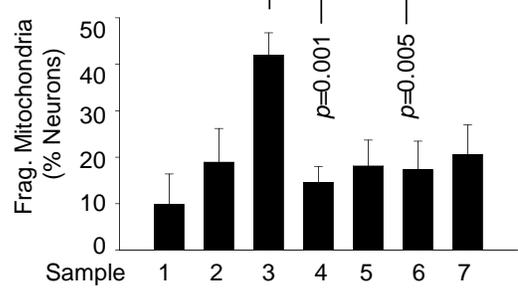
**Figure 12: CNP1 prevent Aβ-induced mitochondrial fragmentation.**

(A) Fluorescence micrographs (scale bar, 50 μm) and 3 x zoom of boxed regions of mitochondrial morphology in neurons expressing DsRed2-Mito and (a) left untreated or treated with (b) CNP1 (100 nM) (3 h pretreatment), (c) or A*β* 25-35 (10 μM), (d) CNP1 and A*β* 25-35, (e) NAC (50 μM) (3 h pretreatment), (f) NAC and A*β* 25-35, (g) or the reverse A*β* 35-25 (10 μM) peptide for six hours. (B) Mitochondrial fragmentation in neurons expressing DsRed2-Mito and after treatment for six hours with CNP1, NAC, or A*β* 25-35 alone or in combination with either CNP1 and A*β* 25-35 or NAC and A*β* 25-35. Data are representative of three or more independent experiments. Results are means ± s.d. Statistics: Student's *t* test.
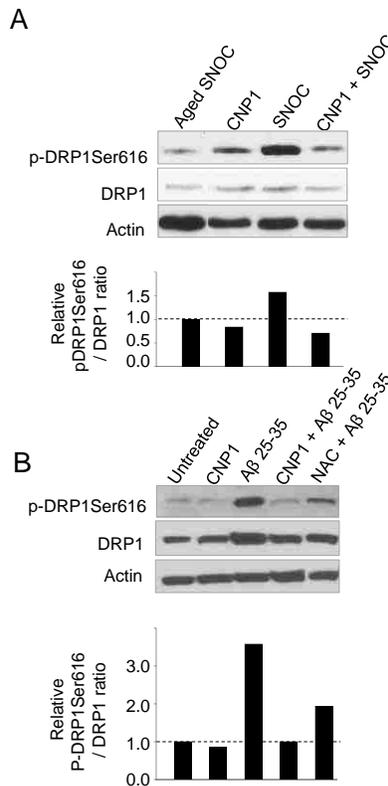


**Figure 13: CNP1 abolish DRP1 phosphorylation at S616 in response to RNS.**

(A) Western blots of p-DRP1 S616, total DRP1, and actin protein levels from neurons exposed for three hours to aged SNOC (100 μM), CNP1 (100 nM) (3 h pretreatment), or fresh SNOC (100 μM) alone or in combination. The bar graph represents the relative ratios of p-Drp1 S616 to total DRP1 protein and normalized to actin. (B) Western blots of p-DRP1 S616, total DRP1, and actin protein levels from neurons exposed to CNP1 (100 nM), preaggregated 10 μM A*β* 25-35 for 6 h, or in combination as well as NAC (50 μM) (3 h pretreatment) with A*β* 25-35. The bar graph illustrates the relative ratios of p-DRP1 S616 to total DRP1 protein, normalized to actin.
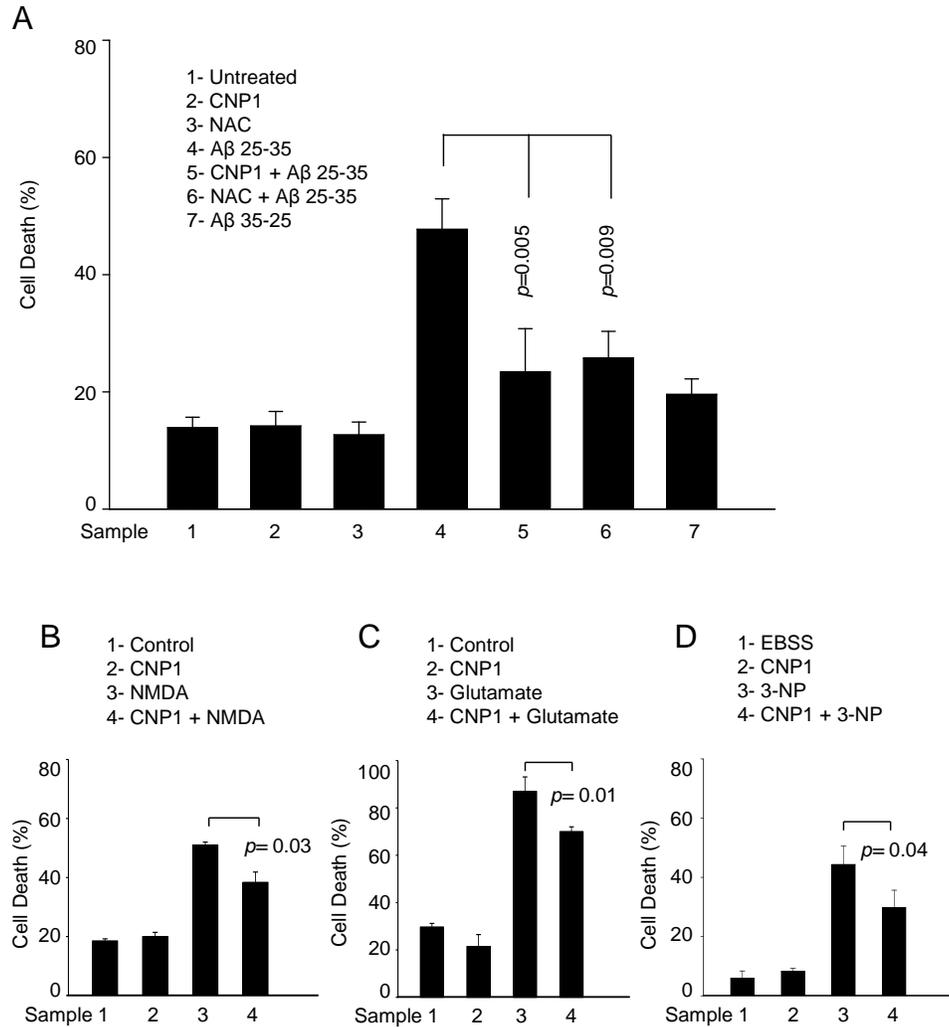
**Figure 14: CNP1 delay neuronal cell death induced by Aβ, NMDA, glutamate, or 3-NP.**

(A) Cell death of neurons treated with either CNP1 (100 nM) (3 h pretreatment), NAC (50 μM) (3 h pretreatment), or A$\beta$ 25-35 (10 μM) alone, or both CNP1 and A$\beta$ 25-35, or NAC and A$\beta$ 25-35 at six hours. Untreated cells or reverse A$\beta$ 35-25 (10 μM) peptide treatment served as negative controls. (B) Excitotoxic cell death of neurons exposed to either NMDA (150 μM), or CNP1 (100 nM) (3 h pretreatment), or in combination of both for 12 hours. (C) Excitotoxic cell death of neurons exposed to either glutamate (150 μM), or CNP1 (100 nM) (3 h pretreatment), or in combination of both for six hours. (D) Cell death of neurons exposed to mitochondrial respiratory complex II inhibitor 3-NP (10 mM), or CNP1 (100 nM) (3 h pretreatment), or in

combination of both for eight hours. Results are representative of three or more independent experiments. Data are means ± s.d. Statistics: Student's *t* test.

# CHAPTER 4: ATPASE/PHOSPHATASE ACTIVITY UNDERLIES THE TOXICITY OF HEXAMETHYLENETETRAMINE-BASED CERIUM OXIDE NANOPARTICLES

## Introduction

Cerium is a rare earth metal that belongs to the Lanthanides series of the periodic table. It has the unique property in that oxygen vacancies are created in their metal oxide nanoparticle form (140). Cerium oxide NPs retain their fluorite lattice structure even with the loss of oxygen, yielding $CeO_{2-x}$, and vacancies are the likely sites for potent reduction-oxidation (redox) reactions (88). It is this property that first made it useful for industrial applications including the removal of carbon monoxide (CO), hydrocarbons and nitric oxide species ($NO_x$) from exhaust gas (87). In addition, the ability to shift between $Ce^{3+}$ and $Ce^{4+}$ states plays an important role in $CeO_2$ NPs capacity to interact with a variety of reactive oxygen species (ROS) and reactive nitrogen species (RNS) species (55, 67, 68, 126). It is this ability to scavenge ROS/RNS species that has led to $CeO_2$ NPs testing in biological systems to reduce potentially harmful ROS/RNS in disease and aging as use as potential therapeutics.

Nanoparticles in general exhibit novel surface properties that can affect their chemistry and their interaction with biological systems. For $CeO_2$ NPs to be a realistic therapeutic, they must be understood completely before human testing can be started and carefully characterized in order to insure safety. Part of that understanding must include the synthesis process in which the $CeO_2$ NPs have been created. The processing and material preparation of $CeO_2$ NPs are wide and varied, this includes creating NPs with the core $CeO_2$ material as well as surface functionalization and/or modifications (66). Even when synthesizing 'bare' $CeO_2$ NPs,

there are numerous synthesis methods that have been employed (141-143). Over the past

decades, better synthesis methods for $CeO_2$ NPs use have been extensively tested for industrial

(144) and biological uses. For use in biological studies, three major synthesis themes have been

described, direct high-temperature exposure processes, heated in solvent synthesis and room

temperature synthesis (66) resulting in various biological responses.  The aim of these new

synthesis methods was to create NPs with high oxygen storage capacity, uniform size, specific

size, and catalytic activity. The use of heated hexamethylenetetramine (HMT) as a solvent

results in finer $CeO_2$ NPs (145) and is routinely employed in the synthesis of $CeO_2$ NPs (65, 146,

147). The catalytic properties of these HMT-based $CeO_2$ NPs have not yet been determined in

biological systems. There are many studies using room temperature/water-based synthesis of

$CeO_2$ NPs in which various catalytic activities have been described (55, 67, 68, 126). The

rationale for this synthesis method is that they seem to be less toxic (60, 148, 149) and the

ability to control the $Ce^{3+}/Ce^{4+}$ ratio (81). Indeed, for $CeO_2$ NPs to be a potential therapy for the

reduction ROS/RNS in disease, the mechanism of action for $CeO_2$ NPs, respective of synthesis

procedure, must be well defined.

The study of the chemical and biological properties of $CeO_2$ NPs has expanded recently.

There are numerous studies that point to $CeO_2$ NPs as a potential new treatment for a wide

variety diseases (58, 98, 99, 150). Although most of the focus has been on the ability of these

materials to reduce reactive oxygen and nitrogen species in biological systems, there are

reports that claim that $CeO_2$ NPs are toxic. Unfortunately, the material synthesis of these

studies varies significantly. Thus it must first be determined whether $CeO_2$ NPs made by

different methods are similar or different in their chemical properties. Then the next step is to

determine the pathways that $CeO_2$ NPs might interfere or augment. Mechanisms for anti-oxidant or pro-oxidant for $CeO_2$ NPs are now just starting to be compared. However, the outcomes of $CeO_2$ NPs exposure can vary as much as the synthesis methods and cell types tested (151-153). This underscores the need to fully understand the nanoparticles synthesis method, resulting catalytic behavior(s) and their influence(s) in biological settings.

Phosphorylation and dephosphorylation play a significant role in a wide range of important regulatory mechanisms in mammals. Control of the addition or removal of phosphate ($PO_4^{3-}$) groups is especially important energy maintenance, specifically adenosine triphosphate (ATP) which is a critical energy storage molecule. The hydrolysis of ATP to adenosine diphosphate (ADP) releases energy (H+) and inorganic phosphate which is then utilized in a wide range of cellular applications such as the movement of organelles (endosomes, lysosomes, mitochondria) along microtubules as well as muscle contractions, small molecule transport, or biosynthetic reactions driving anabolism. Unregulated hydrolysis of ATP to ADP will strain energy metabolism and have a negative impact on a cell's ability to function normally. In this study we compared $CeO_2$ NPs synthesized by two different methods (water-based and HMT-based) to begin to understand the enigma of how $CeO_2$ NPs can be reported to be both toxic and non-toxic when exposed to a variety of organisms and cells in culture at similar concentrations. Based on our results, we hypothesize that the toxicity reported by many investigators may be due to phosphatase activity of $CeO_2$ NPS that proceeds through a poorly understood catalytic mechanism at the surface of the nanoparticle.

## Materials and Methods

### *Preparation of Different Cerium Oxide Nanoparticles*

In this study several cerium oxide nanoparticles were prepared with varying surface oxidation state, surface modification, and morphology. Cerium nitrate hexahydrate (99.999% pure from Sigma Aldrich, St. Louis, MO) were used as a precursor for all of the preparations. Cerium oxide nanoparticles with a higher $Ce^{3+}/Ce^{4+}$ ratio (CNP1) or with lower $Ce^{3+}/Ce^{4+}$ ratio (CNP 2) were prepared using wet chemical method as described previously (154). Surface modified cerium oxide nanoparticles were prepared using hexamethylenetetramine (HMT) (155). Briefly, equal volume of 37.5 mM of cerium nitrate solution and 0.5 M HMT were mixed together and stirred for 24 h at room temperature. Cerium oxide nanoparticles prepared using HMT were washed with either ethanol and acetone or $dH_2O$ for three times and finally resuspended in $dH_2O$. It is important to mention that after washing with ethanol and acetone, CNP-HMT-1 were washed with $dH_2O$ (three times) to remove any trace amount of solvent (ethanol or acetone) before resuspending in $dH_2O$. Cerium oxide nanoparticles washed with ethanol and acetone to remove the maximum amount HMT were designated as CNP-HMT1. CNPs washed with only $dH_2O$ were designated as HMT-CNP2. Different morphology of CNP-HMT3 were prepared by preheating the both the solutions (37.5 mM cerium nitrate precursor and 0.5 M HMT) at 60° C and then equal volume of the solutions were mixed and stirred for 4 h. CNP formed were then washed with ethanol and acetone for three times and finally with $dH_2O$ to remove the solvent before resuspending in $dH_2O$.

*Physico-Chemical Properties of Cerium Oxide Nanoparticles (CeO$_2$)*

High resolution transmission electron microscopy (HRTEM) was used to analyzed size and morphology of the nanoparticles. Hydrodynamic radius and surface charge of the nanoparticles were estimated using Zetasizer (Nano-ZS from Malvern Instruments, Houston, TX). X-Ray photoelectron spectroscopy (5400 PHI ESCA) used to determine the surface oxidation state of the nanoparticles. Mg-Ka X-radiation (1253.6 eV) and 350 W power was used during the data collection as previously described (154). Fourier transform infrared (FTIR) spectra were collected to confirm the presence of HMT molecule on the nanoparticle surface using PerkinElmer Spectrum IR Spectrophotometer (Waltham, MA). The amount of HMT that remains on the surface of the nanoparticles was determined with differential scanning calorimetry and thermogravimetric analysis (DSC-TGA) using a TA Instruments SDT-Q600 (New Castle, DE), with open alumina pans under 100 mL/min air flow. Particle size analysis was also carried out by measuring the specific surface area (m$^2$/g) using the Brunauer, Emmett, and Teller (BET) method with a Quantachrome Nova 4200e surface area analyzer (Boynton Beach, FL).

*Drosophila* *melanogaster* *Exposure to Water-based or HMT-based Cerium Oxide Nanoparticles.*

Male and female wild-type *D. melanogaster* (Oregon R) were maintained under optimal conditions in a standard corn meal medium at a temperature of 25°C. Larval exposure to nanoparticles began at the larvae stage and continued through eclosion. Parental crosses were set up in cages with 150 females and 30-40 males on grape plates seeded with live yeast. After 21 hours, each grape plate was changed and hatched larvae removed. Groups of 50 larvae from

grape plates were isolated using a mounting needle under a dissecting microscope and placed

in vials containing 6 ml Jazzmix (Fisher Scientific, Pittsburg, PA) food medium containing 86

µg/mL of nanoparticles, CNP1 or HMT-CNP1. Control larvae were cultured in parallel in food

vials containing only $H_2O$ or 500 µM HMT. All vials were kept at 25°C and checked daily for

pupariation and eclosion.

## Cultivation of HUVECs

Human Umbilical Vein Endothelial Cells (HUVECs) (Lonza Walkerville, Inc., Walkersville, MD)

were maintained at 37°C in a humidified atmosphere containing 5% $CO_2$ in endothelial basal

medium (EBM) (Lonza Walkerville, Inc., Walkersville, MD) supplemented with 2 % fetal bovine

serum (FBS). Only cells from passages 3-6 were utilized in all experiments.

## Cell Viability MTT Assay

HUVECs were cultured in 96-well plates and exposed to $CeO_2$ NPs for 48 h. Thiazoyl blue

tetrazolium bromide (MTT) (Amresco, Solon, OH) (1.2 mM) was added and cells were

subsequently incubated for 4 h at 37 °C in 5% $CO_2$ atmosphere. To solubilize the dye, 100 µL of

cell lysis solution (10% SDS, 5 mM HCl) was added to each well and the plate was incubated for

an additional 4 h at 37 °C. Absorbance of the soluble dye was recorded at 570 nm using a

Spectra Max 190 spectrophotometer (Molecular Devices, Sunnyvale, CA). Cell viability was

determined by dividing the absorbance of treated samples to untreated controls and reported

as a percentage of control cells. Results were collected from at least three independent

experiments and are expressed as mean ± standard deviation (s.d.). Statistical analysis of two populations was compared using two-tailed non-paired Student's *t* test.

*Analysis of Intracellular ATP Levels*

HUVECs were cultured in opaque-walled 96-well plates and treated with $CeO_2$ NPs for 48 h. Plates were equilibrated to room temperature and cells were lysed according manufacturer instructions. CellTiter-Glo® Reagent was added, plates were incubated for 10 min to stabilize the luminescent signal. Luminescence was then recorded with a Varian Cary Eclipse fluorescence spectrophotometer (Palo Alto, CA) using 1 second integration time per well. Results were collected from at least three or more independent experiments and are expressed as mean ± standard deviation (s.d.). Statistical analysis of two populations was compared using two-tailed non-paired Student's *t* test.

*ICP-MS Uptake of $CeO_2$ NPs Studies*

HUVECs culture monolayers were incubated for 24 h with nanoparticles. Cells were washed two-times to remove extracellular nanoparticles and then collected by typsination and washed with PBS again to remove excess media and particles that could be adsorbed on the surface of the cells. Cells exposed to CNPs were analyzed for their cerium content using a Thermo Electron X-Series inductively coupled plasma mass spectrometer (ICP-MS, Thermo Scientific, Pittsburgh, PA) following APHA method 3125B to determine the amount of CNPs taken up by the cells.

*Live Cell Imaging of HUVECs Exposed to CeO$_2$ NPs*

HUVECs were cultured on Lab-Tek$^®$ II chambered coverglass (NUNC, Rochester, NY) slides in phenol red-free EBM (Lonza, Walkersville, MD) supplemented with  2 % FBS. Cells were exposed to various preparations of CeO$_2$ NPs for 36 h. To visualize nuclei, Hoechst 33342 dye (Molecular Probes, Invitrogen, Eugene, OR) (1µg/mL) was added in medium for 10 min at 37°C in a humidified 5% CO$_2$ incubator. Dye was removed and replaced with pre-warmed medium. Chamber slides with cultured HUVECs was placed under phase-contrast 40x air objective on a Nikon fluorescence microscope and images acquired at 37°C in a humidified 5% CO$_2$ atmosphere.

*Confocal Microscopy*

HUVECs were exposed to nanoparticles for 24 h and subsequently washed, trypsinized and seeded onto glass coverslips for 4 h (to allow for cell attachment). Cell were then fixed in 4 % formaldehyde for 20 min at RT. Cells were washed two times in PBS and then labeled with wheat germ agglutinin (WGA), Alexa Fluor$^®$ 488 (Molecular Probes, Invitrogen, Eugene, OR) (5 µg/mL) for identification of plasma membranes (green channel, excitation 405nm/emission 498) and Hoechst 33342 for identification of nuclei (blue channel, excitation 405/emission 428). Cells were washed and mounted in anti-fade mounting media (Calbiochem, St. Louis, MO) and slides cured 24h at RT. Slides were stored at 4 °C until simultaneous confocal and bright field imaging by Leica TCS SP5 laser scanning confocal microscope with 40×/1.25 oil objective lens.

*Phosphatase Mimetic Assay*

To measure the phosphatase activity of various $CeO_2$ NPs, 1.2 mM of *p*-nitrophenyl phosphate (pNPP) (New England BioLabs Inc., Ipswich, MA) was incubated in a 96-well plate in the presence of various concentrations of $CeO_2$ NPs (4.3, 8.6, 17, 34 µg/mL) in a total volume of 200 µL $H_2O$. The ability of $CeO_2$ NPs to catalyze the hydrolysis of pNPP to *p*-nitrophenyl was measured by following the increasing absorbance (405 nm) every minute for 20 min using a Spectramax 190 UV-visible spectrophotometer (Molecular Devices, Sunnyvale, CA).

*ATPase Activity Assays*

The concentration of inorganic phosphate liberated by various preparations of $CeO_2$ NPs was determined using a malachite green assay (R&D Systems, Minneapolis, MN). Nanoparticles (34 µg/mL) were added to ATP or GTP (Sigma Aldrich St. Louis, MO) (34 µg/mL) at various time points (0, 30 sec, 1 min, 2 min, 4 min, 6 min, 8 min ,10 min) at RT in 50 mM Tris buffer at pH 8.0. A phosphate standard curve was generated to enable quantitative determination of phosphate. The Malachite Green solutions were added to each well and the absorbance (620 nm) was determined using a Spectramax 190 UV-visible spectrophotometer (Molecular Devices, Sunnyvale, CA) after a 20 min incubation to stabilize the dye/$PO_4$ complex.

The concentration of inorganic phosphate liberated by various preparations of $CeO_2$ NPs was also determined using EnzCheck Phosphate Assay (Invitrogen). The EnzCheck phosphate reaction is a fast, quantitative enzymatically linked assay in which in the presence of $P_i$, the substrate 2-amino-6-mercapto-7-methylpurine riboside (MESG) is converted enzymatically by purine nucleoside phosphorylase (PNP) to ribose 1-phosphate and 2-amino-6-mercapto-7-

methyl purine. The conversion of MESG can be followed by the increase in absorbance at 360

nm. Nanoparticles (34 µg/mL) were added to varying concentrations of ATP (Sigma Aldrich St.

Louis, MO) and phosphate release followed every 30 sec for 30 min at 360 nm using a

Spectramax 190 UV-visible spectrophotometer (Molecular Devices, Sunnyvale, CA) after an

initial10 min incubation. A phosphate standard curve was generated to enable quantitative

determination of phosphate in solution. Baseline changes due to hydrolysis of phosphate from

ATP only controls was subtracted from each concentration to determine free phosphate

liberated only by addition of $CeO_2$ NPs. The kinetic parameters, $V_{max}$ and $K_m$ were calculated by

using SigmaPlot® 10 software (Systat Software, Inc., Point Richmond, CA).

*Analysis of DNA Stability in the Presence of Cerium Oxide Nanoparticles*

Preparations of nanoparticles were heated at $65^o$ C for 15 minutes to denature possible

endogenous (contaminating) DNase activity. The treated solutions were allowed to cool to

room temperature. 1 µL (500 ng) of DNA ladder (Lambda *Hind*III digestion) was added

nanoparticles in water and EDTA at a final concentration of 5 mM. Cerium oxide nanoparticle

levels were varied in the presence of the same concentration of DNA. One set of incubations

was placed at room temperature, and another was carried out at 37º C. DNA was analyzed by

agarose gel electrophoresis using a 1% agarose gel in Tris-Acetate EDTA (TAE) buffer as

previously described (156). DNA was analyzed by staining with ethidium bromide and viewed

under trans illumination with UV light.

<u>Results</u>

*Cerium Oxide Nanoparticles (CeO$_2$ NPs) Vary in Size, Shape, and Charge Depending Upon Synthesis Method*

Careful characterization of nanoparticle preparations used in a study is critical when addressing biological relevance. It is rare that the actual synthesis procedure is used as a variable. In this study we chose two types of synthesis procedures for making cerium oxide nanoparticles. These two methods have been frequently used in the literature since it has been established that biological properties vary depending upon the synthesis method (66). TEM images of CeO$_2$ NPs prepared using water-based or hexamethylenetetramine (HMT) (synthesis methods are shown in Supplementary Figure 1. In general, the water-based NPs are smaller and rounder than the HMT-based NPs which display a sharp, angular shape. This figure demonstrates that depending upon synthesis method and the various conditions during synthesis (see Materials and Methods) nanoparticles of the same core cerium oxide composition (CeO$_2$) can be very different morphologically yet the biological relevance of these differences is poorly understood.

*Physico-Chemical Properties of Cerium Oxide Nanoparticles (CeO$_2$)*

Nanoparticles in general exhibit novel surface properties that can affect their chemistry and their interaction with biological systems. Supplementary Figure 2 contains a chart outlining the physico-chemical characteristics of all CeO$_2$ NPs used throughout this study. Distribution of the hydrodynamic radius of individual particles is shown in Supplementary Figure S1A-E. Surface charge differences of water-based CNPs (CNP1 and CNP2) were estimated in dH$_2$O

suspension. The surface oxidation state ($Ce^{3+}/Ce^{4+}$ ratio) of the $CeO_2$ NPs preparations were calculated from x-ray photoelectron spectroscopy (XPS) data as described previously (157). The intensity of peaks at 880.8, 885.8, 899.3 and 903.5 eV corresponding to the cerium (III) oxidation state and intensity of peaks at 881.9, 888.4, 897.9, 901.2, 906.8 and 916.3 eV corresponding to the cerium (IV) were determined and ratios calculated. Deconvoluted XPS spectra for all nanoparticles used in this study are shown in Figure S2A-E. Fourier transform infrared spectroscopy (FTIR) spectrum of hexamethyltetramine (HMT) and HMT-CNP1 revealed residual HMT on the surface of the HMT-CNP1 as compared with water-based CNP1 (Figure S3). The level of the organic was determined to contain HMT and was estimated by calculating differential scanning calorimetry - thermogravimetric analysis (DSC-TGA) by the percentage of weight loss (158). TGA-plot of thermal decomposition of HMT present on the surface of the HMT-based HMT-CNPs is shown in Figure S4A-C.

Water-based $CeO_2$ NPs (CNP1 and CNP2) were comprised of a crystalline lattice and due to their nanometer length scale, and based on previous reports, oxygen defects at the surface are present that yield reactive sites (140). Within these sites, water-based $CeO_2$ NPs have the ability to interchange between the $3^+$ and $4^+$ oxidation state (55). Two water-based $CeO_2$ NPs exhibiting mixed $Ce^{3+}/Ce^{4+}$valence states were synthesized (81). $CeO_2$ NPs with a higher $3^+/4^+$ ratio of approximately 1.28 (CNP1) exhibit efficient superoxide dismutase (SOD) activity (55, 126) when compared to $CeO_2$ NPs with lower $3^+/4^+$ ratio of approximately 0.37 (CNP2). It should be noted that $CeO_2$ NPs with lower $3^+/4^+$ ratio (CNP2) exhibit increased catalase mimetic activity (67) as well as the ability to effectively scavenge soluble nitric oxide ($\cdot$NO) (68). HMT-based $CeO_2$ NPs (HMT-CNP1, HMT-CNP2 or HMT-CNP3) contained lower $3^+/4^+$ ratios measuring

70

0.37, 0.36, 0.32 respectively, very similar to CNP2, however their catalytic natures towards superoxide, hydrogen peroxide or ·NO has not yet been reported. HMT-CNP1 and HMT-CNP3 as synthesized contained very similar concentrations of HMT, 1.68 % and 1.78 % HMT respectively however, they differ in their shape with HMT-CNP1 morphology as polygonal and HMT-CNP3 morphology as round (Supplementary Figure 1). HMT-CNP1 differed from HMT-CNP2 in the amount of HMT present on the surface of the nanoparticles. In addition, the mean hydrodynamic ratios of all three HMT-CNP's were increased when compared to the two water-based CNP's. This becomes important when attempting to understand the biochemical properties of NPs in presence of biological molecules such as proteins. The type of biomolecule and type of interaction that nanoparticles can participate in can be preferentially affected by both size and surface properties of the nanoparticles (159).

Nanoparticles have high surface area to volume ratios and the physical properties of a nanoparticle can be dominated by the nature of the nanoparticle surface (160). The surface areas, as determined by BET, closely ranged between 71 and 118 $m^2$/g and it appears that the presence of HMT had no dramatic influence on surface area. Particle size and surface area are important features when considering *in vivo* nano-bio reactivity (161). High surface areas can also increase surface reactivity leading to catalytic activities that can be both beneficial and detrimental to cells (66). Though consisting of identical core materials, $CeO_2$, the physicochemical properties $CeO_2$ nanoparticles produced by different methods can differ extensively and have implications that must be thoughtfully considered when adapting them for use in biological systems. These material properties can affect how cells respond to nanoparticles including whether or not they exhibit toxicity.

*HMT-based Nanoparticles are More Toxic Than Water-based Cerium Oxide Nanoparticles*

The rapid development of cerium oxide nanoparticles for various applications in many

years has led to numerous studies evaluating $CeO_2$ NPs toxicity or biocompatibility. We

employed the primary cell type Human Umbilical Vein Endothelial Cells (HUVECs) as a biological

model to test toxicity in the context of human tissue. To investigate whether different particles

made using different synthesis methods can effect overt toxicity, HUVEC cells were exposed to

increasing $CeO_2$ NPs concentrations (0, 0.02, 0.08, 0.86, 8.6, 17 µg/mL) for 48 h (Figure 15). It

should be noted that the HMT-CNP NPs were extensively washed during synthesis to avoid

adsorption of background molecules of HMT onto the NPs so to prevent the residual HMT from

affecting the NPS surface chemistry or be present in the aqueous portion of the samples (See

Materials & Methods). We observed a reduced toxicity for CNP1, as previously reported (162)

(Figure 15A) with similar observations for CNP2 (Figure 15B). Even at the highest concentrations

(17 µg/mL), CNP1 and CNP2 only had modest effects on cell viability (80 %) whereas HMT-CNP1

showed a greater reduction in cell viability (70 %). However, at a ten-fold lower concentration

(0.86 µg/mL) the HMT-CNP1 begin to exhibit a derogatory effect whereas the water-based,

CNP1 and CNP2 did not (Figure 15C). To address whether the HMT concentration was

responsible for the deceased cell viability, HMT-CNP2s which contain 8.16 % HMT (Figure 15D)

were also tested and MTT results are similar to HMT-CNP1 (Figure 15C). Finally, to address if

shape of the nanoparticle was a factor in toxicity, HMT-CNP3 containing similar concentration

of HMT as HMT-CNP1 however having a rounder appearance, similar to CNP1 and CNP2

(Supplementary Figure 1), were tested. MTT results for HMT-CNP3 (Figure 15E) were again

similar to HMT-CNP1 strongly suggesting that increasing HMT concentration or shape did not

play a role in the decreased HUVEC viability of HMT-CNP1 when compared to water-based CNP1 and CNP2. Additionally, all three HMT-CNPs started to show decreased cell viability at 0.86 µg/mL concentration whereas the both CNPs do not exhibit any toxicity at the 0.86 µg/mL concentration. To rule out the decreased cell viability was due solely to the presences of the HMT solvent, we test the higher concentrations of HMT solvent only and found no toxicity to be attributed to the presence of the solvent alone (Figure 15F). The MTT assay relies upon metabolically active cells to reduce the MTT dye. Mitochondria are the cell's source of energy by producing adenosine-5'-triphosphate (ATP) through oxidative phosphorylation. This led us to determine if intracellular ATP levels of HUVECs exposed to various preparations of $CeO_2$ NPs would be affected.

*Exposure to HMT-CNP Leads to Decreases in Intracellular ATP Levels*

To analyze if there was a link between exposure to HMT-CNPs and reduced HUVEC viability, we treated HUVECs with increasing $CeO_2$ NPs concentrations (0, 0.02, 0.08, 0.86, 8.6, 17 µg/mL) and measured ATP levels in cell lysates at 48 h as an alternative to MTT reduction. At the higher two exposure concentrations, both CNP1 (Figure 16A) and CNP2 (Figure 16B) had diminished ATP levels (85-68%, respectively) as compared to controls. However, HMT-CNP1 treated cells showed dramatically reduced ATP levels at a ten-fold lower exposure of 0.86 µg/mL (42 %) Figure 16C. We found similar decreases at the 0.86 µg/mL concentrations using HMT-CNP2 (Figure 15D) and HMT-CNP3 (Figure 16E). Similar to our MTT results, HMT solvent alone had no effect on ATP concentration. Thus exposure to HMT-CNPs at lower doses resulted in a significant reduction in ATP levels than CNP1 or CNP2 exposure.

HMT-CNP1 aggregate in exposed HUVEC cells. Cerium oxide nanoparticles are readily internalized by cells due to their small size however to visualize nanoparticles, high resolution transmission electron microscopy or a fluorescent tag is normally utilized (46, 98). Since the HMT-CNPs all had similar toxicities (Figures 15 & 16) we chose to use HMT-CNP1 for additional in depth comparisons with CNP1 and CNP2. Untreated HUVECs as well as CNP1 and CNP2 (8.6 µg/mL) treated HUVECs exhibited no visible changes (Figure 17A - C). Strikingly, HUVECs treated with HMT-CNP1 at the same concentration exhibited visible changes in morphology with bright field microscopy (Figure 17D). The addition of a nuclear stain helped us to localize their subcellular location and highlight the presumed HMT-CNP1's aggregation in HUVECs. The ability to see nanoparticles using unaided microscopy techniques is uncommon. In the study by Yokel, *et. al.*, similar $CeO_2$ NPs agglomerations were seen in light microscope images of spleen of rats treated with 250 mg/kg $CeO_2$ NPs after only 1 h (163). These intracellular accumulations do not appear to have a specific sub-cellular localization and led us to probe the biological interaction of our $CeO_2$ NPs with HUVECs.

*Confocal Laser Scanning Microscopy (CLSM) Images Reveal Perinuclear Aggregation of HMT-CNP in HUVECs*

It has been reported that $CeO_2$ NPs dispersed directly into cultures media may form aggregates on cells (164). To confirm whether the dense granules visualized by bright field microscopy were actually HMT-CNP1 aggregates within the cell and not simply associated outside the cells, HUVECs were treated for 24 h with nanoparticles, washed repeatedly, trypsinized and seeded onto glass coverslips for 4 h (to allow for cell attachment) before

fixation. Using immunocytochemistry we labeled the plasma membranes of HUVECs with wheat germ agglutinin (WGA) with fluorescein conjugate and took simultaneous fluorescent and bright field imaging using confocal microscopy. Untreated, CNP1 and CNP2 (8.6 µg/mL) treated HUVECs under bright field and merged channels show no evidence of nanoparticle aggregation (Figure 18A & B). By contrast, HUVECs treated with HMT-CNP1 (8.6 µg/mL) showed a robust increase in agglomerated, granular material in both the bright field and merged channels (Figure 18D). This aggregation becomes even more evident in HUVECs treated with a higher concentration of HMT-CNP1 (86 µg/mL) (Figure 19). Notably, CLSM highly suggested that the apparent dense granules were in fact intracellular HMT-CNP1s and their subcellular location was peri-nuclear. The subcellular localization is in agreement with previous studies testing $CeO_2$ NPs using *in vitro* cell culture models (165).

*HMT-CNP1 are Transported into HUVECs More Efficiently Than Water-based Cerium Oxide Nanoparticles*

Uptake of nanomaterial varies vastly between materials tested and cell types (166, 167). Based upon the morphological changes in HUVECs treated with HMT-CNP1 easily seen by light microscopy, we incubated HUVECs with increasing concentrations (0, 1.7, 8.6, 17, 86 µg/mL) of CNP1, CNP2 and HMT-CNP1 and harvested cells after 24 h. We used inductively coupled plasma mass spectrometry (ICP-MS) to determine the concentration of cerium inside the cells. Interestingly, CNP2 uptake was more efficient than CNP1 uptake and cellular uptake of HMT-CNP1 was greatly increased in HUVECs at every concentration tested (Figure 20). Taken together, this clearly shows that HMT-CNP1s are readily internalized by HUVEC cells and this

could be a contributing factor as to the toxicity previously observed in a *Caenorhabditis elegans* model (65). We tested CNP1 and HMT-CNP1 in a comparable model system, *Drosophila melanogaster* and found that CNP1 were not toxic and HMT-CNP1 NPs were only marginally toxic at a concentration of 860 µg/mL (Figure 21). Thus, uptake must be taken under consideration when determining toxicity. Our data shows that the CNP2 are also readily taken up and yet they have not shown toxicity at the same level as HMT-CNP1 in HUVECs. It should be noted that CNP2 exhibit catalase mimetic activity and scavenge ·NO (67, 68) and therefore these catalytic activities could be at the basis for their lack of toxicity (98).

*CeO$_2$ NPs with Increased Surface 4+ Character Exhibit Phosphatase and ATPase Activity*

Phosphorylation and dephosphorylation play significant roles signaling, energy transfer and utilization within cells. Phosphate ester hydrolysis of biological molecules by CeO$_2$NPs would have important implications in their potential toxicity. In order to test any potential phosphatase activity of CNPs and HMT-CNPs, we first used *p*-nitrophenyl phosphate (pNPP) as a screening substrate (168). This assay uses an artificial chromogenic substrate that is readily hydrolysed by phosphatases and allowed us to detect any potential phosphatase mimetic activity. We found that CNP2 as well as HMT-CNP1 were able to de-phosphorylate pNPP whereas CNP1 did not (Figure 22A). These results agreed with previous observations for water-based ceria (168). Our initial results strongly suggested that cerium oxide nanoparticles with increased 4+ shared a similar catalytic activity. In order to corroborate the phosphatase mimetic activity and possibly explain the mechanism of cell death, we used ATP as the substrate and looked at free phosphate production using two different assays. Our results show again

76

that CNP1 did not act as a phosphatase using ATP for the substrate (Figures 22A and 23E). $SiO_2$

NPs, a metal oxide NP of similar size was used as a negative control and also did not cause the

release of phosphate (Figure 22A and B). However, CNP2 and HMT-CNP1 did release phosphate

from ATP with CNP2 showing a robust activity (Figure 22B). To obtain quantitative information

on the effect of CNP2 and HMT-CNP1, we determined the apparent $K_m$. Experimentally, we

followed the kinetics of $P_i$ released in a continuous reaction and determined the initial rates of

free phosphate release from 34 µg/mL NPs in the presence of increasing concentrations of ATP

(Figure 23A-D). The apparent $K_m$ for HMT-CNP1 was 39.9 ± 8.2 µM. CNP2 were efficient

phosphatases at lower substrate concentrations however when approaching physiological

concentrations of ATP, CNP2s reached saturation and rates declined however CNP2 apparent

$K_m$ was determined to be 48.4 ± 10.6 µM. We compared the kinetic behavior of $CeO_2$ NPs with

an established, physiologically relevant ATPase, dynein ATPase which has reported $K_m$ of 20 µM

(169). We chose to compare to a motor protein since they have multiple active sites (170),

which is similar to nanoparticles having numerous engineered vacancies for  reactions to occur.

In addition, dynein ATPase is located in the cytoplasm, along the same location as we saw the

aggregation of HMT-CNP1 NPs (Figures 17 and 18). However, $CeO_2$ NPs differ from dynein

ATPase in terms of turnover rate. Dynein APTase $V_{max}$ is 0.22 µM/s (169) however the $V_{max}$

values for CNP2 and HMT-CNP1 were 0.017 nmol/ min and 0.024 nmol/min (respectively).

Collectively, these results suggest that $CeO_2$ NPs with increased level of 4+, regardless of their

synthesis method, are competent phosphatases. They were able to hydrolyze various

substrates including pNPP (Figure 22A), ATP (Figure 22B and Figure 23A-D) and GTP (data not

shown). However, HMT-CNP1 is more readily taken up by cells so the concentration of the

catalyst is higher in cells than those exposed to CNP2. The combination of uptake and catalytic activity must be considered when determining toxicity.

*Synthesis Method Determines Surface Catalytic Character of CeO$_2$ NPs*

Having identified ATPase as a critical catalytic character for HMT-CNPs in terms of toxicity, we tested these preparations of CeO$_2$ NPs to assess the effect of synthesis on their catalytic activity at a broader level. To evaluate the potential catalytic activities we tested HMT-CNP1s for their ability to scavenge ·NO or to act as SOD or catalase mimetics. Unlike CNP1 or CNP2, HMT-CNP1s did not show any reactivity ·NO (Figure 24A), superoxide (Figure 24C), and hydrogen peroxide (Figure 24D).

Reduction of Ce$^{4+}$ to Ce$^{3+}$ causes oxygen vacancies or defects on the surface of the crystalline lattice structure of the particles, generating a cage for redox reactions to occur (125). It has been established that the specificity of some of the catalytic activities depend upon the ratio of Ce$^{3+}$/Ce$^{4+}$ (68, 94). Table 2 chart highlights water-based synthesis method of CeO$_2$ NPs leads to unique physical and catalytic characteristics that are not found in CeO$_2$ NPs synthesized by HMT-based method. In addition, these catalytic activities seem to correlate with the 3+/4+ ratio, specifically NPs with more Ce$^{4+}$ displaying phosphatase activity. This reiterates the need for the careful characterization of nanoparticle preparations and a thorough understanding of their catalytic activities.

Discussion

The toxicology and surface reactivity of $CeO_2$ nanoparticles synthesized by two different methods were compared in this work in order to elucidate the mechanisms behind the varied observations with biological models in the current literature. Due to the small size of NPs, TEM is an appropriate technique to use for visualizing NPs inside cells, since light microscopy fails to resolve NPs at a single particle level (171). However, HMT-CNP1 are readily taken up by HUVECs and their aggregation was visible using conventional light microscopy techniques (Figures 5 and 6). An increase in the uptake of HMT-CNP1 certainly could have a negative effect on a HUVEC cell's metabolism. The increased uptake may be due to electrostatic interactions, given the fact that the zeta potential of HMT1 and CNP2 are more positive than CNP1 (Figure 2.) A positively charged particles would more readily be taken up by a negatively charged cell. We also observed significant aggregation of HMT-CNP1 in intracellular vesicles in HUVEC cells (Figures 5& 6). It has been reported that, under hydrothermal conditions, HMT can promote the formation of well-aligned and highly crystallized ZnO nanorods and nanowires when a ZnO seed layer was adopted (172). So, it is certainly possible that similar nucleation events may exist in our current HMT-CNP system as well. However, the CNP2 are also readily taken up but do not aggregate (Figures 5 & 6) and yet they do not show the level of toxicity that the HMT-CNP1 demonstrated. CNP2, though also taken up by HUVECS (Figure 7), also are catalase mimetics (67) and scavenge soluble ·NO (68). Therefore CNP2s may reduce the level of $H_2O_2$ as well reduce the downstream damage caused by excessive ·NO. Peroxynitrite ($ONOO^-$), formed by the diffusion limited inter-action of superoxide ($O_2^{\cdot-}$) with ·NO, is a potent oxidant that can lead to the detrimental, 3-nitrotyrosine, post-translational modification of tyrosine residues in

79

proteins (34) as well oxidize lipids and DNA. There are efficient cellular means reduce both $O_2^{\cdot -}$

and $\cdot NO$ during normal cellular metabolism however in a diseased state, an imbalance can

occur due leading to the cells inability to remove excess $O_2^{\cdot -}$ and $\cdot NO$. Therefore, decreasing the

precursors of the strong oxidizer $ONOO^-$ would reduce tissue damage in all the major

biomolecules. It should be noted that when cells are cultured in 21 % $O_2$, cells in culture are

generally seen as being under constant oxidative stress (173).

The intercellular location of the HMT-CNP1 may also play a role in their toxic nature. We

found the HMT-CNP1 aggregated in a peri-nuclear location (Figure 5) aligning with the

endoplasmic reticulum (ER) as visualized by wheat germ agglutinin (WGA) antibody (Figure 6).

Since this antibody labels glycoproteins, we see an increase of signal from the ER and Golgi, the

location in the cells where sugars are incorporated into proteins in cells, in all cell images.

Disrupted energy metabolism leads to increased ROS and therefore increased free radicals and

the resulting downstream damage of protein modification, lipid peroxidation and DNA damage

(174). The peri-nuclear location of the HMT-CNP1s may interfere with normal cellular

processes, such as protein post-translational modifications (*i.e.* phosphate) or energy

metabolism, leading to adverse cellular responses. In addition to the location of HMT-CNP1

affecting the cell, their catalytic ATPase ability would have a further negative affect on cell

survival due to decreased ATP levels. This two-fold hit on cells by HMT-CNP1 might explain the

drastic difference in toxicity as compared to CNP1 or CNP2.

Nanoparticles in general exhibit novel surface properties that can affect their chemistry

and their interaction with biological systems. In addition, we have demonstrated that synthesis

methods of $CeO_2$ NPs can further affect surface properties. For non-redox active

nanoparticles, varying the synthesis procedure may not have a substantial effect but our data demonstrates that it is not the case when dealing with redox active nanomaterials. A slight change in physico-chemical properties (Figure 2) can give you a vast difference in the redox properties of the nanomaterials (Figure 9). During the synthesis of water-based $CeO_2$ NPs, oxygen vacancies are created at the surface yielding reactive sites. Within these sites, $CeO_2$ NPs have the ability to interchange between the 3+ and 4+ oxidation state (55). The cerium atoms on the surface of these vacancies are in the 3+ state (125). Kuchma *et. al*. report that the phosphatase activity appears to be dependent upon the Cerium(III) sites (168). It is possible that the ATPase activity seen in the CNP2 and HMT-CNP1 may be due to a nucleophile attraction of the $Ce^{3+}$ and the terminal phosphate on an ATP molecule. Paradoxically, CNP1, which have more vacancies on the surface are not phosphatases. Additionally, there are phosphate esters on the backbone of nucleic acids. It is known that lanthanide ions effectively hydrolyze DNA and RNA (175) with $Ce^{IV}$ ions being the most active for DNA (176). We tested if $CeO_2$ NPs with varying ratios of $Ce^{3+}/Ce^{4+}$ would be able to hydrolyze other types of phosphate bonds. We exposed DNA to increasing concentrations of CNP1, CNP2 and HMT-CNP1 ranging from 0, 86, 172, 430 μg/mL at both room temperature and 37° C. There was no apparent change in the sizes of the DNA (Supplementary Figure 3). Although CNP2 and HMT-CNP1s act as phosphatase mimetics, the phosphate diester groups on DNA remains intact in the presence of these NPs and therefore $CeO_2$ NPs are not nuclease mimetics. $CeO_2$ NPs exhibit specificity towards phosphate ester linkages and the mechanism of hydrolysis will need to be experimentally determined to understand this apparent specificity.

The study of the chemical and biological properties of $CeO_2$ NPs has expanded recently. Although most of the focus has been on the ability of these materials to reduce reactive oxygen and nitrogen species in biological systems (46), there are reports that claim that nanoceria are toxic. Unfortunately, the material synthesis methods used are not always significantly reported and it is likely that these observed toxicities are the result in the variations of synthesis methods. The $CeO_2$ NPs synthesized in HMT resulted in different surface chemistry which resulted in different catalytic activities than the water-based NPs. The increased uptake and phosphatase/ATPase activity of HMT-CNP1 may underlie their toxicity. With the recent burgeoning growth of the use of $CeO_2$ NPs as potential therapeutics, synthesis method and surface chemistries must be emphasized.

**Figure 15: Cell viability of HUVECs exposed to various preparations of CeO$_2$ NPs.**

HUVEC cells were exposed to increasing CeO$_2$ NPs concentrations (0, 0.02, 0.08, 0.86, 8.6, 17 µg/mL). A) CNP1. B) CNP2. C) HMT-CNP1. D) HMT-CNP2. E) HMT-CNP3. Cell viability was determined by dividing the absorbance of treated samples to untreated controls and reported as a percentage of control cells. The mean of at least 4 independent cultures is plotted with standard deviation as error.
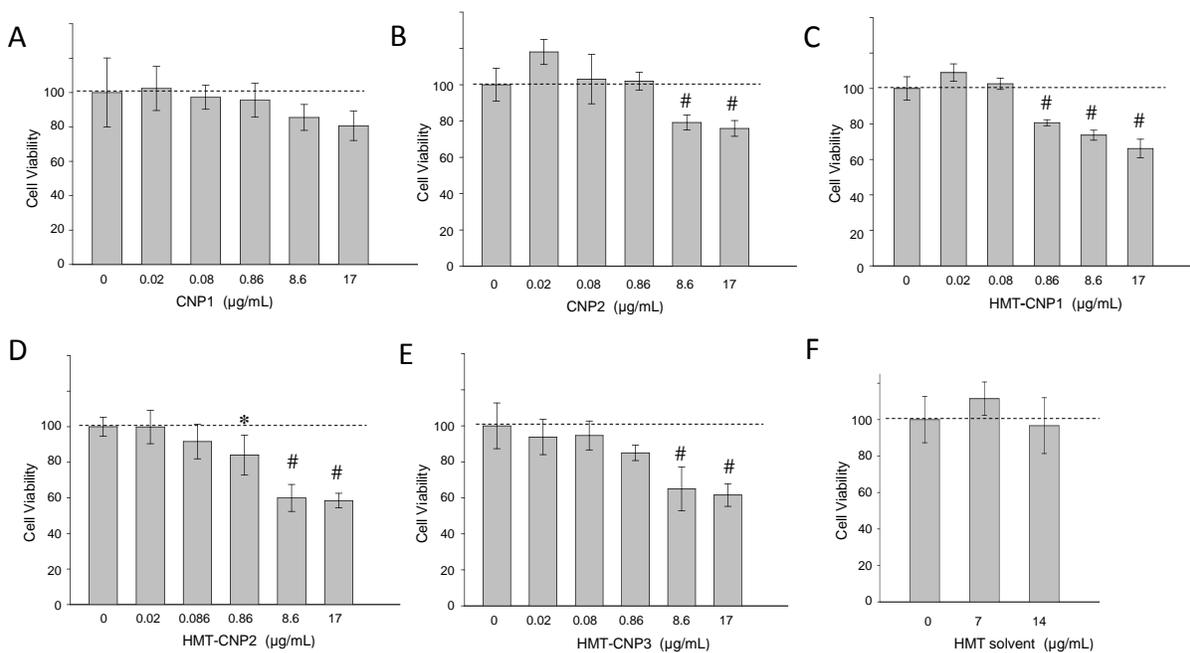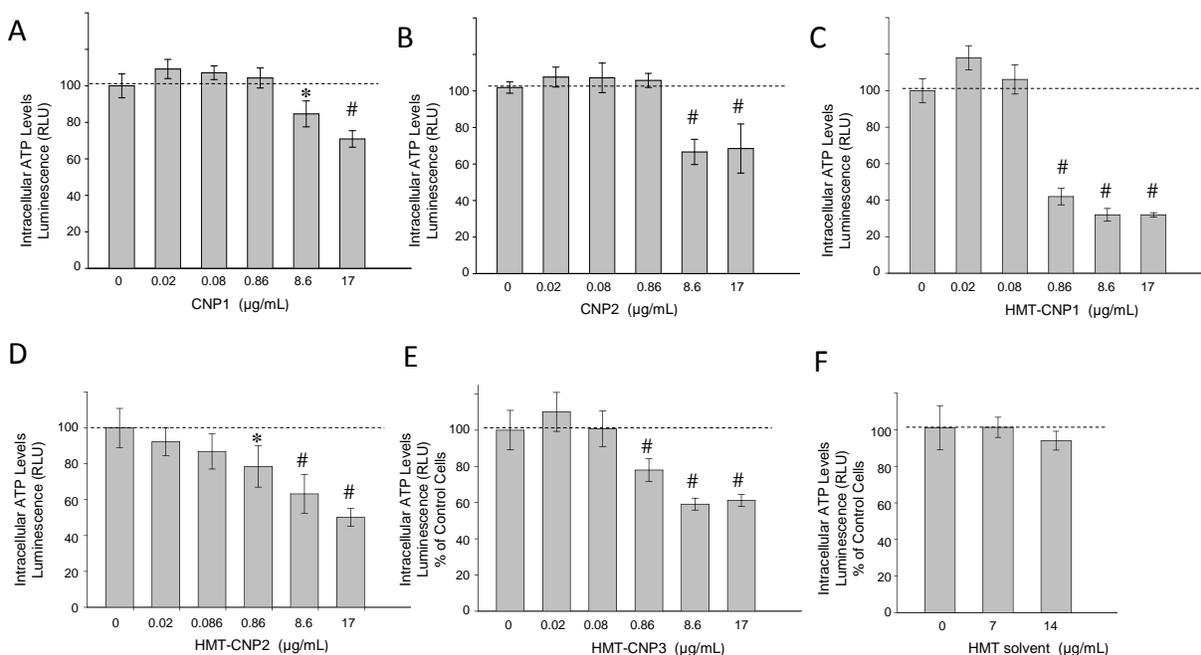
**Figure 16: Intercellular ATP levels of HUVECs exposed to various preparations of CeO$_2$ NPs.**

HUVEC cells were exposed to increasing CeO$_2$ NPs concentrations (0.02, 0.08, 0.86, 8.6 17 μg/mL). A) CNP1. B) CNP2. C) HMT-CNP1. D) HMT-CNP2. E) HMT-CNP3. ATP level was determined by dividing the luminescence of treated samples to untreated controls and reported as a percentage of control cells. The mean of at least 4 independent cultures is plotted with standard deviation as error. *, $p \leq 0.05$, #, $p \leq 0.001$.
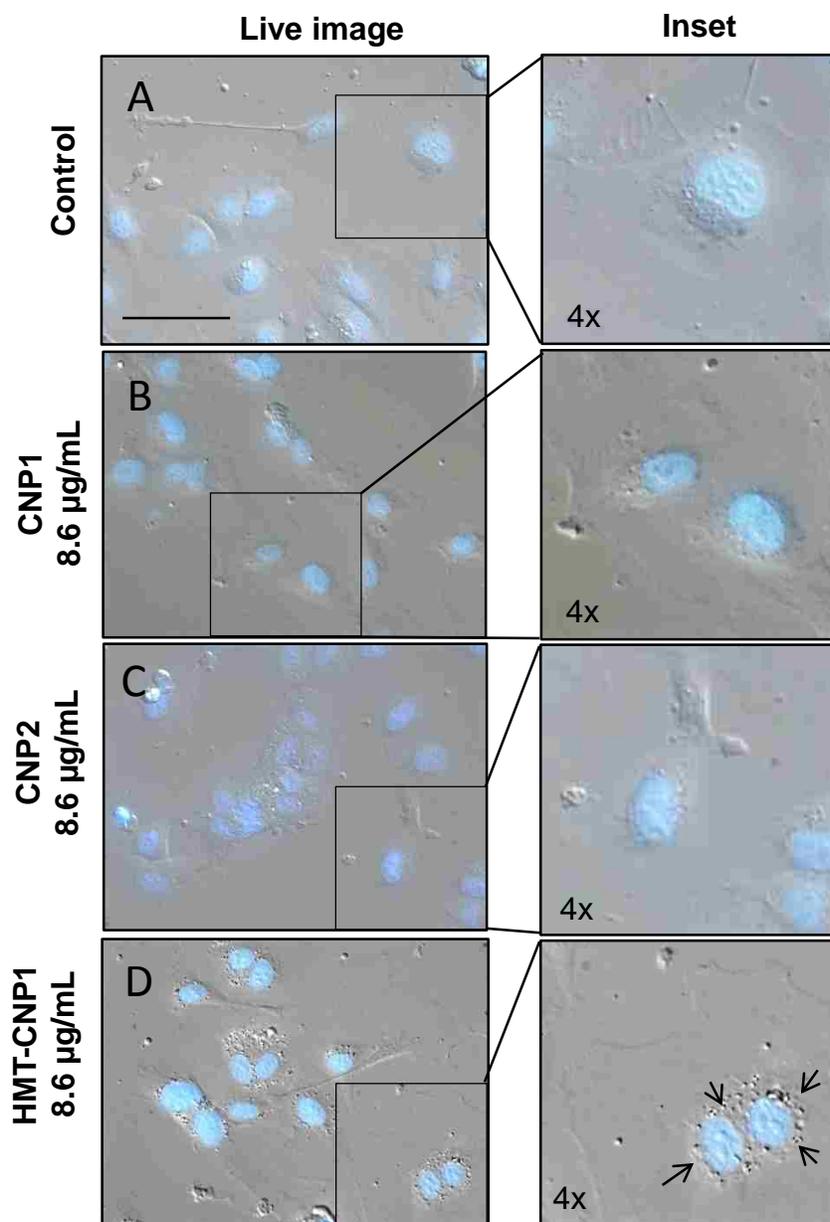
**Figure 17: Live cell examination of HUVEC cells exposed to HMT-CNP1.**

HUVEC cells were exposed to 8.6 µg/mL CeO$_2$ NPs for 20 h. A) Control cells. B) CNP1. C) CNP2. D) HMT-CNP1. Hoescht dye was added just before imaging to show location of nuclei. Representative images feature 4x zoom of region of interest. Scale bar = 50 µm.
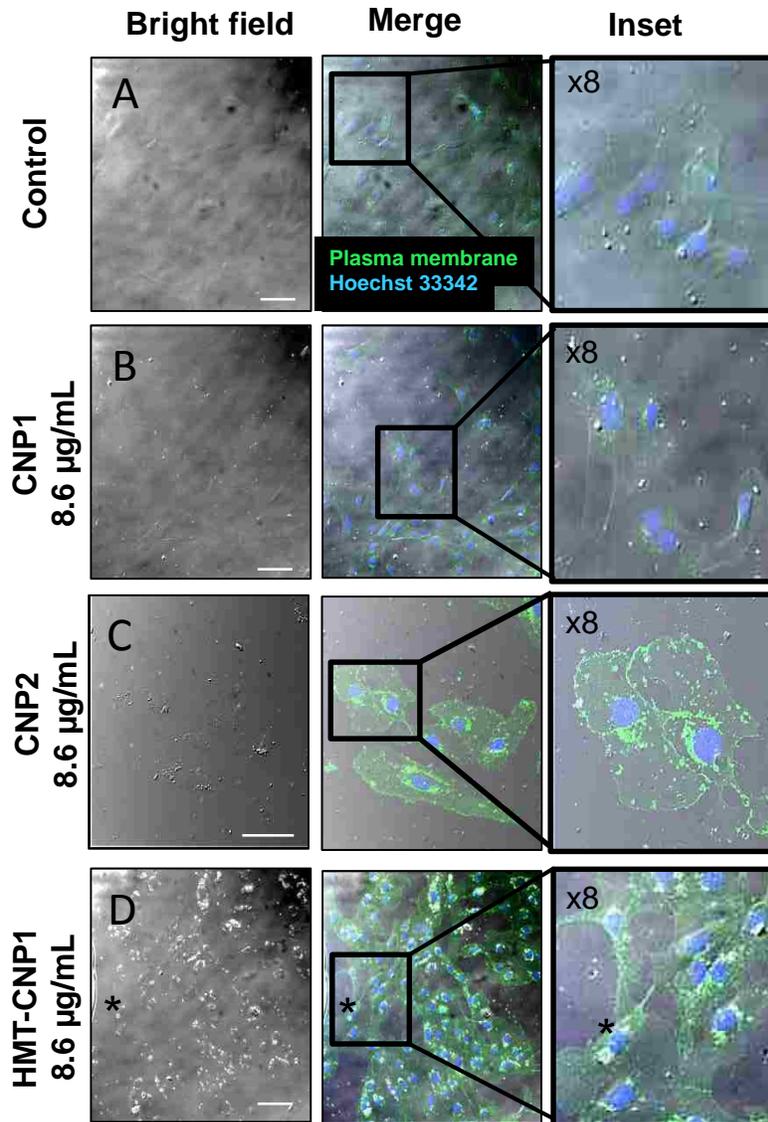
**Figure 18: Intracellular aggregation of HMT-CNP1 as viewed by confocal laser scanning microscopy (CLSM).**

Cells were exposed to nanoparticles for 24 h, washed, trypsinized and seeded onto glass coverslips for 4 h (to allow for attachment), fixed and labeled with antibody for identification of plasma membranes (green channel) and Hoechst 33342 (blue channel) for identification of nuclei. A) Control/no treatment B) 86 μg/mL CNP1 C) 86 μg/mL CNP2 D) 86 μg/mL HMT-CNP1. Scale bar = 50 μM. Asterisk follows representative region of HMT-CNP1 aggregation.
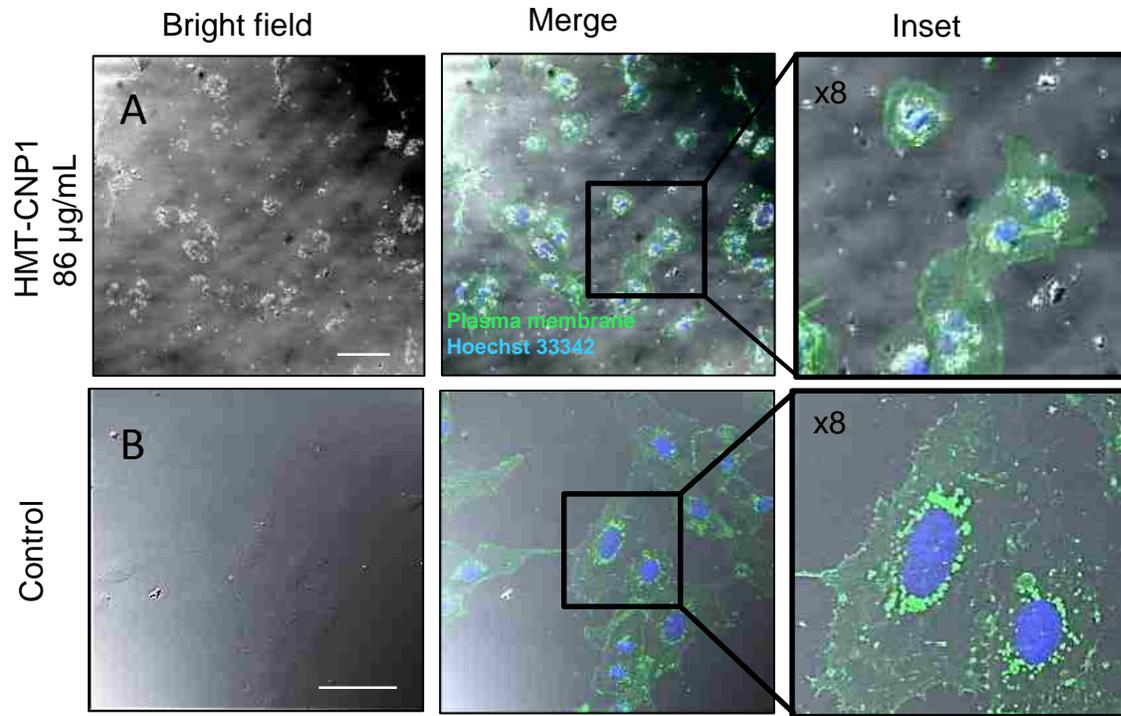
**Figure 19: CLSM images of HUVECs showing intracellular aggregation after exposure to 86 µg/mL HMT-CNP1.**

Cells were treated for 24 h with nanoparticles, washed, trypsinized and seeded onto glass coverslips for 4 h (to allow for attachment), fixed and then labeled with WGA for identification of plasma membranes (green channel) and Hoechst 33342 (blue channel) for identification of nuclei. A) 86 µg/mL HMT-CNP1. B) Control/no treatment. Scale bar = 50 µM.
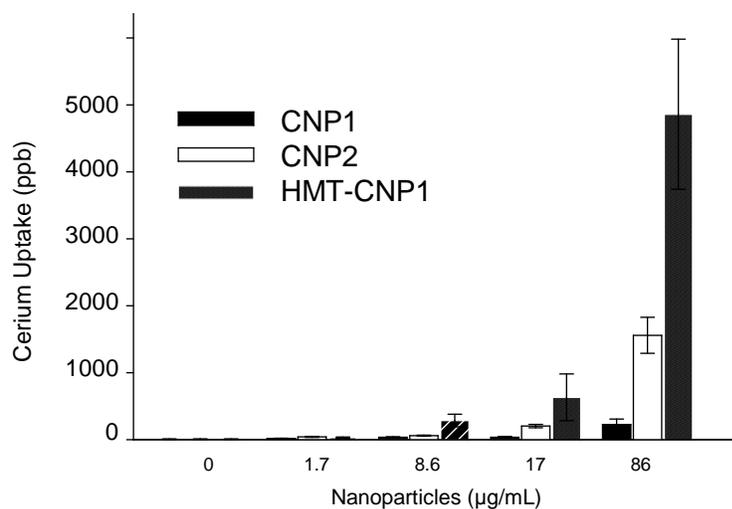
**Figure 20: Increased uptake of HMT-CNP1 as measured by ICP-MS.**

HUVEC cells were incubated with various $CeO_2$ NPs for 24 h, washed two-times to remove extracellular nanoparticles, collected by typsination and washed with PBS again to remove excess media and particles which may be adsorbed on the surface of the cells. The concentration of cerium inside cells was measured by ICP-MS as described in methods.
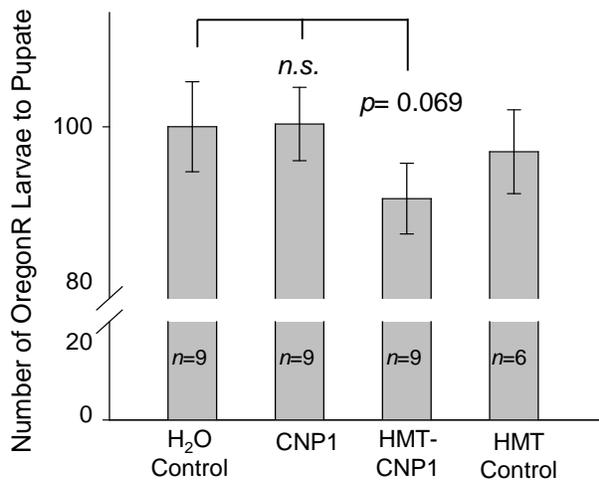
**Figure 21: Exposure of Drosophila melanogaster to CeO$_2$ NPs does not significantly alter development.**

Oregon-R (OR) wild-type larvae were fed JazzMix® supplemented with 86 µg/mL of CeO$_2$ NPs or appropriate solvent control. Wild-type larvae survival to reach pupariation was tabulated. Minimum 50 larvae per condition per experiment. $p$=0.069 by One way ANOVA followed by Tukey Post Hoc Tests.
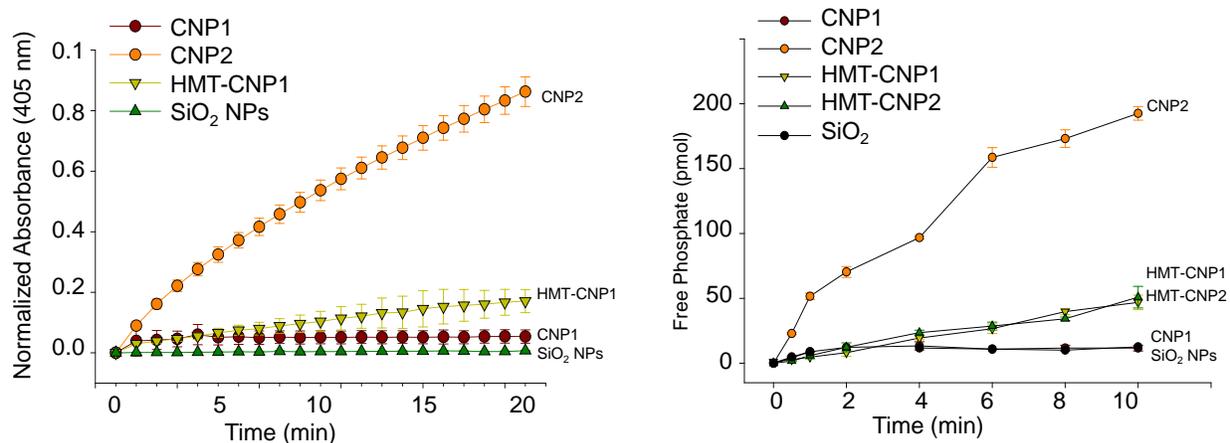
**Figure 22: p-nitrophenyl phosphate (pNPP) and ATP hydrolysis by various preparations of CeO₂ NPs.**

(A) 34.4 µg/mL CeO$_2$ NPs were incubated with pNPP and conversion to *p*-nitrophenyl was measured by following its absorbance at 405 nm. (B) Free phosphate released by NPs was quantified by malachite green assay using 200 µM ATP as substrate comparing 34.4 µg/mL of indicated nanoparticles in 50 mM Tris buffer at pH 8.0. Traces were recorded using Spectra Max 190 spectrophotometer. Graphs are representative of 3 or experiments.
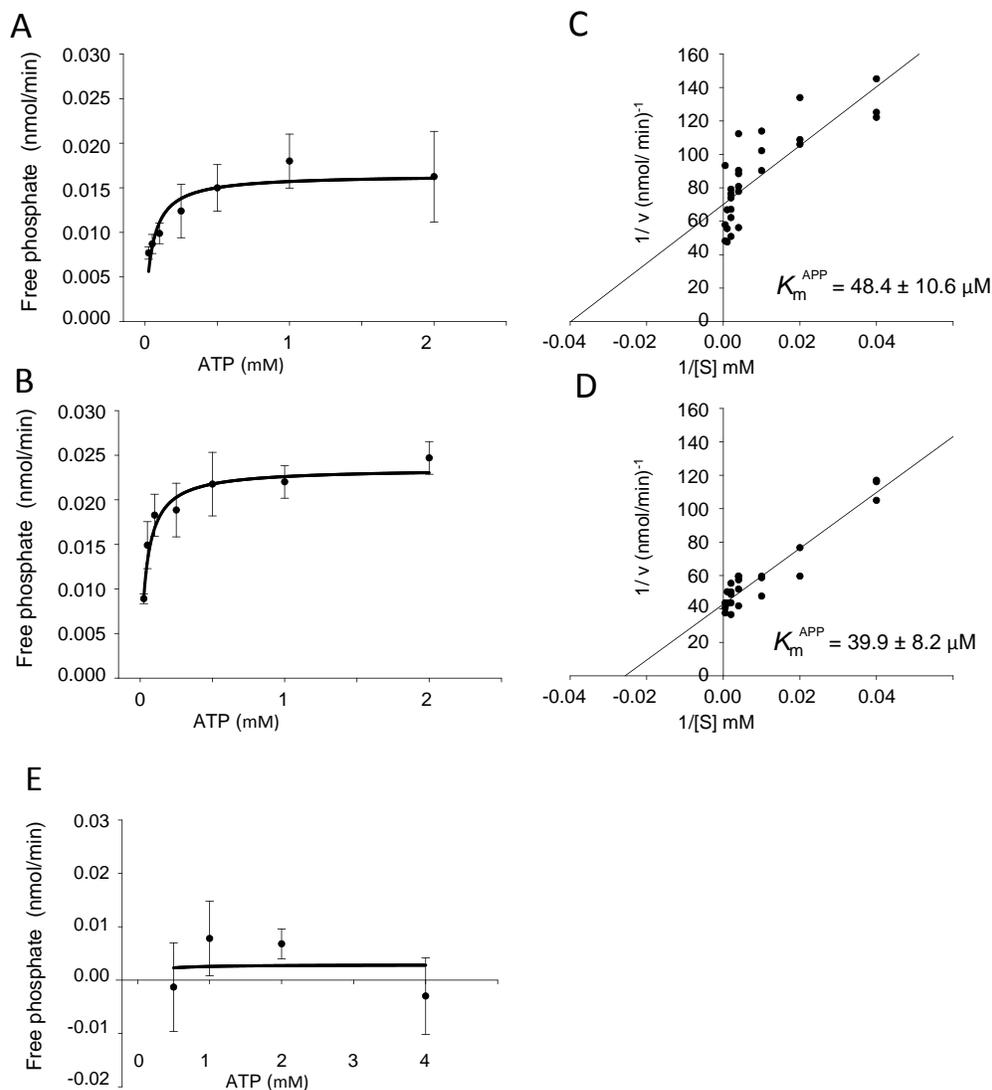
**Figure 23: CNP2 and HMT-CNP1s exhibit significant ATPase activity at physiological relevant concentrations of ATP.**

ATPase activity of $CeO_2$ NPs was quantified by measuring phosphate released with EnzCheck® phosphate assay using varying concentrations of ATP with 34 µg/mL NPs. (A) CNP2 (B) HMT-CNP1 (E) CNP1. Line plot is representative of 3 or more experiments. Double reciprocal plots of ATPase activity of (C) CNP2 and (D) HMT-CNP1, with ATP as substrate while keeping constant the concentration of NPs (34 µg/mL).
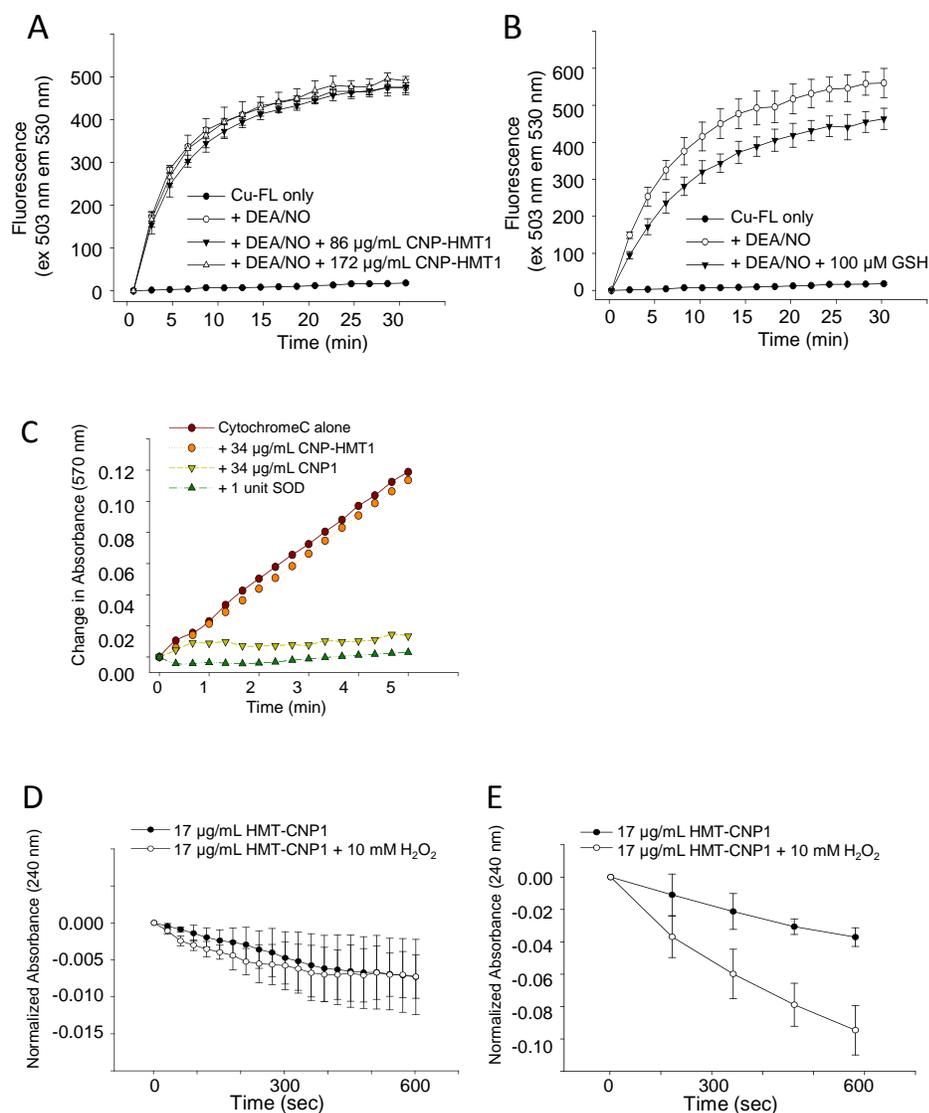
**Figure 24: CNP-HMT1 do not exhibit the ·NO scavenging, SOD mimetic or catalase mimetic of CNP1 and CNP2.**

A&B) Fluorescence emission was monitored at 530 nm upon excitation at 503 nm in the presence of the ·NO generator, 100 µM DEA/NO (Dowding et.al., ChemComm2012). A) Scavenging of ·NO in presence of HMT-CNP1 at concentrations indicated. B) Scavenging of ·NO in the presence of 100 µM Glutathione (GSH). C) Ferricytochrome C reduction was followed spectroscopically by measuring increase in absorbance at 550 nm (Korvics et. al., ChemComm 2007). SOD = superoxide dismutase. D&E) Hydrogen peroxide concentration was followed by changes in absorbance of the reaction monitoring absorbance at 240 nm (Pirmohamed et. al., ChemComm 2010). D) Reduction of H2O2 concentration in the presence of HMT-CNP1.  E) Reduction of H2O2 concentration in the presence of CNP2. Graphs are representative of 3 or more experiments.

**Table 2: Synthesis method determines surface character and catalytic activities of CeO$_2$ NPs.**

| Catalytic activity | Assay | CNP1 | CNP2 | HMT-CNP1 | SiO$_2$ |
|---|---|---|---|---|---|
| **Phosphatase** | pNPP | no | yes | yes | no |
| **ATPase** | Malachite Green | no | yes | yes | no |
| | ENZCheck | no | yes | yes | n/d |
| **·NO Scavenger** | CuFl assay | no (68) | yes (68) | no | no (68) |
| **Catalase Mimetic** | UV-visible | no (177) | yes (177) | no | no |
| **SOD Mimetic** | Cytochrome C | yes (56) | no (56) | no | no |

Various properties of CeO$_2$ NPs have been tested for their ability to exhibit SOD mimetic, catalase mimetic, ·NO scavenging, phosphatase or ATPase activities.

# APPENDIX A: COPYRIGHT PERMISSIONS

Dear Janet

The Royal Society of Chemistry (RSC) hereby grants permission for the use of your paper(s) specified below in the printed and microfilm version of your thesis. You may also make available the PDF version of your paper(s) that the RSC sent to the corresponding author(s) of your paper(s) upon publication of the paper(s) in the following ways: in your thesis via any website that your university may have for the deposition of theses, via your university's Intranet or via your own personal website. We are however unable to grant you permission to include the PDF version of the paper(s) on its own in your institutional repository. The Royal Society of Chemistry is a signatory to the STM Guidelines on Permissions (available on request).

Please note that if the material specified below or any part of it appears with credit or acknowledgement to a third party then you must also secure permission from that third party before reproducing that material.

Please ensure that the thesis states the following:

*Reproduced by permission of The Royal Society of Chemistry*

and include a link to the paper on the Royal Society of Chemistry's website.

Please ensure that your co-authors are aware that you are including the paper in your thesis.

Regards

Gill Cockhead
Publishing Contracts & Copyright Executive

Gill Cockhead (Mrs), Publishing Contracts & Copyright Executive
Royal Society of Chemistry, Thomas Graham House
Science Park, Milton Road, Cambridge CB4 0WF, UK
Tel +44 (0) 1223 432134, Fax +44 (0) 1223 423623
http://www.rsc.org

-----Original Message-----
From: Janet M Dowding [mailto:jdowding@mail.ucf.edu]
Sent: 14 September 2012 18:12
To: CONTRACTS-COPYRIGHT (shared)
Subject: Website Email: Copyright permission to include data from publication in my PhD dissertation

To: Contracts
This Email was sent from the following RSC.ORG page:

Dear ChemComm,

I am in the process of compiling my PhD dissertation and would like to include the data that was published in your journal earlier this year entitled "Cerium oxide nanoparticles scavenge nitric oxide radical (NO). DOI: 10.1039.c2cc30485f. I require copyright permission. Please let me know how to proceed.

Thank you for your help!

Janet Dowding

Membership No. :

# APPENDIX B: CHAPTER 4 SUPPLEMENTARY FIGURES
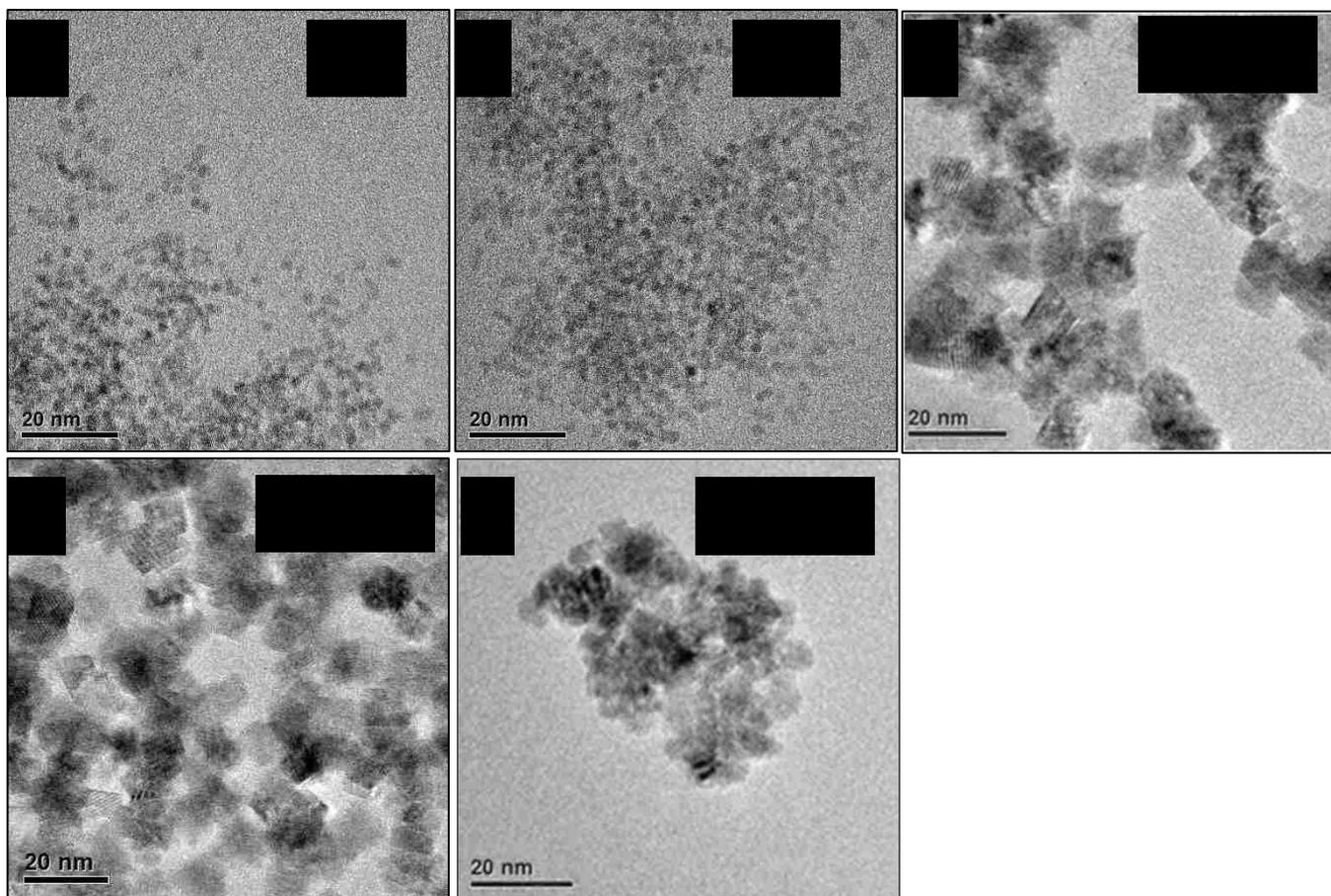
**Supplementary Figure 1: Size, shape, and morphology variation of Cerium Oxide Nanoparticles (CeO$_2$) NPs synthesized by two different synthesis methods.**

TEM images of CeO$_2$ NPs prepared using water-based (A & B) or solvent HMT (C – E) synthesis methods.  A) CNP1. B) CNP2. C) HMT-CNP1. D) HMT-CNP2. E) HMT-CNP3.

| Particle Characteristics | CNP1 | CNP2 | HMT-CNP1 | HMT-CNP2 | HMT-CNP3 |
|---|---|---|---|---|---|
| Morphology | round | round | polygonal | polygonal | round |
| Crystalline property | crystalline fluorite structure | crystalline fluorite structure | crystalline fluorite structure | crystalline fluorite structure | crystalline fluorite structure |
| Size (TEM) (nm) | 3-5 | 5-8 | 10-15 | 10-15 | 8-10 |
| Hydrodynamic radii (nm) | 30.84 ±2.8 | 69.26 ±4.5 | 147.70 ±6.4 | 83.56 ±3.2 | 129.20 ±4.1 |
| Zeta potential (mV) | 18.6 ±0.6 | 30.2 ±1.5 | 34.6 ±1.7 | 38.6 ±2.3 | 36.7 ±2.1 |
| Hexamethyltetramine (% wt) | - | - | 1.68 ±0.2 | 8.16 ±0.7 | 1.78±0.3 |
| Surface $Ce^{3+}/Ce^{4+}$ ratio | 1.28 | 0.37 | 0.37 | 0.36 | 0.32 |
| BET ($m^2$/g) | 92 | 102 | 86 | 71 | 118 |

**Supplementary Figure 2: Physico-chemical properties of cerium oxide nanoparticles (CeO$_2$) prepared by water-based or HMT-based method.**

# REFERENCES

1.    Harman D (1996) Aging and disease: extending functional life span. (Translated from eng) *Annals of the New York Academy of Sciences* 786:321-336 (in eng).
2.    Harman D (1956) Aging: a theory based on free radical and radiation chemistry. (Translated from eng) *Journal of gerontology* 11(3):298-300 (in eng).
3.    Ryter SW, Kim, Hong Pyo, Hoetzel, Alexsander, Park, Jeohg W., Nakahira, Kiichi, Wang, Xue, Choi, Augustine M.K., (2007) Protective Functions of Heme Oxygenase-1 and Carbon Monoxide in the Respiratory System. *Antioxidants & Redox Signaling* 9(1):49-89.
4.    Mates JM, Pérez-Gómez C, & De Castro IN (1999) Antioxidant enzymes and human diseases. *Clinical Biochemistry* 32(8):595-603.
5.    Knepler JL, Jr*., et al.* (2001) Peroxynitrite causes endothelial cell monolayer barrier dysfunction. (Translated from eng) *American journal of physiology* 281(3):C1064-1075 (in eng).
6.    Vivekananthan DP, Penn MS, Sapp SK, Hsu A, & Topol EJ (2003) Use of antioxidant vitamins for the prevention of cardiovascular disease: meta-analysis of randomised trials. (Translated from eng) *Lancet* 361(9374):2017-2023 (in eng).
7.    Ku HH, Brunk UT, & Sohal RS (1993) Relationship between mitochondrial superoxide and hydrogen peroxide production and longevity of mammalian species. (Translated from eng) *Free radical biology & medicine* 15(6):621-627 (in eng).
8.    Sharpe MA, Ollosson R, Stewart VC, & Clark JB (2002) Oxidation of nitric oxide by oxomanganese-salen complexes: a new mechanism for cellular protection by superoxide dismutase/catalase mimetics. (Translated from eng) *The Biochemical journal* 366(Pt 1):97-107 (in eng).
9.    Calabrese V*, et al.* (2005) Oxidative stress, mitochondrial dysfunction and cellular stress response in Friedreich's ataxia. (Translated from eng) *Journal of the neurological sciences* 233(1-2):145-162 (in eng).
10.   Silva JoP, Proença F, & Coutinho OP (2008) Protective role of new nitrogen compounds on ROS/RNS-mediated damage to PC12 cells. *Free Radical Research* 42(1):57 - 69.
11.   Vanessa P.M. van Empel M, Anne T. Bertrand, PhD, Ralph J. van Oort, MSc, Roel van der Nagel, BS, Markus Engelen, MD, Harold V. van Rijen, PhD, Pieter A. Doevendans, MD, PhD, Harry J. Crijns, MD,PhD, Suan L.Ackerman, PhD, Wim Sluiter, PhD, Leon J. Windt,PhD (2006) EUK-8, a Superoxide Dismutase and Catalse Mimetic, Reduces Cardiac Stress and Ameliorates Pressure Overload-Induced Heart Failure in the Harlequin Mouse Mutant. *Journal of the American College of Cardiology* 48:824-832.
12.   Gilgun-Sherki Y, Melamed E, & Offen D (2001) Oxidative stress induced-neurodegenerative diseases: the need for antioxidants that penetrate the blood brain barrier. (Translated from eng) *Neuropharmacology* 40(8):959-975 (in eng).
13.   Chaturvedi RK & Beal MF (2008) Mitochondrial approaches for neuroprotection. (Translated from eng) *Annals of the New York Academy of Sciences* 1147:395-412 (in eng).
14.   Craggs L & Kalaria RN (2011) Revisiting dietary antioxidants, neurodegeneration and dementia. (Translated from eng) *Neuroreport* 22(1):1-3 (in eng).
15.   Crimi E*, et al.* (2006) The role of oxidative stress in adult critical care. (Translated from eng) *Free radical biology & medicine* 40(3):398-406 (in eng).
16.   Frei B (2004) Efficacy of dietary antioxidants to prevent oxidative damage and inhibit chronic disease. (Translated from eng) *J Nutr* 134(11):3196S-3198S (in eng).

17.     Greenberg ER*, et al.* (1994) A clinical trial of antioxidant vitamins to prevent colorectal adenoma. Polyp Prevention Study Group. (Translated from eng) *The New England journal of medicine* 331(3):141-147 (in eng).
18.     Drew B & Leeuwenburgh C (2002) Aging and the role of reactive nitrogen species. (Translated from eng) *Annals of the New York Academy of Sciences* 959:66-81 (in eng).
19.     Lipton SA*, et al.* (1993) A redox-based mechanism for the neuroprotective and neurodestructive effects of nitric oxide and related nitroso-compounds. (Translated from eng) *Nature* 364(6438):626-632 (in eng).
20.     Foster MW, McMahon TJ, & Stamler JS (2003) S-nitrosylation in health and disease. (Translated from eng) *Trends in molecular medicine* 9(4):160-168 (in eng).
21.     Ischiropoulos H (1998) Biological tyrosine nitration: A pathophysiological function of nitric oxide and reactive oxygen species. (Translated from English) *Arch Biochem Biophys* 356(1):1-11 (in English).
22.     Into T*, et al.* (2008) Regulation of MyD88-dependent signaling events by S nitrosylation retards toll-like receptor signal transduction and initiation of acute-phase immune responses. (Translated from eng) *Mol Cell Biol* 28(4):1338-1347 (in eng).
23.     Sha Y & Marshall HE (2012) S-nitrosylation in the regulation of gene transcription. *Biochimica et Biophysica Acta (BBA) - General Subjects* 1820(6):701-711.
24.     Foster MW, Hess DT, & Stamler JS (2009) Protein S-nitrosylation in health and disease: a current perspective. *Trends in molecular medicine* 15(9):391-404.
25.     van der Vliet A, Eiserich JP, Kaur H, Cross CE, & Halliwell B (1996) [16] Nitrotyrosine as biomarker for reactive nitrogen species. *Methods in Enzymology*, ed Lester P (Academic Press), Vol Volume 269, pp 175-184.
26.     Bonfoco E, Krainc D, Ankarcrona M, Nicotera P, & Lipton SA (1995) Apoptosis and necrosis: two distinct events induced, respectively, by mild and intense insults with N-methyl-D-aspartate or nitric oxide/superoxide in cortical cell cultures. (Translated from eng) *Proceedings of the National Academy of Sciences of the United States of America* 92(16):7162-7166 (in eng).
27.     Radi R, Beckman JS, Bush KM, & Freeman BA (1991) Peroxynitrite oxidation of sulfhydryls. The cytotoxic potential of superoxide and nitric oxide. (Translated from eng) *The Journal of biological chemistry* 266(7):4244-4250 (in eng).
28.     Radi R, Beckman JS, Bush KM, & Freeman BA (1991) Peroxynitrite-induced membrane lipid peroxidation: the cytotoxic potential of superoxide and nitric oxide. (Translated from eng) *Archives of biochemistry and biophysics* 288(2):481-487 (in eng).
29.     Beckman JS, Beckman TW, Chen J, Marshall PA, & Freeman BA (1990) Apparent hydroxyl radical production by peroxynitrite: implications for endothelial injury from nitric oxide and superoxide. (Translated from eng) *Proceedings of the National Academy of Sciences of the United States of America* 87(4):1620-1624 (in eng).
30.     King PA*, et al.* (1992) A stable solid that generates hydroxyl radical upon dissolution in aqueous solutions: reaction with proteins and nucleic acid. *Journal of the American Chemical Society* 114(13):5430-5432.
31.     Radi R (1998) Peroxynitrite reactions and diffusion in biology. (Translated from eng) *Chemical research in toxicology* 11(7):720-721 (in eng).
32.     Belik J, Jankov RP, Pan J, & Tanswell AK (2004) Peroxynitrite inhibits relaxation and induces pulmonary artery muscle contraction in the newborn rat. (Translated from eng) *Free radical biology & medicine* 37(9):1384-1392 (in eng).
33.     Pacher P, Beckman JS, & Liaudet L (2007) Nitric oxide and peroxynitrite in health and disease. (Translated from eng) *Physiol Rev* 87(1):315-424 (in eng).

34. Pietraforte D, Salzano AM, Marino G, & Minetti M (2003) Peroxynitrite-dependent modifications of tyrosine residues in hemoglobin. Formation of tyrosyl radical(s) and 3-nitrotyrosine. (Translated from eng) *Amino Acids* 25(3-4):341-350 (in eng).

35. Radi R (2004) Nitric oxide, oxidants, and protein tyrosine nitration. *Proceedings of the National Academy of Sciences* 101(12):4003-4008.

36. Radi R, Rodriguez M, Castro L, & Telleri R (1994) Inhibition of mitochondrial electron transport by peroxynitrite. (Translated from eng) *Archives of biochemistry and biophysics* 308(1):89-95 (in eng).

37. Tohgi H, *et al.* (1999) Alterations of 3-nitrotyrosine concentration in the cerebrospinal fluid during aging and in patients with Alzheimer's disease. (Translated from eng) *Neurosci Lett* 269(1):52-54 (in eng).

38. Fuenzalida K, *et al.* (2007) Peroxisome proliferator-activated receptor gamma up-regulates the Bcl-2 anti-apoptotic protein in neurons and induces mitochondrial stabilization and protection against oxidative stress and apoptosis. (Translated from eng) *The Journal of biological chemistry* 282(51):37006-37015 (in eng).

39. Shibuya A, *et al.* (2002) Nitration of PPARgamma inhibits ligand-dependent translocation into the nucleus in a macrophage-like cell line, RAW 264. (Translated from eng) *FEBS Lett* 525(1-3):43-47 (in eng).

40. Balavoine GG & Geletii YV (1999) Peroxynitrite scavenging by different antioxidants. Part I: convenient assay. (Translated from eng) *Nitric Oxide* 3(1):40-54 (in eng).

41. Poole LB, Hall A, & Nelson KJ (2011) Overview of peroxiredoxins in oxidant defense and redox regulation. (Translated from eng) *Curr Protoc Toxicol* Chapter 7:Unit7 9 (in eng).

42. Bartlett D, Church DF, Bounds PL, & Koppenol WH (1995) The kinetics of the oxidation of L-ascorbic acid by peroxynitrite. (Translated from eng) *Free Radic Biol Med* 18(1):85-92 (in eng).

43. Quijano C, Alvarez B, Gatti RM, Augusto O, & Radi R (1997) Pathways of peroxynitrite oxidation of thiol groups. (Translated from eng) *Biochem J* 322 ( Pt 1):167-173 (in eng).

44. Whiteman M, Ketsawatsakul U, & Halliwell B (2002) A Reassessment of the Peroxynitrite Scavenging Activity of Uric Acid. *Annals of the New York Academy of Sciences* 962(1):242-259.

45. Ferrer-Sueta G, Batinic-Haberle I, Spasojevic I, Fridovich I, & Radi R (1999) Catalytic scavenging of peroxynitrite by isomeric Mn(III) N-methylpyridylporphyrins in the presence of reductants. (Translated from English) *Chemical Research in Toxicology* 12(5):442-449 (in English).

46. Singh S, Kumar A, Karakoti A, Seal S, & Self WT (2010) Unveiling the mechanism of uptake and sub-cellular distribution of cerium oxide nanoparticles. (Translated from eng) *Mol Biosyst* 6(10):1813-1820 (in eng).

47. Flora SJS (2009) Structural, Chemical and Biological Aspects of Antioxidants for Strategies Against Metal and Metalloid Exposure. *Oxidative Medicine and Cellular Longevity* 2(4):191-206.

48. Melov S, *et al.* (2000) Extension of life-span with superoxide dismutase/catalase mimetics. (Translated from eng) *Science* 289(5484):1567-1569 (in eng).

49. Faulkner KM, Liochev SI, & Fridovich I (1994) Stable Mn(III) porphyrins mimic superoxide dismutase in vitro and substitute for it in vivo. (Translated from eng) *J Biol Chem* 269(38):23471-23476 (in eng).

50. Rong Y, Doctrow SR, Tocco G, & Baudry M (1999) EUK-134, a synthetic superoxide dismutase and catalase mimetic, prevents oxidative stress and attenuates kainate-induced neuropathology. (Translated from eng) *Proc Natl Acad Sci U S A* 96(17):9897-9902 (in eng).

51. Salvemini D, *et al.* (2001) Pharmacological manipulation of the inflammatory cascade by the superoxide dismutase mimetic, M40403. (Translated from eng) *Br J Pharmacol* 132(4):815-827 (in eng).

52.     Zhang Feng PW, J. Koberstein, S. Khalid, Siu-Wai Chan (2004) Cerium oxidation state in ceria nanoparticles studied with X-ray photoelectron spectroscopy and absorption near edge spectroscopy. *Surface Science* 563:74-82.

53.     Babu S, Schulte, Alfons, and Sela, Sudipta (2008) Defects and symmetry influences on visable emmission of Eu doped nanoceria. *Applied Physics Letters* 92(12).

54.     Davis VT & Thompson JS (2002) Measurement of the electron affinity of cerium. (Translated from eng) *Physical review letters* 88(7):073003 (in eng).

55.     Heckert EG, Karakoti AS, Seal S, & Self WT (2008) The role of cerium redox state in the SOD mimetic activity of nanoceria. (Translated from eng) *Biomaterials* 29(18):2705-2709 (in eng).

56.     Korsvik C, Patil S, Seal S, & Self WT (2007) Superoxide dismutase mimetic properties exhibited by vacancy engineered ceria nanoparticles. (Translated from eng) *Chem Commun (Camb)* (10):1056-1058 (in eng).

57.     Chen J, Patil S, Seal S, & McGinnis JF (2006) Rare earth nanoparticles prevent retinal degeneration induced by intracellular peroxides. *Nat Nano* 1(2):142-150.

58.     Kong L*, et al.* (2011) Nanoceria extend photoreceptor cell lifespan in tubby mice by modulation of apoptosis/survival signaling pathways. (Translated from eng) *Neurobiol Dis* 42(3):514-523 (in eng).

59.     Niu J, Azfer A, Rogers LM, Wang X, & Kolattukudy PE (2007) Cardioprotective effects of cerium oxide nanoparticles in a transgenic murine model of cardiomyopathy. pp 549-559.

60.     Niu J, Wang K, & Kolattukudy PE (2011) Cerium oxide nanoparticles inhibit oxidative stress and nuclear factor-kappaB activation in H9c2 cardiomyocytes exposed to cigarette smoke extract. (Translated from eng) *J Pharmacol Exp Ther* 338(1):53-61 (in eng).

61.     Rabkin SW & Klassen SS (2008) Metalloporphyrins as a therapeutic drug class against peroxynitrite in cardiovascular diseases involving ischemic reperfusion injury. (Translated from eng) *Eur J Pharmacol* 586(1-3):1-8 (in eng).

62.     van Empel VP*, et al.* (2006) EUK-8, a superoxide dismutase and catalase mimetic, reduces cardiac oxidative stress and ameliorates pressure overload-induced heart failure in the harlequin mouse mutant. (Translated from eng) *J Am Coll Cardiol* 48(4):824-832 (in eng).

63.     Hardas SS*, et al.* (Rat brain pro-oxidant effects of peripherally administered 5 nm ceria 30 days after exposure. *NeuroToxicology* (0).

64.     Ma JY*, et al.* (2011) Cerium oxide nanoparticle-induced pulmonary inflammation and alveolar macrophage functional change in rats. (Translated from eng) *Nanotoxicology* 5(3):312-325 (in eng).

65.     Zhang H*, et al.* (2011) Nano-CeO2 exhibits adverse effects at environmental relevant concentrations. (Translated from eng) *Environ Sci Technol* 45(8):3725-3730 (in eng).

66.     Karakoti AS*, et al.* (2012) Preparation and characterization challenges to understanding environmental and biological impacts of ceria nanoparticles. *Surface and Interface Analysis*:n/a-n/a.

67.     Pirmohamed T*, et al.* (2010) Nanoceria exhibit redox state-dependent catalase mimetic activity. (Translated from eng) *Chem Commun (Camb)* 46(16):2736-2738 (in eng).

68.     Dowding JM, Dosani T, Kumar A, Seal S, & Self WT (2012) Cerium oxide nanoparticles scavenge nitric oxide radical ( NO). (Translated from eng) *Chem Commun (Camb)* 48(40):4896-4898 (in eng).

69.     Ferri CP*, et al.* (2005) Global prevalence of dementia: a Delphi consensus study. (Translated from eng) *Lancet* 366(9503):2112-2117 (in eng).

70.     Markesbery WR (1997) Oxidative stress hypothesis in Alzheimer's disease. (Translated from eng) *Free radical biology & medicine* 23(1):134-147 (in eng).

71.    Barsoum MJ*, et al.* (2006) Nitric oxide-induced mitochondrial fission is regulated by dynamin-related GTPases in neurons. (Translated from eng) *EMBO J* 25(16):3900-3911 (in eng).
72.    Boczkowski J*, et al.* (2001) Peroxynitrite-mediated mitochondrial dysfunction. (Translated from eng) *Biol Signals Recept* 10(1-2):66-80 (in eng).
73.    Lin MT & Beal MF (2006) Mitochondrial dysfunction and oxidative stress in neurodegenerative diseases. (Translated from eng) *Nature* 443(7113):787-795 (in eng).
74.    Swerdlow RH, Burns JM, & Khan SM (2010) The Alzheimer's disease mitochondrial cascade hypothesis. (Translated from eng) *J Alzheimers Dis* 20 Suppl 2:S265-279 (in eng).
75.    Smith MA, Richey Harris PL, Sayre LM, Beckman JS, & Perry G (1997) Widespread peroxynitrite-mediated damage in Alzheimer's disease. (Translated from eng) *J Neurosci* 17(8):2653-2657 (in eng).
76.    Texel SJ & Mattson MP (2011) Impaired adaptive cellular responses to oxidative stress and the pathogenesis of Alzheimer's disease. (Translated from eng) *Antioxid Redox Signal* 14(8):1519-1534 (in eng).
77.    Shankar GM*, et al.* (2007) Natural oligomers of the Alzheimer amyloid-beta protein induce reversible synapse loss by modulating an NMDA-type glutamate receptor-dependent signaling pathway. (Translated from eng) *J Neurosci* 27(11):2866-2875 (in eng).
78.    Reynolds MR*, et al.* (2006) Tau nitration occurs at tyrosine 29 in the fibrillar lesions of Alzheimer's disease and other tauopathies. (Translated from eng) *J Neurosci* 26(42):10636-10645 (in eng).
79.    Reyes JF*, et al.* (2008) A possible link between astrocyte activation and tau nitration in Alzheimer's disease. (Translated from English) *Neurobiol Dis* 31(2):198-208 (in English).
80.    Karakoti A, Singh S, Dowding JM, Seal S, & Self WT (2010) Redox-active radical scavenging nanomaterials. (Translated from eng) *Chem Soc Rev* 39(11):4422-4432 (in eng).
81.    Patil S, Kuiry SC, Seal S, & Vanfleet R (2002) Synthesis of nanocrystalline ceria particles for high temperature oxidation resistant coating. (Translated from English) *J Nanopart Res* 4(5):433-438 (in English).
82.    Murphy ME & Noack E (1994) Nitric oxide assay using hemoglobin method. (Translated from eng) *Methods Enzymol* 233:240-250 (in eng).
83.    Lim MH*, et al.* (2006) Direct nitric oxide detection in aqueous solution by copper(II) fluorescein complexes. (Translated from eng) *J Am Chem Soc* 128(44):14364-14373 (in eng).
84.    Knott AB & Bossy-Wetzel E (2009) Nitric oxide in health and disease of the nervous system. (Translated from eng) *Antioxid Redox Signal* 11(3):541-554 (in eng).
85.    Isenovic E*, et al.* (2011) Regulation of endothelial nitric oxide synthase in pathophysiological conditions. (Translated from Eng) *Cardiovasc Hematol Disord Drug Targets*  (in Eng).
86.    Martinez MC & Andriantsitohaina R (2009) Reactive nitrogen species: molecular mechanisms and potential significance in health and disease. (Translated from eng) *Antioxid Redox Signal* 11(3):669-702 (in eng).
87.    Masui T, Ozaki T, Machida K, & Adachi G (2000) Preparation of ceria-zirconia sub-catalysts for automotive exhaust cleaning. (Translated from English) *J Alloy Compd* 303:49-55 (in English).
88.    Tsai YY*, et al.* (2008) Reactive oxygen species scavenging properties of ZrO2-CeO2 solid solution nanoparticles. (Translated from English) *Nanomedicine-Uk* 3(5):637-645 (in English).
89.    Ferrizz RM, Egami T, Wong GS, & Vohs JM (2001) Reaction of NO on CeO2 and Rh/CeO2 thin films supported on alpha-Al2O3(0001) and YSZ(100). (Translated from English) *Surf Sci* 476(1-2):9-21 (in English).
90.    Niwa M, Furukawa Y, & Murakami Y (1982) Adsorption of Nitric-Oxide on Cerium Oxide. (Translated from English) *J Colloid Interf Sci* 86(1):260-265 (in English).

91. Qi GS, Yang RT, & Chang R (2004) MnOx-CeO2 mixed oxides prepared by co-precipitation for selective catalytic reduction of NO with NH3 at low temperatures. (Translated from English) *Appl Catal B-Environ* 51(2):93-106 (in English).

92. Martinez-Arias A*, et al.* (1995) NO reaction at surface oxygen vacancies generated in cerium oxide. *Journal of the Chemical Society, Faraday Transactions* 91(11).

93. Lim MH, Xu D, & Lippard SJ (2006) Visualization of nitric oxide in living cells by a copper-based fluorescent probe. (Translated from eng) *Nat Chem Biol* 2(7):375-380 (in eng).

94. Singh S*, et al.* (2011) A phosphate-dependent shift in redox state of cerium oxide nanoparticles and its effects on catalytic properties. (Translated from eng) *Biomaterials* 32(28):6745-6753 (in eng).

95. Ignarro LJ ed (2000) *Nitric Oxide Biology and Pathobiology* (Academic Press, San Diego).

96. Wayland BB & Olson LW (1974) Spectroscopic Studies and Bonding Model for Nitric-Oxide Complexes of Iron Porphyrins. (Translated from English) *Journal of the American Chemical Society* 96(19):6037-6041 (in English).

97. Filipovic MR*, et al.* (2008) NO Dismutase Activity of Seven-Coordinate Manganese(II) Pentaazamacrocyclic Complexes. (Translated from English) *Angew Chem Int Edit* 47(45):8735-8739 (in English).

98. Estevez AY*, et al.* (2011) Neuroprotective mechanisms of cerium oxide nanoparticles in a mouse hippocampal brain slice model of ischemia. (Translated from eng) *Free Radic Biol Med* 51(6):1155-1163 (in eng).

99. Niu J, Azfer A, Rogers LM, Wang X, & Kolattukudy PE (2007) Cardioprotective effects of cerium oxide nanoparticles in a transgenic murine model of cardiomyopathy. (Translated from eng) *Cardiovasc Res* 73(3):549-559 (in eng).

100. Radi R, Peluffo G, Alvarez MN, Naviliat M, & Cayota A (2001) Unraveling peroxynitrite formation in biological systems. (Translated from eng) *Free radical biology & medicine* 30(5):463-488 (in eng).

101. Karakoti A, Singh S, Dowding JM, Seal S, & Self WT (2010) Redox-active radical scavenging nanomaterials. (Translated from English) *Chem Soc Rev* 39(11):4422-4432 (in English).

102. Radi R (1996) Kinetic analysis of reactivity of peroxynitrite with biomolecules. (Translated from eng) *Methods Enzymol* 269:354-366 (in eng).

103. Pompella A, Visvikis A, Paolicchi A, De Tata V, & Casini AF (2003) The changing faces of glutathione, a cellular protagonist. (Translated from eng) *Biochem Pharmacol* 66(8):1499-1503 (in eng).

104. Setsukinai K, Urano Y, Kakinuma K, Majima HJ, & Nagano T (2003) Development of novel fluorescence probes that can reliably detect reactive oxygen species and distinguish specific species. (Translated from eng) *J Biol Chem* 278(5):3170-3175 (in eng).

105. Whiteman M & Halliwell B (1996) Protection against peroxynitrite-dependent tyrosine nitration and alpha 1-antiproteinase inactivation by ascorbic acid. A comparison with other biological antioxidants. (Translated from eng) *Free Radic Res* 25(3):275-283 (in eng).

106. Pacher P, Beckman JS, & Liaudet L (2007) Nitric oxide and peroxynitrite in health and disease. (Translated from English) *Physiol Rev* 87(1):315-424 (in English).

107. Knott AB & Bossy-Wetzel E (2010) Impact of nitric oxide on metabolism in health and age-related disease. (Translated from eng) *Diabetes Obes Metab* 12 Suppl 2:126-133 (in eng).

108. Ghatan S*, et al.* (2000) p38 MAP kinase mediates bax translocation in nitric oxide-induced apoptosis in neurons. (Translated from eng) *J Cell Biol* 150(2):335-347 (in eng).

109. Martinez-Ruiz A, Cadenas S, & Lamas S (2011) Nitric oxide signaling: classical, less classical, and nonclassical mechanisms. (Translated from eng) *Free radical biology & medicine* 51(1):17-29 (in eng).

110. Stamler JS, Lamas S, & Fang FC (2001) Nitrosylation. the prototypic redox-based signaling mechanism. (Translated from eng) *Cell* 106(6):675-683 (in eng).
111. Knott AB, Perkins G, Schwarzenbacher R, & Bossy-Wetzel E (2008) Mitochondrial fragmentation in neurodegeneration. (Translated from eng) *Nat Rev Neurosci* 9(7):505-518 (in eng).
112. Bossy-Wetzel E*, et al.* (2004) Crosstalk between nitric oxide and zinc pathways to neuronal cell death involving mitochondrial dysfunction and p38-activated K+ channels. (Translated from eng) *Neuron* 41(3):351-365 (in eng).
113. Yamamoto T*, et al.* (2002) Selective nitration of mitochondrial complex I by peroxynitrite: involvement in mitochondria dysfunction and cell death of dopaminergic SH-SY5Y cells. (Translated from eng) *J Neural Transm* 109(1):1-13 (in eng).
114. Wallace DC (2005) A mitochondrial paradigm of metabolic and degenerative diseases, aging, and cancer: a dawn for evolutionary medicine. (Translated from eng) *Annu Rev Genet* 39:359-407 (in eng).
115. Manczak M, Calkins MJ, & Reddy PH (2011) Impaired mitochondrial dynamics and abnormal interaction of amyloid beta with mitochondrial protein Drp1 in neurons from patients with Alzheimer's disease: implications for neuronal damage. (Translated from eng) *Hum Mol Genet* 20(13):2495-2509 (in eng).
116. Cho DH*, et al.* (2009) S-nitrosylation of Drp1 mediates beta-amyloid-related mitochondrial fission and neuronal injury. (Translated from eng) *Science (New York, N.Y* 324(5923):102-105 (in eng).
117. Bossy B*, et al.* (2010) S-Nitrosylation of DRP1 does not affect enzymatic activity and is not specific to Alzheimer's disease. (Translated from eng) *J Alzheimers Dis* 20 Suppl 2:S513-526 (in eng).
118. Wang X*, et al.* (2009) Impaired balance of mitochondrial fission and fusion in Alzheimer's disease. (Translated from eng) *J Neurosci* 29(28):9090-9103 (in eng).
119. Taguchi N, Ishihara N, Jofuku A, Oka T, & Mihara K (2007) Mitotic phosphorylation of dynamin-related GTPase Drp1 participates in mitochondrial fission. (Translated from eng) *The Journal of biological chemistry* 282(15):11521-11529 (in eng).
120. Yamano K & Youle RJ (2011) Coupling mitochondrial and cell division. (Translated from eng) *Nat Cell Biol* 13(9):1026-1027 (in eng).
121. Nguyen MD, Mushynski WE, & Julien JP (2002) Cycling at the interface between neurodevelopment and neurodegeneration. (Translated from eng) *Cell death and differentiation* 9(12):1294-1306 (in eng).
122. Crews L & Masliah E (2010) Molecular mechanisms of neurodegeneration in Alzheimer's disease. (Translated from eng) *Hum Mol Genet* 19(R1):R12-20 (in eng).
123. Ikiz B & Przedborski S (2008) A sequel to the tale of p25/Cdk5 in neurodegeneration. (Translated from eng) *Neuron* 60(5):731-732 (in eng).
124. Qu J*, et al.* (2011) S-Nitrosylation activates Cdk5 and contributes to synaptic spine loss induced by beta-amyloid peptide. (Translated from eng) *Proceedings of the National Academy of Sciences of the United States of America* 108(34):14330-14335 (in eng).
125. Esch F*, et al.* (2005) Electron localization determines defect formation on ceria substrates. (Translated from eng) *Science* 309(5735):752-755 (in eng).
126. Korsvik C, Patil S, Seal S, & Self WT (2007) Superoxide dismutase mimetic properties exhibited by vacancy engineered ceria nanoparticles. (Translated from English) *Chemical Communications* (10):1056-1058 (in English).
127. Dowding J, Dosani T, Kumar A, Seal S, & Self WT (2012) Cerium oxide nanoparticles scavenge nitric oxide radical (NO). *Chem Commun*.

128. Liot G, *et al.* (2009) Complex II inhibition by 3-NP causes mitochondrial fragmentation and neuronal cell death via an NMDA- and ROS-dependent pathway. (Translated from eng) *Cell death and differentiation* 16(6):899-909 (in eng).

129. Song W, *et al.* (2011) Mutant huntingtin binds the mitochondrial fission GTPase dynamin-related protein-1 and increases its enzymatic activity. (Translated from eng) *Nat Med* 17(3):377-382 (in eng).

130. Song W, *et al.* (2008) Assessing mitochondrial morphology and dynamics using fluorescence wide-field microscopy and 3D image processing. (Translated from eng) *Methods* 46(4):295-303 (in eng).

131. Singh S, Kumar A, Karakoti A, Seal S, & Self WT (2010) Unveiling the mechanism of uptake and sub-cellular distribution of cerium oxide nanoparticles. (Translated from eng) *Molecular Biosystems* 6(10):1813-1820 (in eng).

132. Liaudet L, Vassalli G, & Pacher P (2009) Role of peroxynitrite in the redox regulation of cell signal transduction pathways. (Translated from eng) *Front Biosci* 14:4809-4814 (in eng).

133. Cho D-H, *et al.* (2009) S-Nitrosylation of Drp1 Mediates β-Amyloid-Related Mitochondrial Fission and Neuronal Injury. *Science (New York, N.Y* 324(5923):102-105.

134. Chan DC (2006) Mitochondria: dynamic organelles in disease, aging, and development. (Translated from eng) *Cell* 125(7):1241-1252 (in eng).

135. Zhu X, Raina AK, Perry G, & Smith MA (2004) Alzheimer's disease: the two-hit hypothesis. *The Lancet Neurology* 3(4):219-226.

136. Reddy PH (2008) Mitochondrial medicine for aging and neurodegenerative diseases. (Translated from eng) *Neuromolecular Med* 10(4):291-315 (in eng).

137. Jang JH & Surh YJ (2005) AP-1 mediates beta-amyloid-induced iNOS expression in PC12 cells via the ERK2 and p38 MAPK signaling pathways. (Translated from eng) *Biochem Biophys Res Commun* 331(4):1421-1428 (in eng).

138. Swerdlow RH (2007) Pathogenesis of Alzheimer's disease. (Translated from eng) *Clin Interv Aging* 2(3):347-359 (in eng).

139. Chen J, Patil S, Seal S, & McGinnis JF (2006) Rare earth nanoparticles prevent retinal degeneration induced by intracellular peroxides. (Translated from eng) *Nat Nanotechnol* 1(2):142-150 (in eng).

140. Campbell CT & Peden CH (2005) Chemistry. Oxygen vacancies and catalysis on ceria surfaces. (Translated from eng) *Science* 309(5735):713-714 (in eng).

141. Bumajdad A, Eastoe J, & Mathew A (2009) Cerium oxide nanoparticles prepared in self-assembled systems. (Translated from eng) *Adv Colloid Interface Sci* 147-148:56-66 (in eng).

142. Karakoti AS, Kuchibhatla SVNT, Babu KS, & Seal S (2007) Direct synthesis of nanoceria in aqueous polyhydroxyl solutions. (Translated from English) *J Phys Chem C* 111(46):17232-17240 (in English).

143. Sathyamurthy S, Leonard KJ, Dabestani RT, & Paranthaman MP (2005) Reverse micellar synthesis of cerium oxide nanoparticles. (Translated from English) *Nanotechnology* 16(9):1960-1964 (in English).

144. He H-W, *et al.* (2012) Synthesis of crystalline cerium dioxide hydrosol by a sol–gel method. *Ceramics International* 38, Supplement 1(0):S501-S504.

145. Zhou XD, Huebner W, & Anderson HU (2003) Processing of nanometer-scale CeO2 particles. (Translated from English) *Chem Mater* 15(2):378-382 (in English).

146. Lee TL, Raitano JM, Rennert OM, Chan SW, & Chan WY (2012) Accessing the genomic effects of naked nanoceria in murine neuronal cells. (Translated from eng) *Nanomedicine* 8(5):599-608 (in eng).

147.     Schubert D, Dargusch R, Raitano J, & Chan SW (2006) Cerium and yttrium oxide nanoparticles are neuroprotective. (Translated from eng) *Biochem Biophys Res Commun* 342(1):86-91 (in eng).

148.     Chen J, Patil S, Seal S, & McGinnis JF (2006) Rare earth nanoparticles prevent retinal degeneration induced by intracellular peroxides. (Translated from eng) *Nature Nanotechnology* 1(2):142-150 (in eng).

149.     Hirst SM*, et al.* (2011) Bio-distribution and in vivo antioxidant effects of cerium oxide nanoparticles in mice. (Translated from Eng) *Environ Toxicol* (in Eng).

150.     Angelo B*, et al.* (Cerium Oxide Nanoparticles Trigger Neuronal Survival in a Human Alzheimer Disease Model By Modulating BDNF Pathway. *Current Nanoscience* 5(2):167-176.

151.     Hussain S*, et al.* (2012) Cerium dioxide nanoparticles induce apoptosis and autophagy in human peripheral blood monocytes. (Translated from eng) *ACS Nano* 6(7):5820-5829 (in eng).

152.     Suh WH, Suslick KS, Stucky GD, & Suh YH (2009) Nanotechnology, nanotoxicology, and neuroscience. (Translated from eng) *Prog Neurobiol* 87(3):133-170 (in eng).

153.     Tseng MT*, et al.* (2012) Alteration of hepatic structure and oxidative stress induced by intravenous nanoceria. *Toxicology and Applied Pharmacology* 260(2):173-182.

154.     Das S*, et al.* (2012) The induction of angiogenesis by cerium oxide nanoparticles through the modulation of oxygen in intracellular environments. (Translated from Eng) *Biomaterials* (in Eng).

155.     Zhang F, Jin Q, & Chan S-W (2004) Ceria nanoparticles: Size, size distribution, and shape. *Journal of Applied Physics* 95(8):4319-4326.

156.     Maniatis T, Fritsch EF, & Sambrook J (1989) Molecular cloning : a laboratory manual / J. Sambrook, E.F. Fritsch, T. Maniatis.  (New York : Cold Spring Harbor Laboratory Press).

157.     Deshpande S, Patil S, Kuchibhatla SVNT, & Seal S (2005) Size dependency variation in lattice parameter and valency states in nanocrystalline cerium oxide. (Translated from English) *Appl Phys Lett* 87(13) (in English).

158.     Taguchi M*, et al.* (2012) Synthesis of surface-modified monoclinic ZrO2 nanoparticles using supercritical water. (Translated from English) *Crystengcomm* 14(6):2132-2138 (in English).

159.     Lundqvist M*, et al.* (2008) Nanoparticle size and surface properties determine the protein corona with possible implications for biological impacts. (Translated from eng) *Proc Natl Acad Sci U S A* 105(38):14265-14270 (in eng).

160.     Nel A, Xia T, Madler L, & Li N (2006) Toxic potential of materials at the nanolevel. (Translated from eng) *Science* 311(5761):622-627 (in eng).

161.     Nel AE*, et al.* (2009) Understanding biophysicochemical interactions at the nano-bio interface. (Translated from eng) *Nat Mater* 8(7):543-557 (in eng).

162.     Das M*, et al.* (2007) Auto-catalytic ceria nanoparticles offer neuroprotection to adult rat spinal cord neurons. *Biomaterials* 28(10):1918-1925.

163.     Yokel RA*, et al.* (2009) Biodistribution and oxidative stress effects of a systemically-introduced commercial ceria engineered nanomaterial. (Translated from English) *Nanotoxicology* 3(3):234-248 (in English).

164.     Horie M*, et al.* (2011) Cellular responses induced by cerium oxide nanoparticles: induction of intracellular calcium level and oxidative stress on culture cells. (Translated from eng) *J Biochem* 150(4):461-471 (in eng).

165.     Xia T*, et al.* (2008) Comparison of the mechanism of toxicity of zinc oxide and cerium oxide nanoparticles based on dissolution and oxidative stress properties. (Translated from eng) *ACS Nano* 2(10):2121-2134 (in eng).

166.     Hillegass JM*, et al.* (2010) Assessing nanotoxicity in cells in vitro. *Wiley Interdisciplinary Reviews: Nanomedicine and Nanobiotechnology* 2(3):219-231.

167.     Sohaebuddin S, Thevenot P, Baker D, Eaton J, & Tang L (2010) Nanomaterial cytotoxicity is composition, size, and cell type dependent. *Particle and Fibre Toxicology* 7(1):22.

168. Kuchma MH*, et al.* (2010) Phosphate ester hydrolysis of biologically relevant molecules by cerium oxide nanoparticles. (Translated from eng) *Nanomedicine* 6(6):738-744 (in eng).
169. Anderson SA & Purich DL (1982) A Reinvestigation of Dynein Atpase Kinetics and the Inhibitory-Action of Vanadate. (Translated from English) *J Biol Chem* 257(12):6656-6658 (in English).
170. Lark E, Omoto CK, & Schumaker MF (1994) Functional Multiplicity of Motor Molecules Revealed by a Simple Kinetic-Analysis. (Translated from English) *Biophys J* 67(3):1134-1140 (in English).
171. Brandenberger C*, et al.* (2010) Intracellular imaging of nanoparticles: Is it an elemental mistake to believe what you see? *Particle and Fibre Toxicology* 7(1):15.
172. Gao MD, Li MM, & Yu WD (2005) Flowerlike ZnO nanostructures via hexamethylenetetramine-assisted thermolysis of zinc-ethylenediamine complex. (Translated from English) *J Phys Chem B* 109(3):1155-1161 (in English).
173. Westfall SD*, et al.* (2008) Identification of oxygen-sensitive transcriptional programs in human embryonic stem cells. (Translated from eng) *Stem Cells Dev* 17(5):869-881 (in eng).
174. Murphy MP*, et al.* (2011) Unraveling the biological roles of reactive oxygen species. (Translated from eng) *Cell Metab* 13(4):361-366 (in eng).
175. Franklin SJ (2001) Lanthanide-mediated DNA hydrolysis. (Translated from eng) *Curr Opin Chem Biol* 5(2):201-208 (in eng).
176. Komiyama M, Takeda N, & Shigekawa H (1999) Hydrolysis of DNA and RNA by lanthanide ions: mechanistic studies leading to new applications. (Translated from English) *Chem Commun* (16):1443-1451 (in English).
177. Pirmohamed T*, et al.* (2010) Nanoceria exhibit redox state-dependent catalase mimetic activity. *Chem Commun* 46(16):2736-2738.